(12) B.S.

(14) DNA | WT-394 (EX)

EXTRACTED VERSION

(19)

(6)

OPERATION JANGLE.

Airborne Particle Studies. Project 2.5a-1.

Armed Forces Special Weapons Project
Washington, D.C.

(10) C. Robbins

Nevada Proving Grounds
1 Oct [redacted]—Nov [redacted]51.

(15) DNA 191-79-C-0455

NOTICE

This is an extract of WT-394, Operation JANGLE, Project 2..5a.1, which remains classified Secret/ Restricted Data as of this date.

Extract version prepared for:
Director
DEFENSE NUCLEAR AGENCY
Washington, D.C. 20305

(11) 1 Oct [redacted]79

(12) 191

346420

DISCLAIMER NOTICE

THIS DOCUMENT IS BEST QUALITY PRACTICABLE. THE COPY FURNISHED TO DTIC CONTAINED A SIGNIFICANT NUMBER OF PAGES WHICH DO NOT REPRODUCE LEGIBLY.

Unclassified

SECURITY CLASSIFICATION OF THIS PAGE (When Data Entered)

REPORT DOCUMENTATION PAGE		READ INSTRUCTIONS BEFORE COMPLETING FORM
1. REPORT NUMBER WT-394 (EX)	2. GOVT ACCESSION NO.	3. RECIPIENT'S CATALOG NUMBER
4. TITLE (and Subtitle) Operation JANGLE, Project 2.5a.1, Airborne Particle Studies		5. TYPE OF REPORT & PERIOD COVERED WT-394 (EX) 6. PERFORMING ORG. REPORT NUMBER
7. AUTHOR(s) LTC C. Robbins		8. CONTRACT OR GRANT NUMBER(s)
9. PERFORMING ORGANIZATION NAME AND ADDRESS Chemical and Radiological Laboratories Army Chemical Center, Maryland		10. PROGRAM ELEMENT, PROJECT, TASK AREA & WORK UNIT NUMBERS
11. CONTROLLING OFFICE NAME AND ADDRESS		12. REPORT DATE July 1952 13. NUMBER OF PAGES
14. MONITORING AGENCY NAME & ADDRESS(if different from Controlling Office)		15. SECURITY CLASS. (of this report) Unclassified 15a. DECLASSIFICATION/DOWNGRADING SCHEDULE

16. DISTRIBUTION STATEMENT (of this Report)

Approved for public release; unlimited distribution.

17. DISTRIBUTION STATEMENT (of the abstract entered in Block 20, if different from Report)

18. SUPPLEMENTARY NOTES

This report has had the classified information removed and has been republished in unclassified form for public release. This work was performed by the General Electric Company-TEMPO under contract DNA001-79-C-0455 with the close cooperation of the Classification Management Division of the Defense Nuclear Agency.

19. KEY WORDS (Continue on reverse side if necessary and identify by block number)

Nuclear Atmospheric Tests
Operation JANGLE
Radioactivity Measurements
Instruments (Design/Calibration) Fractionation
Radioactive Particles

20. ABSTRACT (Continue on reverse side if necessary and identify by block number)

The object of this study was to obtain data relative to the close-in ground level airborne and fallout hazard associated with each detonation in Operation JANGLE. The airborne particle studies reported herein were undertaken by the Chemical Corps to answer questions which were raised regarding the internal hazard due to the radioactive particulate matter associated with the cloud and base surge produced by a surface and underground detonation of an atomic weapon.

DD FORM 1 JAN 73 1473 EDITION OF 1 NOV 65 IS OBSOLETE

Unclassified

SECURITY CLASSIFICATION OF THIS PAGE (When Data Entered)

PROJECT 2.5a-1

ABSTRACT

The object of this study was to obtain data relative to the close-in ground level airborne and fall-out hazard associated with each detonation in Operation JANGLE. For this purpose samples of the aerosol and fall-out were obtained from 46 stations located between 4000 feet upwind and 50,000 feet downwind. Several types of instruments were used in this study; filter samplers, cascade impactors, conifuges, particle separators, electrostatic precipitators, Brookhaven continuous air monitors, Tracerlab continuous air monitors and fall-out trays.

The concentration of beta activity in the cloud near ground zero a few minutes after the shot was found to be approximately 10^{-3} and 10^{-1} microcuries per cubic centimeter for the surface and underground shots respectively. The number median diameters of the particles in the surface and underground shots were 1.0 and 1.5 microns respectively at stations 4000 ft. downwind, decreasing in both cases to less than 0.1 microns at 50,000 ft. Data were also obtained on the variation of activity with particle size, as well as the percentage of the number of particles which were radioactive for both the aerosol and the fall-out. In addition, a study of fractionation and its manifestations was made.

FOREWORD

This report has had classified material removed in order to make the information available on an unclassified, open publication basis, to any interested parties. This effort to declassify this report has been accomplished specifically to support the Department of Defense Nuclear Test Personnel Review (NTPR) Program. The objective is to facilitate studies of the low levels of radiation received by some individuals during the atmospheric nuclear test program by making as much information as possible available to all interested parties.

The material which has been deleted is all currently classified as Restricted Data or Formerly Restricted Data under the provision of the Atomic Energy Act of 1954, (as amended) or is National Security Information.

This report has been reproduced directly from available copies of the original material. The locations from which material has been deleted is generally obvious by the spacings and "holes" in the text. Thus the context of the material deleted is identified to assist the reader in the determination of whether the deleted information is germane to his study.

It is the belief of the individuals who have participated in preparing this report by deleting the classified material and of the Defense Nuclear Agency that the report accurately portrays the contents of the original and that the deleted material is of little or no significance to studies into the amounts or types of radiation received by any individuals during the atmospheric nuclear test program.

PREFACE

The airborne particle studies reported herein were undertaken by the Chemical Corps to answer questions which were raised regarding the internal hazard due to the radioactive particulate matter associated with the cloud and base surge produced by a surface and underground detonation of an atomic weapon. It is believed that the data developed from this study will assist in evaluating the relative importance of the internal hazard which can result from such a detonation.

ACKNOWLEDGMENT

The authors wish to make the following acknowledgments:

Lt Cdr Walter F. V. Bennett, USN, who made valuable contributions in planning for this test and in reducing the data obtained from the samples. In the early stage of preparation of this report, Lt Cdr Bennett was transferred to sea duty and his services were lost to our organization.

Mr. Curt L. Zitza, of CRL Engineering Division, for the design of equipment.

Mr. Robert C. Tompkins, of CRL Radiological Division, for the radiochemical analysis of samples and results on isotopic content.

Miss Phyllis Beamer for activity measurements.

Mr. Walter R. Van Antwerp, of CRL Test Division, for the sampling, analysis, and results of the cascade impactor.

CONTENTS

ILLUSTRATIONS

PROJECT 2.5a-1

TABLES

CHAPTER 1

INTRODUCTION

1.1 OBJECTIVE

The primary objective of Project 2.5a was to conduct a study of the airborne particulate matter resulting from a surface and underground detonation of a nuclear weapon and to determine the following:

1. Concentration of radioactivity in the aerosol and its variation with distance from ground zero.

2. Variation of radioactivity with particle-size.

3. The variation of the particle-size distribution with distance from the point of detonation.

4. Total particles which are radioactive as a function of particle size.

Secondary objectives of this project were to study similar factors for the fall-out (factors which are inseparable from the aerosol) and the phenomenon of fractionation [1] for both.

An indirect objective of the project was to evaluate the field performance of the several instruments employed.

1.2 HISTORICAL

Chemical Corps results from SANDSTONE[2] derived from the cascade impactor indicated a predominence of particulate matter in the range of 0.1 to 0.4 micron diameter, with some material in the range 1 to 10 microns. The long sampling period and the large integrated sample collected left doubt as to the accuracy of the particle size measurements

---

1 These and certain other terms used in this report are defined in Appendix A.

2 Bernard Siegel, Cdr H. L. Andrews, USPHS, and Raymond E. Murphy, Particle Size of Material in Cloud, Operation SANDSTONE, Task Group 7.6, Project Report, Project 7.1-17/RS(CC)-9, 30 June 1948.

of the active particulates. Tracerlab results from SANDSTONE [3], derived from filters, indicated that in the frequency vs. particle size graph the mode occurred between 4 and 6 microns for particles in the range of 2 to 10 micron diameter. The limit of resolution of the technique was approximately 1 micron, thus no observations were made on particles less than one micron diameter.

Chemical Corps results from Operation GREENHOUSE [4] derived from the cascade impactor indicated that cloud samples taken at 16,000-25,000 feet had a median size of approximately 0.3 micron. The results from the U. S. Naval Radiological Defense Laboratory derived from the electrostatic precipitator on this same Operation indicated a median particle size of 0.15 microns.

In June, 1950, the Joint Chiefs of Staff directed the test of an underground and surface nuclear detonation. The Armed Forces Special Weapons Project requested the Chemical Corps to submit proposals for participation in the test. As a result, Project 2.5a was developed to conduct airborne particle studies on the aerosol resulting from these bursts. Because of the large amount of ground contamination expected, these tests provided an opportunity to determine whether there is a correlation between particle size, isotopic content and decay rate, and to evaluate the internal hazard associated with these types of detonations.

1.3 AEROSOL SAMPLING

It may be safely said that the sampling of particulate aerosols is a field characterized by instrument design difficulties. And this is particularly true of sampling aerosols containing large particles; a condition which is produced by the detonation of atomic weapons near to or under the surface of the ground.

The difficulties, roughly, are two-fold. First, is the problem of introducing the particles into the sampling apparatus without prejudice with respect to particle size. This is the problem of obtaining isokinetic flow into the sampler. The second problem is to remove the particles from the air, again, without selecting for or against different sized particles. This problem is usually aggravated by the desire to remove the particles in such a manner that they may subsequently be subjected to size measurements or other types of analysis.

---

3 Report on Analysis Results and Conclusions Relating to Test Joe, December 1950, Department of the Air Force Contracts with Tracerlab, Inc., 130 High St., Boston, Mass.

4 GREENHOUSE 6.1 Report. Unpublished.

PROJECT 2.5a-1

At the time of planning of this project there were a number of sampling instruments in existence, none of which satisfied the first criteria, but which partially satisfied the second criteria in a number of ways which were suitable to the types of measurements desired. For example, a filter sampler, in common use in the Chemical Corps, would collect all particle sizes to be encountered with better than 99.9 per cent efficiency, and would be excellent for the measurements necessary to determine activity concentration data.

Due to the cost and lack of time adjudged to be necessary to redesign all desired instruments for isokinetic flow, it was deemed necessary either to reduce the number and type of sampling instruments, or to use all instruments as they were, even though sampling was not isokinetic. A decision in favor of the latter course was made at an early stage of planning. The crux of this matter was the extent to which non-isokinetic sampling would affect the data obtained by the instruments. Unfortunately, only a qualitative discussion of this point can be made at the present time.

Anderson[5], working with cement dust less than 50 microns in diameter, reported dust concentrations of 150 to 180 per cent of the true concentrations in the samples taken at one-half of the stream velocity and concentrations of 80 per cent of the true value for samples taken at 140 per cent of stream velocity.

Figure 1.1 illustrates isokinetic flow. The streamlines enter the sampling tube without distortion. Any other condition results in deflection of the streamlines in the vicinity of the orifice, giving samples which are either too low or too high, depending upon whether the ratio of sampling speed to wind speed is less than or greater than one respectively. Figure 1.2 illustrates the sampling speed to wind speed ratio of one-half. In this case the sample will favor the larger particles. Figure 1.3 illustrates the sampling speed to wind speed ratio of two. In this case the sample will favor the smaller particles.

Table 1.1 indicates the deviations of the samplers from isokinetic flow, assuming the intake orifice is pointed into the wind. (Not the case in actual use) The average wind speed at the Nevada Test Site was approximately 5 miles per hour, or 1.34×10^4 cm/min. A value of one for the ratio sampling speed:wind speed, represents isokinetic flow.

5 Evald Anderson, "On the Qualitative Determination of Industrial Gas Dispersoids." Transactions of the American Inst. of Chemical Engineers, 34, 589. (1938)

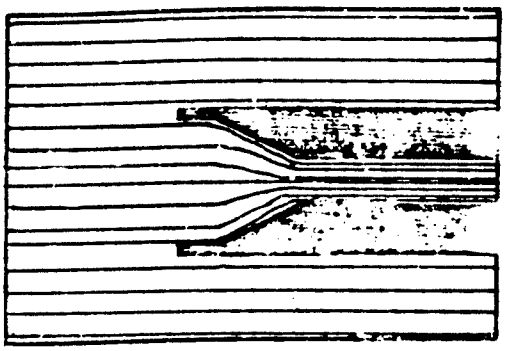

Fig. 1.1 Isokinetic Flow

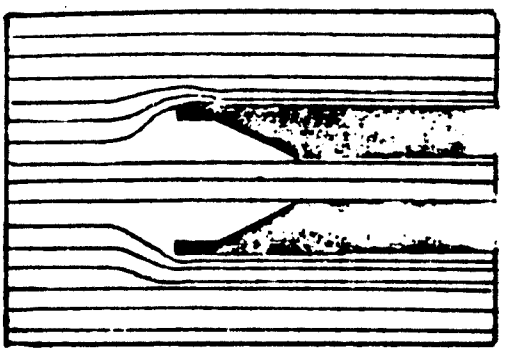

Fig. 1.2 Ratio of Sampling Speed to Wind Speed is 1/2

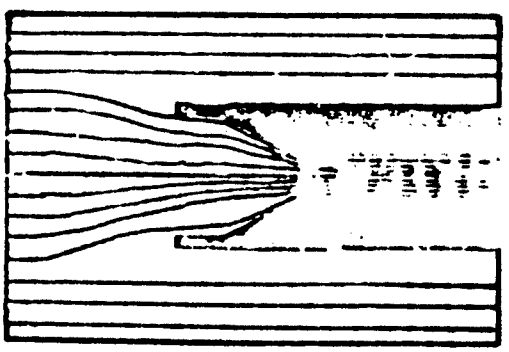

Fig. 1.3 Ratio of Sampling Speed to Wind Speed is 2

PROJECT 2.5a-1

TABLE 1.1

Air Sampling Speed Data

Instrument	Volume Flow Rate cm/min	Sampling Area cm	Sampling Speed cm/min	Sampling Speed / Wind Speed
Filter Sampler	3.4×10^4	100	3.41×10^2	2.54×10^{-2}
Cascade Impactor	1.25×10^4	10	1.2×10^3	8.95×10^{-2}
Centrifuge at 6000 RPM	2.2×10^2	0.18	1.2×10^3	8.95×10^{-2}
Tracerlab Continuous Air Monitor	7.4×10^4	13.2	5.6×10^3	4.18×10^{-1}
Brookhaven Continuous Air Monitor	9.6×10^4	10.4	9.25×10^3	6.90×10^{-1}
Particle Separator	2.83×10^4	52.8	5.38×10^2	4.02×10^{-2}
Radiological Air Sampler	5.0×10^2	0.6	7.94×10^2	5.94×10^{-2}
Electrostatic Precipitator	3.3×10^4	22	1.5×10^3	1.12×10^{-1}

It must be reemphasized that the values given in Table 1.1 are applicable only for the case of the instrument facing continually into the wind i.e. as a weather cock. Actually the filter samplers were mounted perpendicularly to the radii from the zero point so that in general on the "hot" legs they sampled broadside to the wind stream. This and the presence of the sheet metal hood (see Fig. 2.1), tended to make this instrument favor the smaller particles. The cascade impactors were oriented down the axis of radii from the zero point and on the "hot" legs were non-isokinetic to approximately the degree indicated in Table 1.1. All of the other instruments were oriented in the vertical direction and therefore were sampling broadside to the wind and in a manner comparable to the filter sampler, except that they favored the very largest particles which had a Stoke's fall velocity greater than the horizontal wind velocity.

1.4 RADIOACTIVITY MEASUREMENTS

While in any investigation of this nature all three kinds of nuclear radiation can be of interest, the hazard caused by the in-

halation of fission products is predominantly due to beta radiation.[6] For this reason, as well as the heavy counting load caused by the large number of samples, only beta counting was performed in this project. In order to report such quantities as concentration of activity in the aerosol, it was necessary to determine absolute beta disintegration rates, a difficult goal. An uncertainty of the order of 20% can be expected in the reported beta activity data.[7,8] Unless otherwise indicated, corrections for coincidence, sample covering, air path, and tube window were applied to all counting data, in addition to the usual geometry correction. No corrections for self scattering and self absorption or back scattering were made.

1.5 ORGANIZATION

Figure 1.4 shows the organization employed to prosecute this project, and Table 1.2 shows the assignment of stations to personnel.

6 See, for example, The Effects of Atomic Weapons, (U. S. Gov. Printing Office, Sept. 1950), p. 257.

7 G. Friedlander and J. W. Kennedy, Introduction to Radiochemistry, (New York: John Wiley and Sons, 1949), p. 228

8 L. R. Zumwalt, "Absolute Beta Counting Using End-Window Geiger-Mueller Counter Tubes" MDDC -1346, (Oak Ridge: Technical Information Division, 1947) p. 1

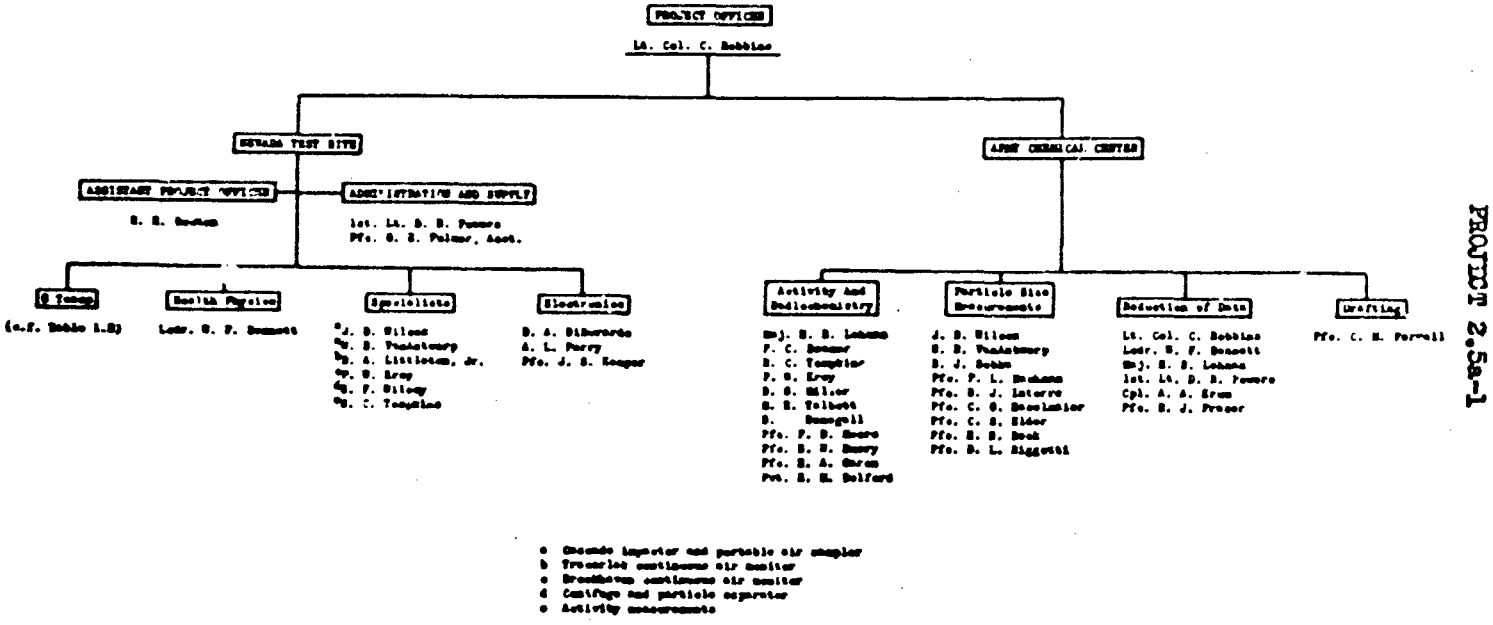

a Chromic impactor and portable air sampler
b Tracerlab continuous air monitor
c Brookhaven continuous air monitor
d Centrifuge and particle separator
e Activity measurements

Fig. 1.4 Organisation of Project 2.5a

TABLE 1.2

Station Assignments to Personnel

Team No.	Group Leader	Organization	Asst. Group Leader	Organization	Station Nos Assigned
1	D. A. Littleton, Jr.	C&RL, ACC	Pfc. D. B. Sullivan	Technical Escort Det. Army Chemical Center	1,7,13,19
2	P. W. Krey	C&RL, ACC	J. L. Lindwarm	Research & Engineering Command, ACC	2,8,14,20 23,27
3	E. P. Sawyer	CmlC Board ACC	Pfc. R. W. Sullivan	Technical Escort Det. Army Chemical Center	3,9,15,21 24,28
4	M. J. Schumchyk	C&RL, ACC	Pvt. R. R. Weber	Technical Escort Det. Army Chemical Center	29,33,36,39
5	E. F. Wilsey	C&RL, ACC	Pvt. S. Wallace	Technical Escort Det. Army Chemical Center	4,10,16,22 26,46
6	J. R. Hendrickson	C&RL, ACC	Pvt. A. Lyons	Technical Escort Det. Army Chemical Center	30,34,37,40
7	E. H. Bouton	C&RL, ACC	A. Owyang	Dugway Proving Ground Tooele, Utah	5,6,11,12 17,18,42,43
8	Capt. G. G. Cannity	CmlC Training Comd.	Pvt. F. N. Gray	Technical Escort Det. Army Chemical Center	31,35,38,41

PROJECT 2.5a-1

CHAPTER 2

INSTRUMENTS

2.1 FILTER SAMPLER

The purpose of this instrument was to filter the particulate matter from a known volume of the aerosol. By measuring the activity on the filter paper and volume of air filtered, the average concentration of activity in the cloud could be estimated.

2.1.1 Design

The filter samplers used in the tests (see Fig. 2.1) consisted of a motor driven suction pump drawing air through a filter paper sampling area of 100 cm^2.

2.1.2 Calibration

All filter samplers were calibrated at the test site with a dry flow-rate meter. For the surface shot the flow rates of several samplers were measured before and after the detonation. The results, given in Table 2.1, show that for the quantity of material filtered there was no appreciable change in resistance of the paper before and after the test. It was therefore considered reasonable to assume that the flow-rate remained constant during the sampling period.

The following code was used in describing the various filter samplers listed in Table 2.1. (For location of the stations, see Figs. 3.1 and 3.2.)

X Consisted of 1 sheet Chemical Corps No. 6 paper and 2 sheets of No. 5 paper. This type was used on all stations at distances greater than 4000 feet from zero. The sampler was located 7 feet above ground.

X_1 Consisted of 1 sheet Cml C No. 6 paper, 2 sheets of Cml C No. 5 paper backed up by 5 sheets of No. 6 paper. The 5 sheets of No. 6 paper served to cut down the flow of air approximately to 1 cubic foot per minute while the filter sampler was operating at full (24 volts) battery voltage. This type of sampler was used on all stations up to and including distances of 4000 feet from ground zero. The sampler was located 7 feet above ground.

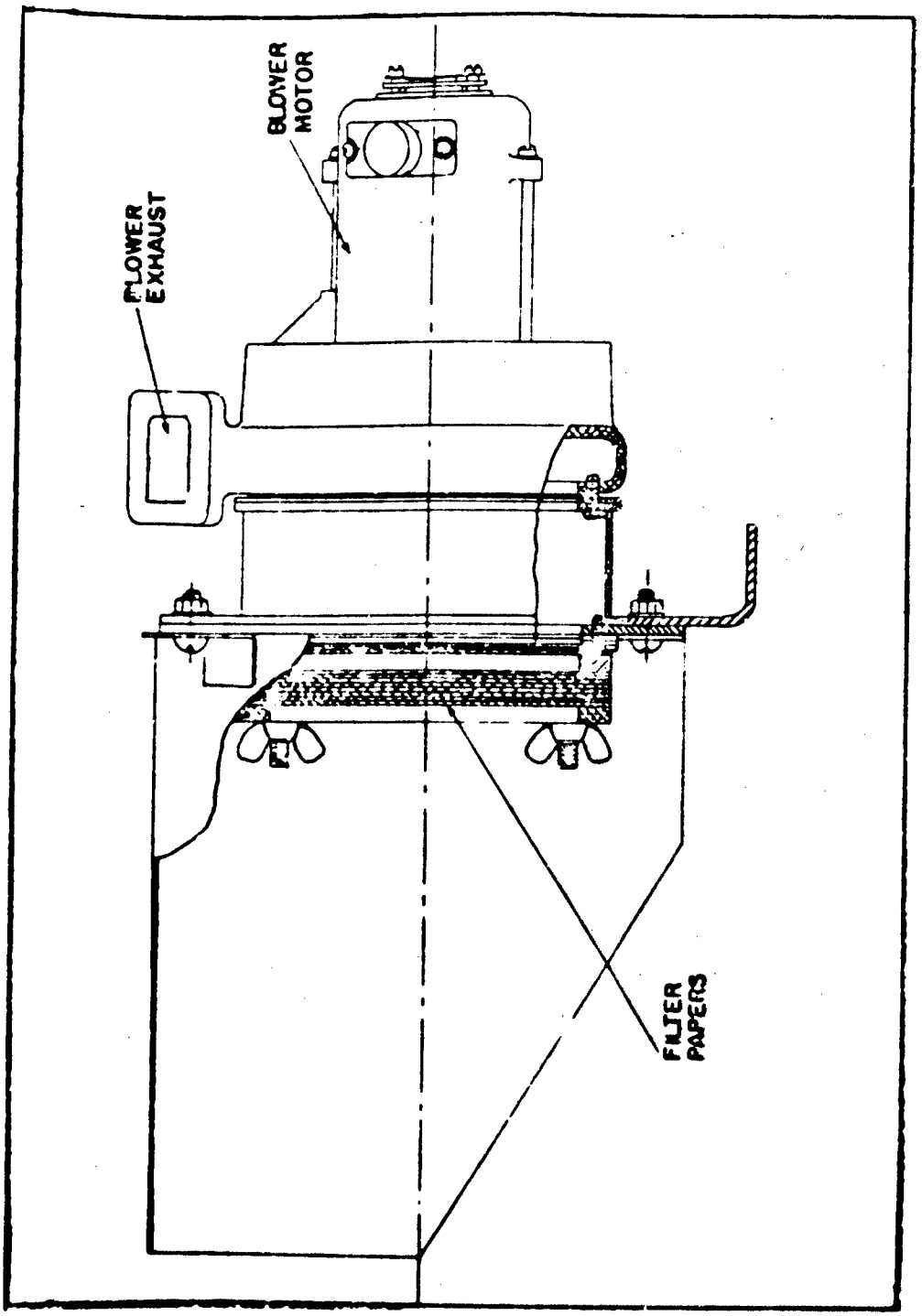

Fig. 2.1 Filter Sampler Assembly

PROJECT 2.5a-1

TABLE 2.1

Filter Sampler Data

Station Number	Location and Type Paper	Flow Rate (cu.ft/min) Before Surface Shot	Flow Rate (cu.ft/min) After Surface Shot	Purpose of Sample	Agency Performing Analysis
1	X_1	1.18	-	activity, decay	NIH, TL
2	X_1	1.36	damaged by blast	activity, decay	NIH, ACC
3	X_1	1.32	-	activity, autoradiograph	NIH, LASL, ACC
4	X_1	0.75	-	activity	NIH, TL
5	X_1	0.83	-	activity	NIH, ACC
6	X_1	1.36	-	activity	NIH, ACC
7	X_1	1.24	-	activity	NIH, TL
8	X_1	1.43	1.43	activity	NIH, TL
9	X_1	1.28	-	activity	NIH, TL
10	X_1	0.59	-	activity	NIH, TL
11	X_1	1.23	-	activity	NIH, ACC
12	X_1	1.38	-	activity	NIH, ACC
13	X_1	1.13	-	activity	NIH, ACC
14	X_1	1.21	1.20	activity	NIH, ACC
	G_1	0.65	0.87	activity	NIH
	L	4.28	4.00	radiochemistry	TL
	L_1	4.06	3.75	radiochemistry	ACC
	A	4.14	3.76	radiochemistry	NIH
15	G_1	0.77	-	activity	NIH
	A	4.28	-	radiochemistry	NIH
	L	4.14	-	radiochemistry	TL
	L_1	3.90	-	radiochemistry	ACC
16	X_1	0.90	-	activity, decay	NIH, TL
	G_1	0.86	-	activity, decay	NIH
	L	4.11	-	radiochemistry	TL
	L_1	4.29	-	radiochemistry	ACC
17	X_1	1.25	-	activity	NIH, ACC
18	X_1	1.32	-	activity	NIH, ACC
19	X	3.30	-	activity	NIH
	G	3.30	-	activity, decay	NIH
20	X	2.86	2.86	activity, decay	NIH, ACC
	G	3.12	3.16	activity	NIH
21	G	3.30	-	activity	NIH
22	X	3.45	-	activity, decay	NIH, TL

PROJECT 2.5a-1

TABLE 2.1 (cont'd)

Filter Sampler Data

Station Number	Location and Type Paper	Flow Rate (cu.ft/min) Before Surface Shot	Flow Rate (cu.ft/min) After Surface Shot	Purpose of Sample	Agency Performing Analysis
23	X	3.16	3.16	activity	NIH,TL
24	X	2.73	-	activity	NIH,TL
25	X	2.83	-	activity,decay autoradiograph	NIH,LASL,ACC
26	X	3.67	-	activity,autoradiograph	NIH,LASL
27	X	3.43	3.40	activity,decay	NIH,TL
28	X+		-	activity,autoradiograph	NIH,LASL
29	X	3.33	-	activity	NIH,TL
	M	3.09	-	activity,particle size	TL
30	X	2.26	-	activity,autoradiograph	NIH,LASL,ACC
	M	3.90	-	activity,particle size	TL
31	X	2.63	-	activity	NIH,TL
	M	3.57	-	activity,particle size	TL
32	X	3.53	-	activity,decay	
	M	4.29	-	activity,particle size	NIH,decay
33	X	3.20	-	activity,autoradiograph	NIH,LASL
34	X	3.00	-	activity,decay autoradiograph	NIH,LASL,ACC
35	X	3.12	-	activity,autoradiograph	NIH,LASL
36	X	3.51	-	activity,autoradiograph	NIH,LASL
37	X	3.53	-	activity,autoradiograph	NIH,LASL
38	X	2.52	-	activity,autoradiograph	NIH,LASL
39	X	3.12	-	activity,autoradiograph	NIH,LASL
40	X	2.46	-	activity,autoradiograph	NIH,LASL
41	X	3.0	-	activity,autoradiograph	NIH,LASL
42	X	2.65	-	activity,autoradiograph	NIH,LASL
43	X	2.38	-	activity,autoradiograph	NIH,LASL
44	X	2.46	-	activity,autoradiograph	NIH,LASL,ACC
45	X	3.37	-	activity,autoradiograph	NIH,LASL
46	X	3.00	-	activity,autoradiograph	NIH,LASL

+plus molecular filter adapter.

G — Same as X in all respects except that the filter sampler was located 2 feet above ground.

L, L_1, A — Consisted of 4 sheets of Chemical Corps No. 5 paper. This is an "open" paper and the purpose is to obtain a large sample for radiochemical analysis. The various letters designate the receiving agencies.

M — Consisted of 4 sheets of polyfiber paper (Air Force) paper. This is an "open" paper and the purpose is to obtain a large sample for radiochemical analysis.

Equipment at stations of the surface shot (1 through 46) was transferred to the corresponding stations of the underground shot (101 through 146). The handling of samples and analytical work for samples collected from the underground shot tests was the same as the surface shot, except that time did not permit the preparation of autoradiographs by the Los Alamos Scientific Laboratory.

The abbreviations of the receiving agencies are as follows:

ACC - Army Chemical Center
NIH - National Institute of Health
TL - Tracerlab, Inc., Boston, Massachusetts
LASL - Los Alamos Scientific Laboratory

2.2 THE CASCADE IMPACTOR

To determine the size-distribution of any heterogeneous cloud, a size-grading sampling method is desirable. It is also desirable to subject the particles to a minimum amount of physical strain as they are collected. The cascade impactor, first developed and described in detail by May[1], is particularly suited to these requirements. It size-grades particles in a manner suitable for analysis with light and/or electron microscopes and also collects the larger particles present (these being the most likely to shatter) at low velocities. The predominate disadvantage of the impactor is that it is not an absolute instrument, i.e., below a certain size, depending on the geometry of the last jet and the physical properties of the particle involved, the probability of collection decreases in a rather complex manner (but presumably monotonic with respect to particle size).

[1] K. R. May, "The Cascade Impactor: An Instrument for Sampling Coarse Aerosols", Journal of Scientific Instruments, 22 (Oct 1945) 187

PROJECT 2.5a-1

The performance of a jet in a cascade impactor is determined by the effects of the previous stages and the flow rate through it, as well as its own physical characteristics; thus the instrument must be designed as a unit, each stage being compatible with both the preceding and the following ones. Since the impactor is to sample efficiently an extended particle size range (0.2-100 microns), five stages were considered necessary for suitable size-grading. The effectiveness of each stage, and therefore of the complete instrument will vary with flow rate. Thus it is necessary to maintain a suitable and constant flow rate.

Although narrower jets will impinge smaller particles efficiently, one might readily assume that the narrowest possible jet should be used for the fifth stage; however, supersonic flow cannot be obtained in a jet of this type. Thus, the flow rate cannot exceed a maximum value, which occurs when sonic velocity is reached in the smallest jet. In actual practice, this feature was used to control the flow rate in the cascade impactor. If a narrower jet had been used, the flow rate would have been reduced correspondingly, thereby reducing the sampling volume.

2.2.1 Design

A theory of impaction is necessarily based on the trajectories of small particles in a moving fluid and extensive studies of the factors effecting particle trajectories have been made by many investigators[2,3,4]. An approximate theory of impaction, by Baurmash[5] et al, is quite flexible, allowing immediate comparison of the efficiencies of various jet widths and velocities. This relation may be derived by considering a jet from which a fluid of density ρ, viscosity

[2] May, Ibid

[3] Johnstone and Roberts, "Deposition of Aerosol Particles from Moving Gas Streams", Industrial and Engineering Chemistry, 32 (1940) 650

[4] Lapple and Shepard, "Calculation of Particle Trajectories", Industrial and Engineering Chemistry, 32

[5] Baurmash, "Development of Continuous Jet Impactor Methods", UCLA 13, AECU-206.

η , slit velocity V, is flowing in an approximately circular path of mean radius of curvature R, as shown in Fig. 2.2. It takes any particle roughly a time equal to

$$t = \frac{\pi R}{2V} \qquad (2.1$$

to traverse the quarter-circle arc. In this time it will have drifted radially outward a distance x equal to

$$x = ut \qquad (2.2)$$

where u is the Stokes velocity

$$u = \frac{D^2 \rho a}{18 \eta} \qquad (2.3)$$

D is the particle diameter and a is the radial acceleration and equal to V^2/R.

If it is assumed that the criterion for impaction is that the radial drift distance x is equal to half the jet width d, then it is possible to calculate the minimum particle diameter D_{min}, which will be impacted. Substituting and solving for D results in

$$D_{min} = 1 \frac{36 \eta d}{\pi \rho V} \qquad (2.4)$$

To check the validity of this formula, the experimental values obtained by May, Johnstone[6], and Casella[7] were compared with

[6] Memo Report, University of Ill., High Velocity Impactor for Sampling Aerosols, 15 March 1949.

[7] C. F. Casella & Co. Ltd., Cascade Impactor, Leaflet 72J, Regent House, Fitzroy Sq. London W. I.

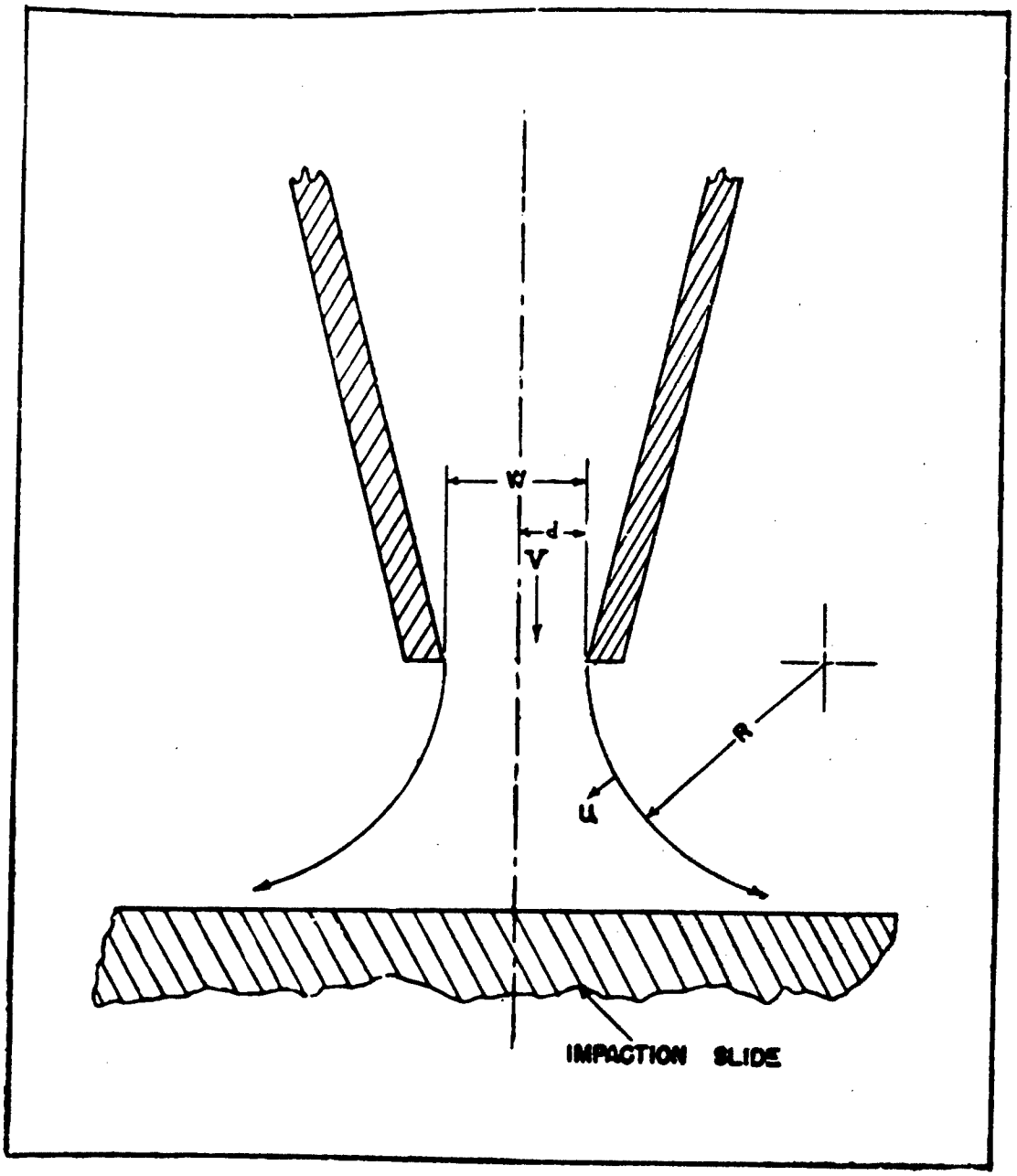

Fig. 2.2 Schematic Drawing of the Idealized Flow From a Cascade Impactor Slit. The slit length (into the paper) is assumed to be much greater than the width w.

those predicted by theory. The results were in excellent agreement.

The impactor described by Voegltin and Hodge[8] was found to be the most sturdy impactor available and since it was designed so that the jets could readily be interchanged it was decided to modify the Hodges model to fit requirements for sampling at Operation JANGLE. After some consideration it was decided to use the 1st, 2nd, and 4th jets of the original Hodge impactor for the first, second, and third jets of the new model and then to design two new jets. The development and performance of this modified Hodges-type impactor as well as refinements to eq. 2.4 have been previously described in detail[9].

A further important modification in this instrument was the inclusion of slides with electron microscope specimen screens set in recesses[10]. As a result, a slide assembly well suited for field use was developed.

2.2.2 Calibration

Critical flow rates of the cascade impactors used are shown in Table 2.2. The critical flow rates were determined using a previously calibrated Dry Test Meter and a vacuum gauge. To be reasonably certain that critical flow was attained, a vacuum of 18.0 inches of mercury was required for critical flow.

Table 2.3 gives the calculated sizes of particles efficiently removed for the modified instrument. Calibration of cascade impactors for actual efficiency for various particle sizes was not necessary for this work due to the heterogeneous density of aerosols expected. The samples were analyzed by direct methods, i.e., measuring and counting of each particle in a known representative area.

---

[8] Voegtlin & Hodge, Pharmacology and Toxicology of Uranium Compounds, Vol. FI-1, p. 483, McGraw-Hill, 1949.

[9] J. D. Wilcox, Design and Development of a New Five Stage Impactor, CRLIR 92, ACC, Md.

[10] J. D. Wilcox, A New Sampling Technique, CRLIR 70, ACC, Md.

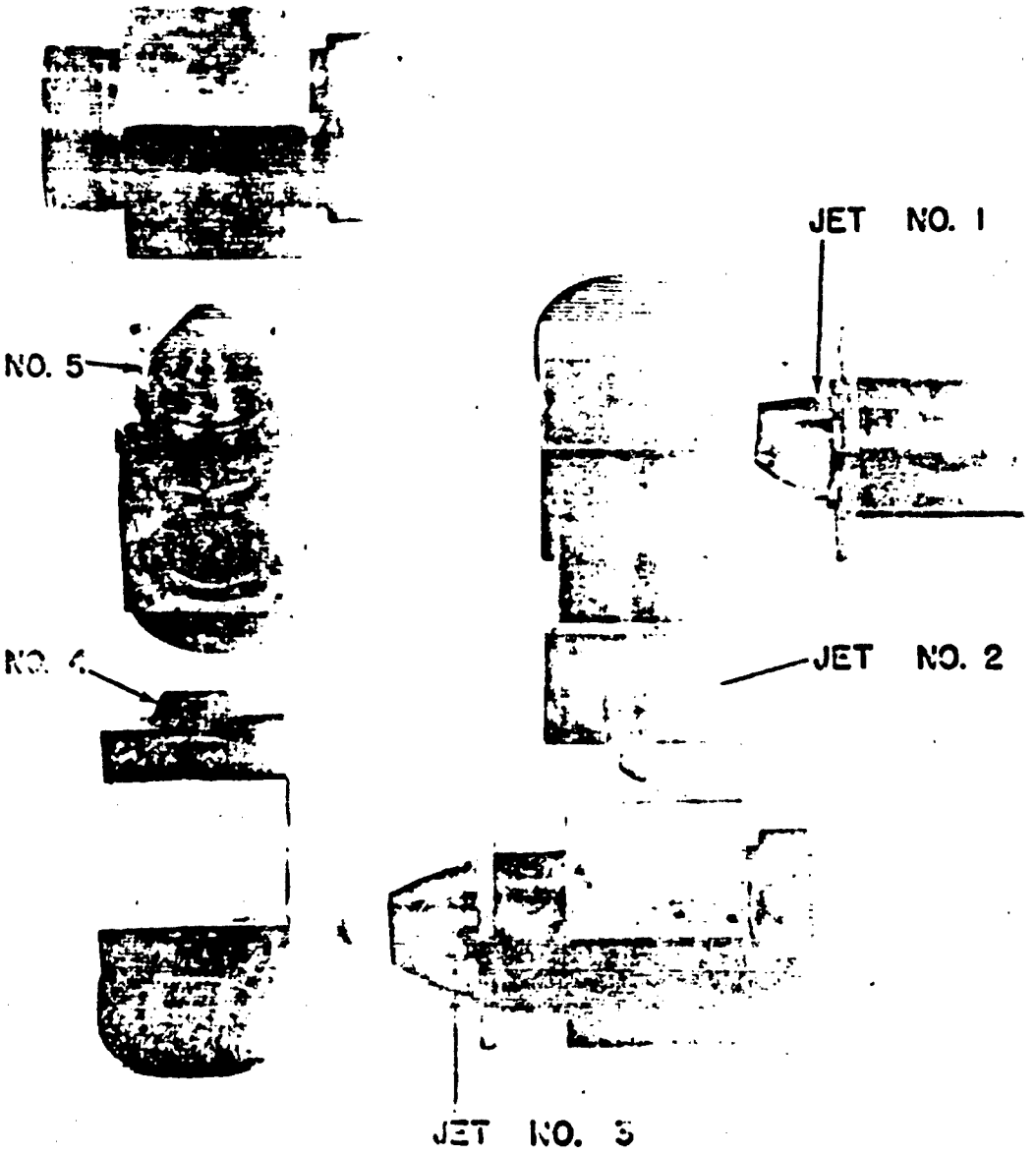

Fig. 2.3 The Jets of the Cascade Impactor in Exploded Arrangement.

TABLE 2.2

Cascade Impactor Critical Flow Rates

Impactor Identification	Flow Rate (liters per min.	Vacuum Between & Pump (inches of Mercury)	Impactor Identification	Flow Rate (liters per min.	Vacuum Between & Pump (inches of Mercury)
A	13.4	18.0	I	12.2	19.0
B	12.1	20.0	J	12.6	19.5
C	13.0	19.0	K	13.6	18.5
D	13.4	18.5	L	12.5	19.5
E	12.9	19.0	M	12.6	19.5
F	12.5	19.5	N	13.1	18.5
G	13.4	18.0	O	12.1	19.5
H	12.6	19.0	PT	12.2	20.0

TABLE 2.3

Cascade Impactor Jet Data[a]

Jet No.	Jet Length	Jet Width	Velocity at Orifice	Minimum Particle Diameter Impacted (D_{min}) microns			
				$\rho = 1$	$\rho = 2$	$\rho = 4$	$\rho = 7.5$
1	13.90mm	5.30 mm	2.83×10^{2} cm/sec	18.0	11.0	7.4	6.2
2	14.35mm	1.38 mm	1.05×10^{3} cm/sec	4.2	2.84	1.98	1.56
3	13.85mm	0.575mm	2.62×10^{3} cm/sec	1.77	1.17	0.84	0.63
4	9.15mm	0.395mm	5.76×10^{3} cm/sec	0.95	0.65	0.47	0.347
5	4.05mm	0.290mm	1.77×10^{4} cm/sec	0.47	0.32	0.224	0.168

[a]Flow rate of 12.6 l/min

2.3 CONIFUGE

The purpose of the conifuge was to provide a size-graded sample of the particulates in the aerosol.

2.3.1 Design

The conifuge consists of a conical head centrifuge formed by an inner and outer cone, arranged co-axially and separated by a narrow annular space through which a steady stream of aerosol is drawn by the self-pumping action of the cones, which are driven by a motor at high rpm. The cloud sample is introduced as a thin film into the annular space through a small tube at the apex of the inner cone. Since the particles are influenced by the transverse velocity of the air stream and the centrifugal velocity of the rotating cones, they follow a trajectory based upon their mass and terminal velocity. The particles pass between the two cones and deposit as a spectrum of particle sizes on the surface of the outer cone which is made of polystyrene plastic with two rows of six evenly spaced screws which carry electron microscope screens.

The thin filament of sampled cloud passing across the gap between the end of the sampling tube and the apex of the inner cone is in unstable equilibrium and is easily displaced by an inequality in the spacing of the two cones. The result is an uneven distribution of the samples on the outer cone. Precise workmanship is therefore essential in the construction of the centrifugal chamber and in the alignment of the whole apparatus. The design must also be robust enough for this adjustment to be retained after dismantling for cleaning and reassembly. Good seals must be obtained around the base of the two cones and around the base of the container. Poor seals give rise to leakage which alter flow rates and destroy regularity of the size separation. For a similar reason, the housing packing must be kept well oiled to prevent leakage through the bearings. To maintain the designed sampling rate, both the sampling inlet and exhaust jet must be subjected to the same external pressure. Figures 2.4 and 2.5 show photographs of the conifuge employed at Operation JANGLE.

The disadvantages of the present instrument are (1) low flow rate and vertical orientation which precludes approximating isokinetic conditions and (2) separation is dependent upon the density of particulates which is likely to be heterogeneous in the aerosol. According to Sawyer[11], "The depositing efficiency of the conifuge is 100

[11] K. F. Sawyer, Porton Technical Paper, No. 86, (Porton, U. K., 14 Dec. 1948)

Fig. 2.5 Assembled Centrifuge Showing Outer Cover in Place

Fig. 2.4 Centrifuge with Outer Cover Removed Showing Plastic Collecting Cone

per cent under all conditions for all particles which do not encounter the walls of the sampling tube on entry or impact upon the inner cone. Re-circulated particles would, if present, show no size separation and form a heterogeneous background to the main deposit".

2.3.2 Calibration

Recent laboratory testing of the conifuge has shown that the rate of sample flow is greater than was first assumed. Flow calibration data was obtained by filling a bottle full of ammonium chloride smoke and drawing the smoke through a 1.17 cm inside diameter glass tubing by the self-pumping action of the conifuge. The point of the smoke was then timed as it flowed through 50 and 100 cm lengths of the glass tubing and into the conifuge inlet tubing. The flow rates shown in Table 2.4 were obtained by the use of a "pipe coefficient" of 0.5 as suggested by Vennard[12] for laminar flow (Re = 380).

TABLE 2.4

Conifuge Flow Calibration

RPM	Corrected Flow Rate (cc/min)
8000	315
7000	265
6000	218
5000	173
4000	130
3000	90

Operating the conifuge at 8000 rpm gives a sampling rate of 173 cc/min with about 3460 cc/min of excess air recycled. The low sampling rate is a serious limitation. For good size separation, the sampling rate must not exceed about five per cent of the total flow rate (total volume circulating between the cones). The design of the Chemical Corps conifuge limited the speed to 8000 rpm when operating at extended periods of time (2-3 hours). For shorter operating times (20-30 min.) the conifuge can be operated at 10,000 rpm. A calibration curve of rpm vs voltage was used to obtain required speeds in the field.

[12] J. K. Vennard, Elementary Fluid Mechanics, (2nd ed) New York: Wiley and Sons, 1947. 7, p. 163.

PROJECT 2.5a-1

Test runs were made on the conifuge using a steel outer cone which had two slits covered by plastic slides along the slant height of the cone. An aerosol containing spherical glass particles was generated into a sampling chamber. Samples were taken with the conifuge, and the particle size distribution was determined with a microscope. Table 2.5 gives data obtained at a speed of 5000 rpm, a sampling time of 6 minutes, and an air flow of approximately 170 cc/min.

TABLE 2.5

Conifuge Particle Size Calibration

Distance From Top Edge	Particle Size (microns)
16 mm	12 -6
20	6 -4
24	4 -2.5
28	2.5-1.8
32	1.8-1.1
36	1.4-0.6
40	0.6-0.4
44	under .4

2.4 PARTICLE SEPARATOR

The purpose of the particle separator was to sample and fractionate the aerosol and fall-out particulate material into size ranges by means of a vertically oriented sifting device.

2.4.1 Design

Each particle separator consisted of:

1. Eleven bronze wire screen sieves which were to fractionate particles into class intervals of 37-43, 44-52, 53-61, 62-73, 74-88, 88-104, 105-124, 125-148, 149-176, 177-209 microns.

2. A porous stainless steel filter to retain particles larger than 1 micron.

3. A molecular filter to separate all the particles which pass through the porous stainless steel disk.

PROJECT 2.5a-1

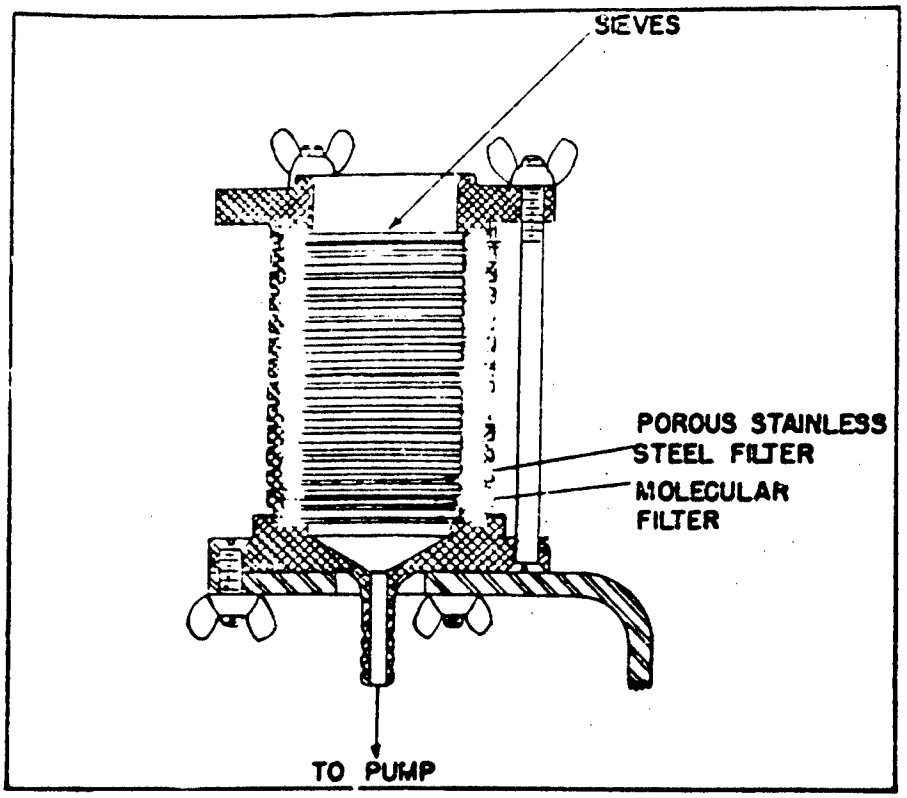

Fig. 2.6 Cross-sectional Drawing of a Particle Separator

TABLE 2.6

Particle Separator Calibration

Station Number	Flow Rate (cu.ft/min)		
	Before Surface Shot	After Surface Shot	After Underground Shot
8	0.89	0.87	0.98
9	0.62	-	0.45
11	0.83	0.90	0.79
15	0.82	-	0.81
20	0.88	0.83	0.92
21	0.89	-	0.85
23	0.89	0.85	1.00
24	0.93	-	0.94
28	0.95	-	0.94
29	0.98	-	1.02
30	0.82	-	0.90

4. A rotary type vacuum pump and hose connection to the particle separator to draw the particles through the apparatus. Air was drawn through the pump at the rate of approximately 1 cubic foot per minute.

The detailed design of the particle soparator [illegible] in Fig. 2.6.

2.4.2 Calibration

Table 2.6 indicates the flow rate through the various filter samplers before and after each test. The results show that no appreciable change in resistance occurred in the particle separators during the test and the rate of flow through the particle separator was constant.

2.5 ELECTROSTATIC PRECIPITATOR

The purpose of the electrostatic precipitator was to sample the particulates. This instrument is not amenable to particle size determination unless microscope slides or screens are incorporated into the sampling cylinder.

2.5.1 Design

This instrument weighs about 50 pounds and consists of a metal cylinder through which air is drawn at the rate of 32 liters per minute at a speed of 25 cm/sec. An electrostatic potential of 300 volts was applied between an outside collecting cylinder and an inside central wire. The particulate matter is precipitated upon the outside cylindrical shell. A schematic diagram of the collecting cylinder is shown in Fig. 2.7.

2.6 CONTINUOUS AIR MONITORS

The purpose of the continuous air monitors was to measure the variation in the concentration of activity in the air with time.

2.6.1 Brookhaven Air Monitor

A filter paper feed system traveling at 4 inches per hour combined with a vacuum pump (3.5 cu ft/min) was employed to collect particulates from the air. A strip of filter paper 3 inches wide moves continuously at a predetermined rate over a rectangular sampling port. (1 in. x 1-3/4 in.) The particulate material in the aerosol was filtered onto the paper which passes under a shielded scintillation counter where

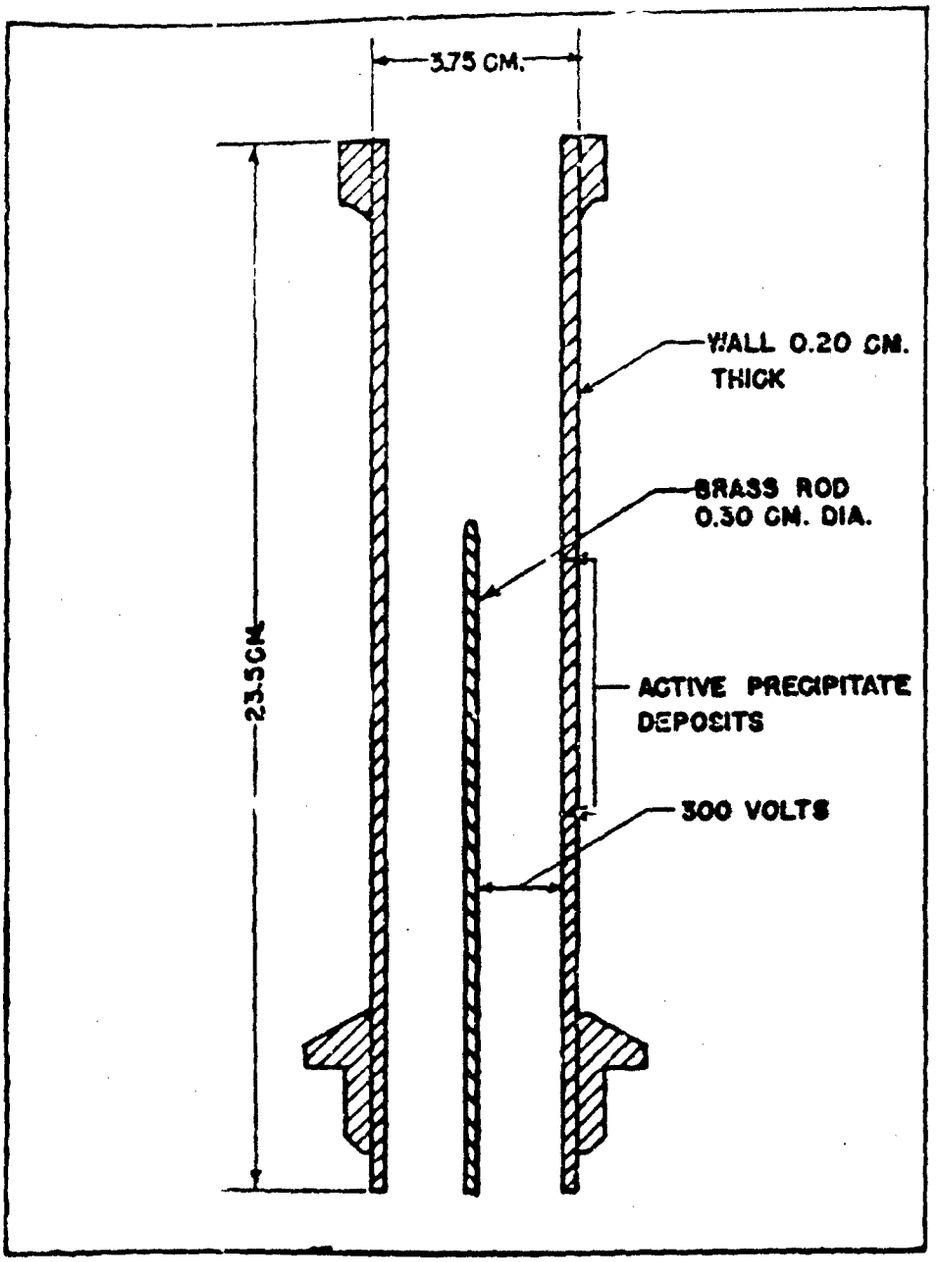

Fig. 2.7 Cross-sectional Drawing of the Electrostatic Precipitator Cylinder.

the activity was measured and a record made on an Esterline-Angus recorder. See Fig. 2.8.

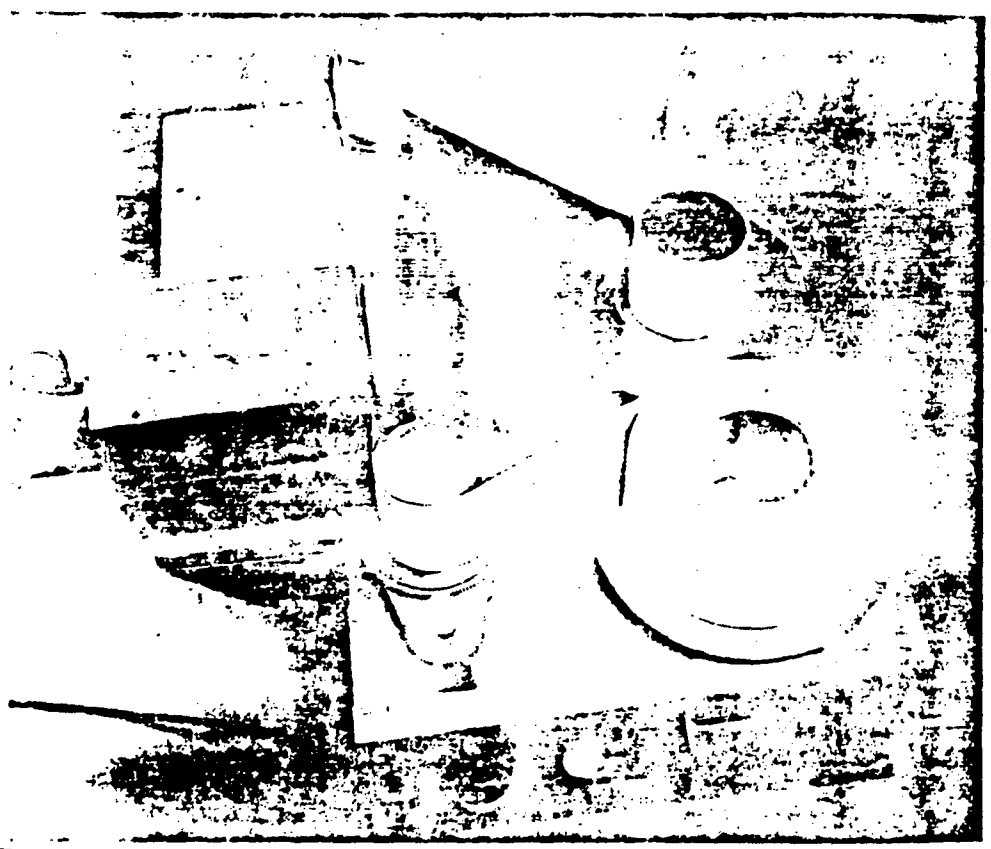

Fig. 2.8 Brookhaven Continuous Air Monitor.
Count Rate Meters Omitted.

The rate-meter and recorder were housed in a shack while the air sampler and scintillation counter were situated in a four foot shelf outside. A plastic cover protected the sampler from fall-out, except at the sampling port. The purpose of this procedure was to sample the cloud and protect the air sampler as much as possible. Cellophane sheet was fed from a roll onto the re-wind spool of the air sampler between successive layers of filter paper to eliminate cross contamination so that the filter paper could be recounted in the event of rate-meter or recorder failure. Rubber foam mats were placed under the electronic equipment to reduce vibration. Electric power (110 volts, 60 cycle) was supplied by a generator driven by a 2-cylinder gasoline engine.

The important feature of this instrument is that the sample is continuously collected on an area 1 in. x 1-3/4 in., the activity measurement is made over a contaminated strip 1 inch in width, and the radiation detector tube off-set approximately 5 inches from the center of the sampling ports, which results in a 30 minute delay between sampling and significant counting. The total time required for a one square inch (the size of the counter face) of filter paper to travel the sampling port is 41.25 minutes. Therefore an estimate of the activity in a cloud is based upon this period of sampling which ends approximately 52.5 minutes prior to counting and recording. A detailed discussion of the calibration of this instrument is given in the Appendix.

2.6.2 Tracerlab Air Monitor

This instrument also employs an air pumping system (2.6 cu.ft/min) with filter paper 6 inches wide traveling at 7 inches per hour or multiples of 1/4, 1/2, 2, and 4 times this rate. Wax paper was fed between successive layers of filter paper to prevent cross contamination. A Tracerlab P-12 alpha scintillation probe and a lead shielded Tracerlab TGC-1 Geiger-Muller tube were employed to detect alpha, beta and gamma radiations. The output voltage from two linear count-rate meters was recorded on a two point chart recorder manufactured by the Brown Instrument Company. The entire unit was housed in a metal cabinet and located in a shack with two air intake pipes, 12 feet long, extending from the instrument through the roof of the shack into the atmosphere. See Figs. 2.9 and 2.10.

The important feature of this monitor was that the radiation detectors were located directly over the sampling ports (2.25 in. diameter) and the activity was measured over this circular area. Inasmuch as deposition of the aerosol and counting occurs simultaneously, no time lag occurs. However, it may be noted that the counter reading at the time of deposition is not the same as when the tape is replayed through the instrument at a later time, despite correction for radioactive decay. A detailed discussion of this and other problems of instrument calibration may be found in Appendix C.

2.7 RADIOLOGICAL AIR SAMPLER

The Radiological Air Sampler (RAS) was a modification, for Operation JANGLE of the Portable Air Sampler (PAS) used previously by Test Division, CRL and Dugway Proving Ground, Utah. Its purpose was to provide an intermittent type of sampler capable of collecting a radioactive

Fig. 2.9 Top View of the Tracerlab Air Monitor Showing the Counters and Filter Tape Transport System.

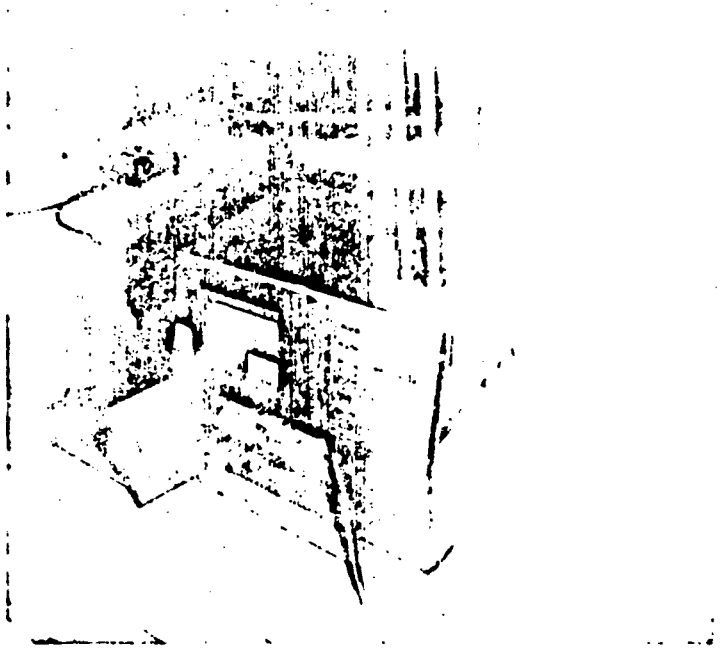

Fig. 2.10 Tracerlab Continuous Air Monitors as Installed, Showing the Two Air Intake Pipes.

aerosol as a function of time. As the sampler contains its own 6 volt DC power supply, the necessity of laying long power lines is avoided, thus simplifying its installation in the field.

2.7.1 Design

The general layout of the components of the RAS are best seen in Fig. 2.11. This instrument was surmounted by twelve plastic "molecular" filter[13] assemblies through which air was pumped successively for ten minutes by means of a rotary solenoid air valve controlled by a cycling mechanism. The sampler was started five minutes prior to shot time by a signal which closed a 24 volt DC latching relay. Each filter in turn sampled the air for ten minutes and then the instrument automatically turned itself off. The complete design details of the RAS have been given previously[14].

2.7.2 Calibration

Calibrations of the instruments at the test site were made by using a molecular filter assembly in the line of flow. The flow calibration data was obtained using a Dry Test Meter and is shown in Table 2.7.

TABLE 2.7

Radiological Air Sampler Flow Calibration

RAS Code	Flow Rate Liters/Minute
A	0.380
B	0.385
C	0.445
D	0.445
E	0.440
F	0.440
H	0.445
I	0.460
K	0.440

[13] Alexander Goetz, "Molecular Filters", Report of Symposium III, Aerosols, Chemical Corps Technical Command, Army Chemical Center, Md. 4 April 1950.

[14] J. D. Wilcox, W. R. Van Antwerp, C. S. Elder. A Radiological Air Sampler - A Modification of a Portable Air Sampler. CRL Interim Rpt. IOS ACC, Md. 12 Apr 52.

Fig. 2.11 Radiological Air Sampler, Showing Filter Heads, Rotary Air Valve, Pump, Timing Mechanism, and Battery.

2.8 FALL-OUT TRAYS

The purpose of the fall-out trays was to collect samples of the fall-out for particle size distribution, activity measurements and radiochemical analysis.

2.8.1 Design

Wooden trays 23x36x2 in. with an effective exposure area of 21x34 in. were lined with thin sheets of polyethylene plastic approximately 0.001 in. thick. The trays were located on top of 7 feet high towers and 8 feet high shacks and covered until approximately 12 hours

before the test when all covers were removed. Several trays were located on the ground wherever shacks were not available or the NRDL thermal precipitator occupied the top of the tower. After the test the trays were covered, returned by truck to the rear area, and several hot particles removed for microscopic analysis at the test site by personnel of the Army Medical Center[15]. The remainder of the sample was bagged, crated, and returned by air to the ACC for particle size analysis and radiochemistry.

A possible disadvantage of the fall-out tray was the uncertainty of the amount of material blown out of or into the tray. Three trays were exposed to atmospheric conditions in the test area for several days and the amount of dust accumulated was too small to be weighed on a torsion balance. On this basis it was reasonable to assume that under normal conditions at the test site, insignificant amounts of material were blown into the trays. Figure 2.12 shows a fall-out tray in position at a typical station.

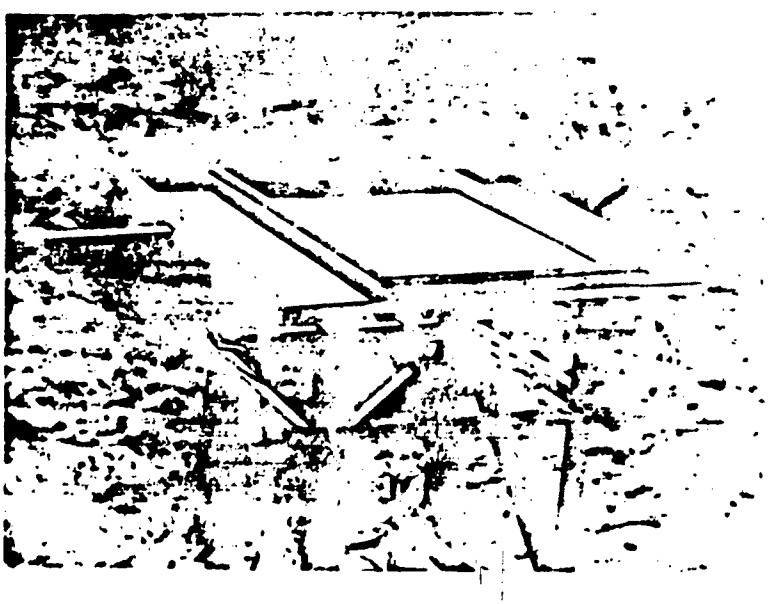

Fig. 2.12 Fall-out Tray Installed at a Typical Station. A filter sampler and a particle separator can also be seen.

[15] Roy D. Maxwell, Radiochemical Studies of Large Particles, Project 2.5a, Operation JANGLE, Army Medical Graduate School, Washington, D.C.

CHAPTER 3

EXPERIMENTAL PROCEDURE

3.1 STATION LAYOUT

On the basis of pre-shot meteorological data accumulated at the test site, 46 sampling stations were located for each shot as shown in Fig. 3.1 and 3.2. The general layout for each shot was the same, however minor changes in position were made to take advantage of differences in ground elevation. Equipment was secured to steel towers which were bolted to concrete foundations (this considerable overdesign of equipment was the result of the change from Operation WINDSTORM to JANGLE) within 4000 feet and wooden foundations beyond 4000 feet of the zero point. Sampling was done at 7 feet and 2 feet above the ground. Figures 2.11 and 3.3 illustrate the appearance of typical stations of this project.

3.2 DISTRIBUTION OF SAMPLING EQUIPMENT

The following items of sampling equipment were used:

1. Filter sampler
2. Cascade impactor
3. Conifuge
4. Particle separator
5. Electrostatic precipitator
6. Continuous air monitor
7. Portable air sampler
8. Fall-out tray

PROJECT 2.5a-1

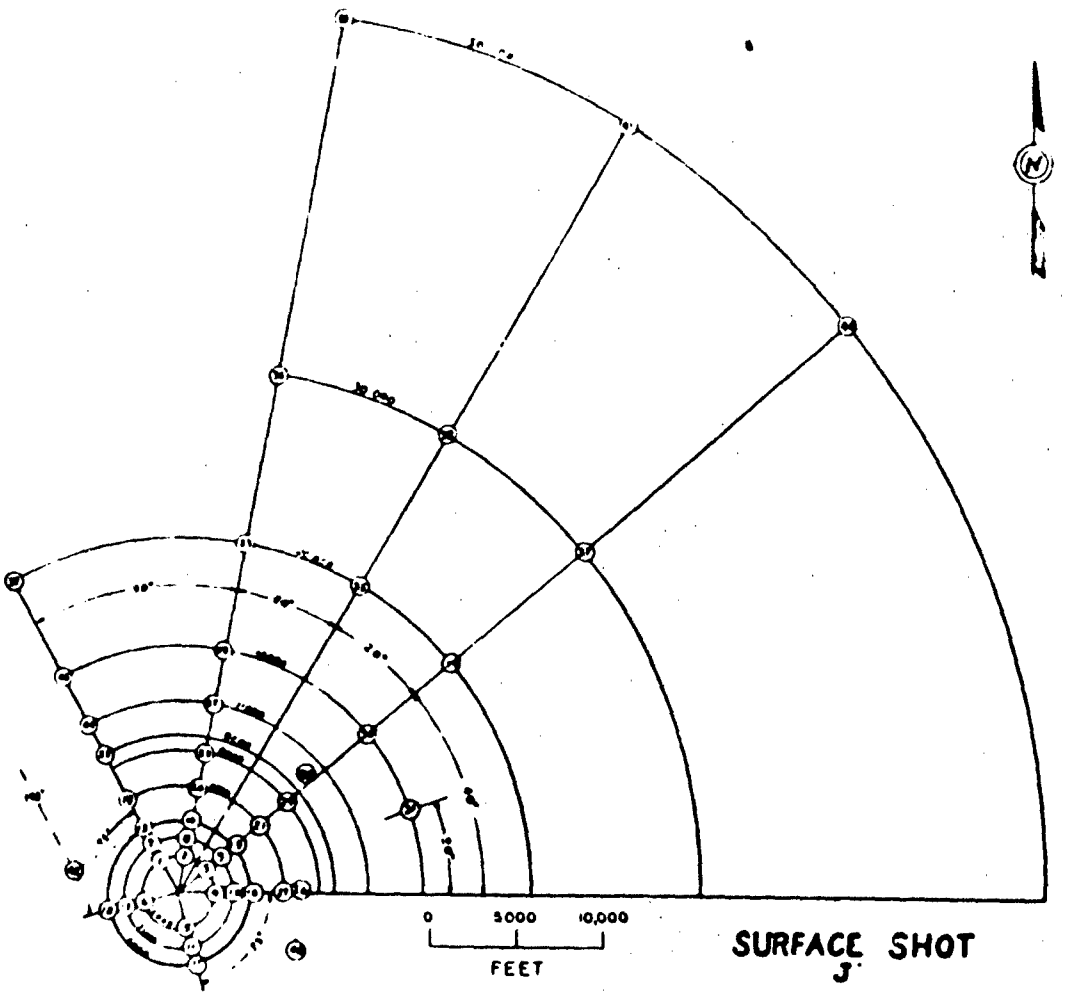

Fig. 3.1 Surface Shot Station Layout

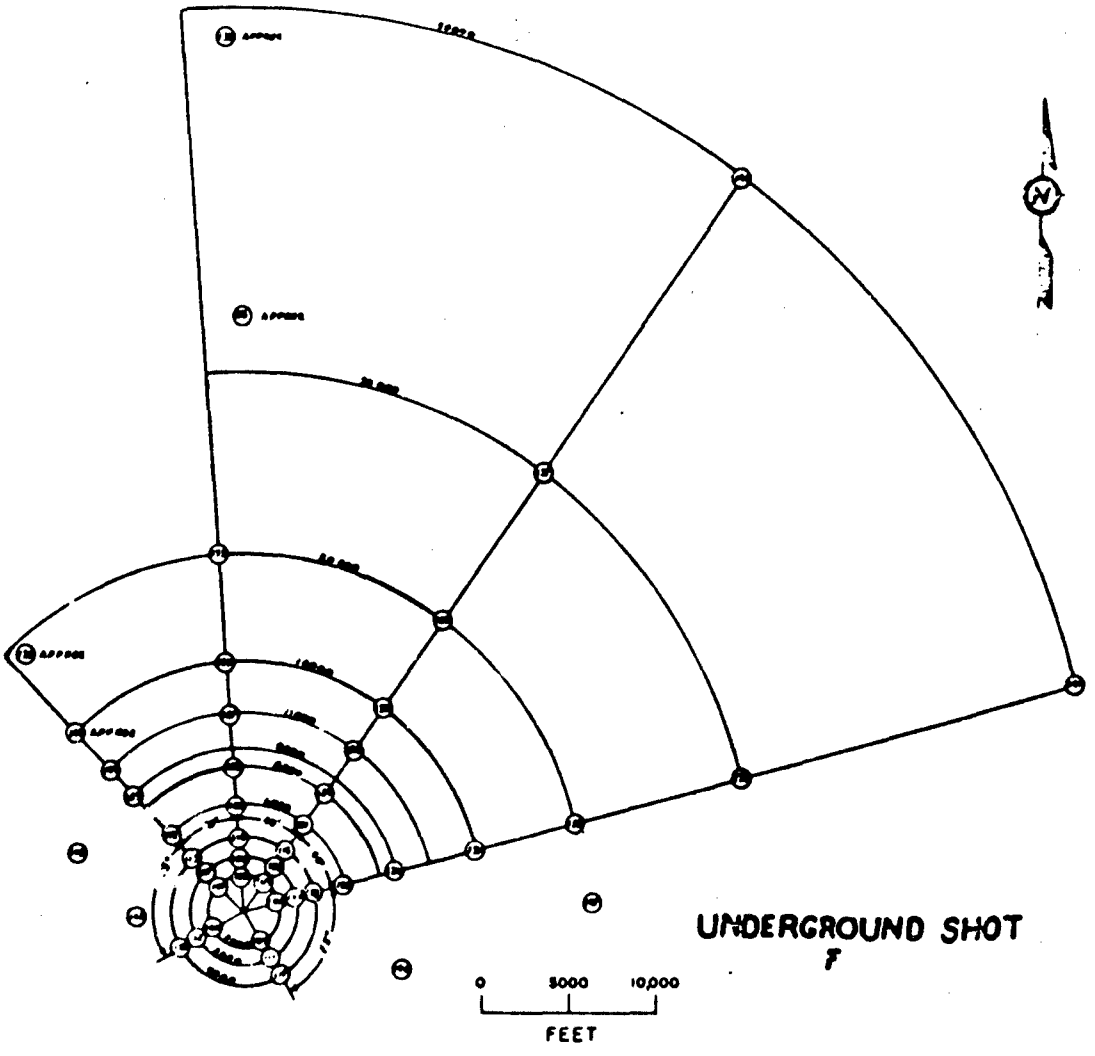

Fig. 2.2 Underground Shot Station Layout

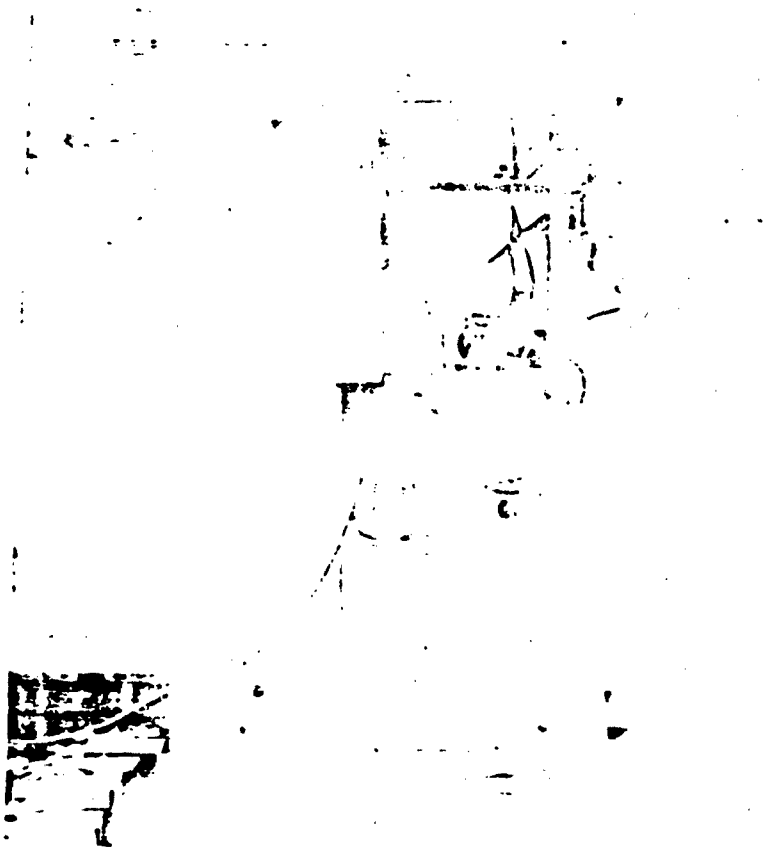

Fig. 3.3 Typical Sampling Station and Equipment. Ground Zero Can Be Seen.

TABLE 3.1

Location of Equipment

Instrument	Station Location
Filter Sampler	All stations; see Table 2.1
Cascade Impactor	13 14[a] 15 19 23 24 25 26 30 32 35[b] 40
Conifuge	13 14 15 19 22 23 24 25 26 30 32 35
Tracerlab Continuous Air Monitor	29 30 31 39 40 41
Brookhaven Continuous Air Monitor	36 37 38
Particle Separator	8 9 14 15 20 21 23 24 28 29 30
Electrostatic Precipitator	33 34 129 130
Portable Air Sampler	14 20 21 27 28 33 36 39 119[b] 120[b] 121[b] 122
Fall-out Tray	1 2 3 4 7 10 14 15 16 19 21 22 23 24 27 29 30 31 33 34 36 37

(a) 3 instruments located here

(b) 2 instruments located here

Table 3.1 shows the manner in which the equipment was distributed. This distribution was based on a prior study of the weather, and the number of samplers available.

3.2.1 A Typical Station

The following instruments represent a typical tower installation; filter sampler, cascade impactor, conifuge, and particle separator. One 24 volt battery rated for 35 ampere hours was placed at each station for each piece of equipment requiring a 24-volt motor. Each motor required 10 ampere hours. One hundred and ten volt AC generators, rated at 3 KW were used at stations which required continuous air monitors, electrostatic precipitators or AC motors.

3.2.2 Triggering

At shot time minus 5 minutes a relay was closed by a signal which activated the clock relay and turned on the power supply.

It is of interest to discuss briefly the clock which controlled the sampling period of the instruments. Figure 3.6 shows the 8 day clock mechanism employed. It is of a type which can be set to open or close a relay for any hour of a particular day. Since shot time could not be accurately forecast, the following modifications were made to allow flexibility in the time of firing. One end of a rigid wire was fastened to the closing latch of a relay and the other end was inserted in the balance wheel of the mechanical clock; the clock was then wound and set so that the micro switches were closed and the relay was open. When the relay was closed at shot time minus five minutes, the rigid wire attached to the closing latch was pulled away from the balance wheel and the clock was started.

At shot time plus one hour and fifty-five minutes the clock mechanism opened the micro switch and caused the relay to open, disconnected the power supply, and stopped the sampling apparatus. Figure 3.5 gives the details of these circuits.

The cascade impactor required a separate timing device because it was necessary to sample for 1 minute when the cloud had arrived at the station. See Fig. 3.6. A longer sampling period would have provided excessive sample which could not be analyzed microscopically for particle size distribution.

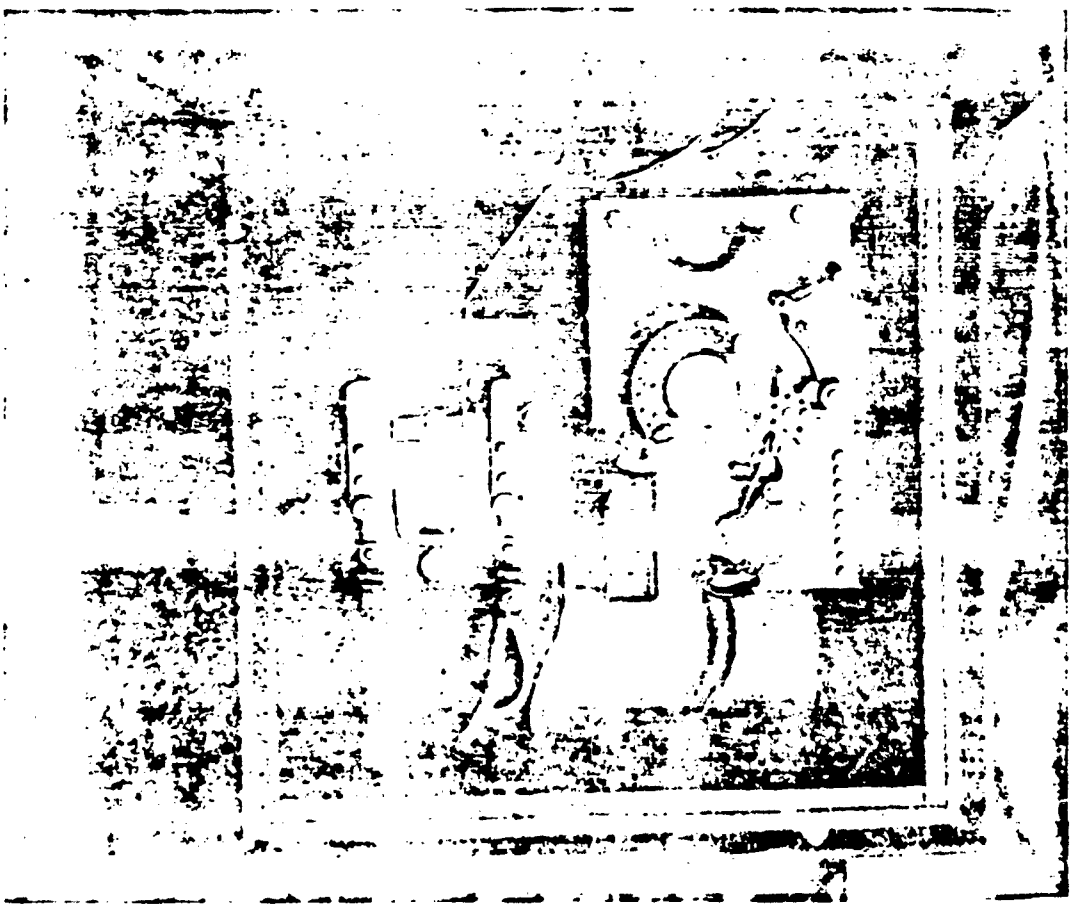

Fig. 3.4 Clock and Triggering Mechanism. The Rigid Wire Leads From the Relay to the Balance Wheel. When the Relay is Closed the Wire Was Withdrawn From the Balance Wheel, Starting the Timing of Equipment. The Outside Dimensions of the Box Are 10-1/2 by 10-1/2 Inches.

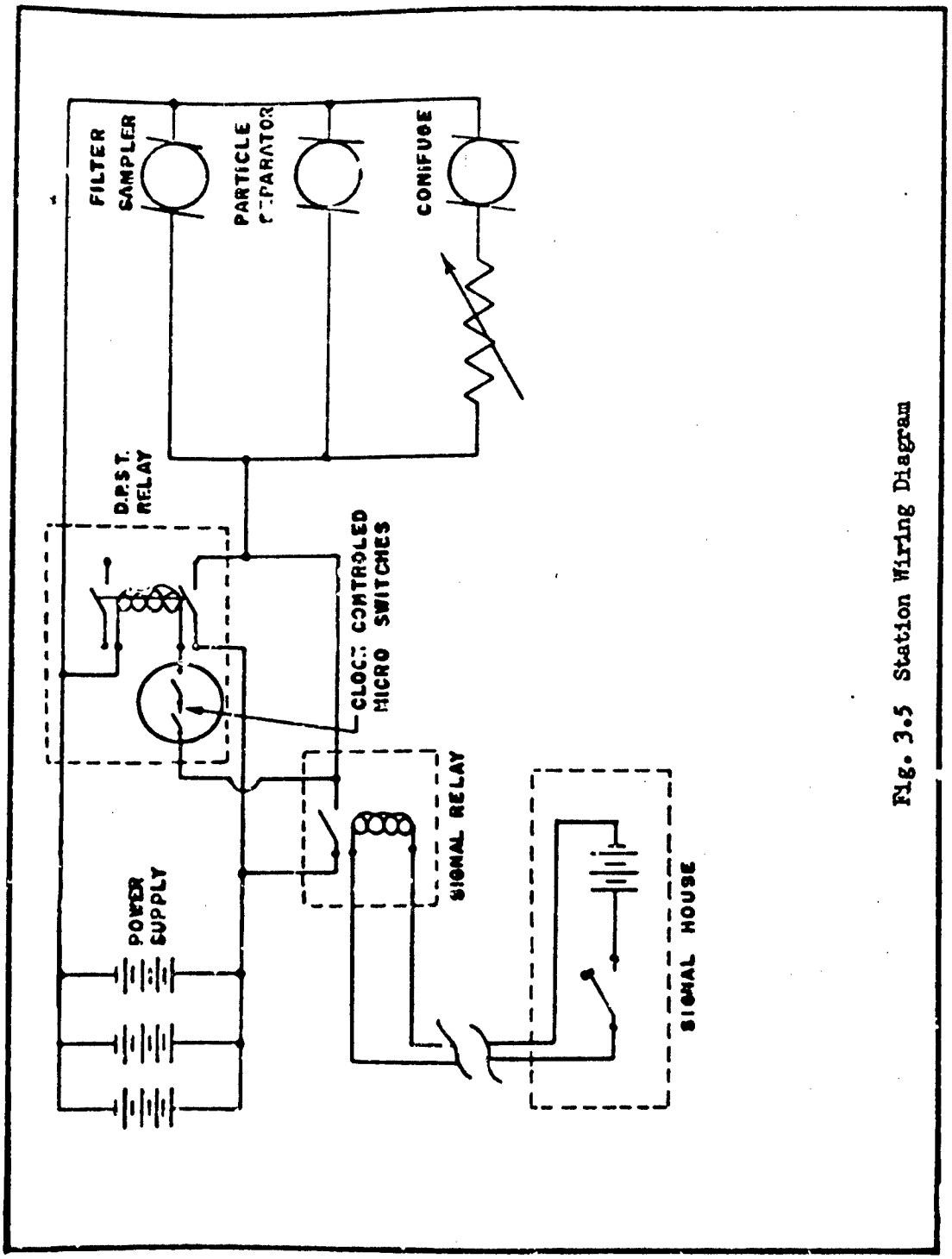

Fig. 3.5 Station Wiring Diagram

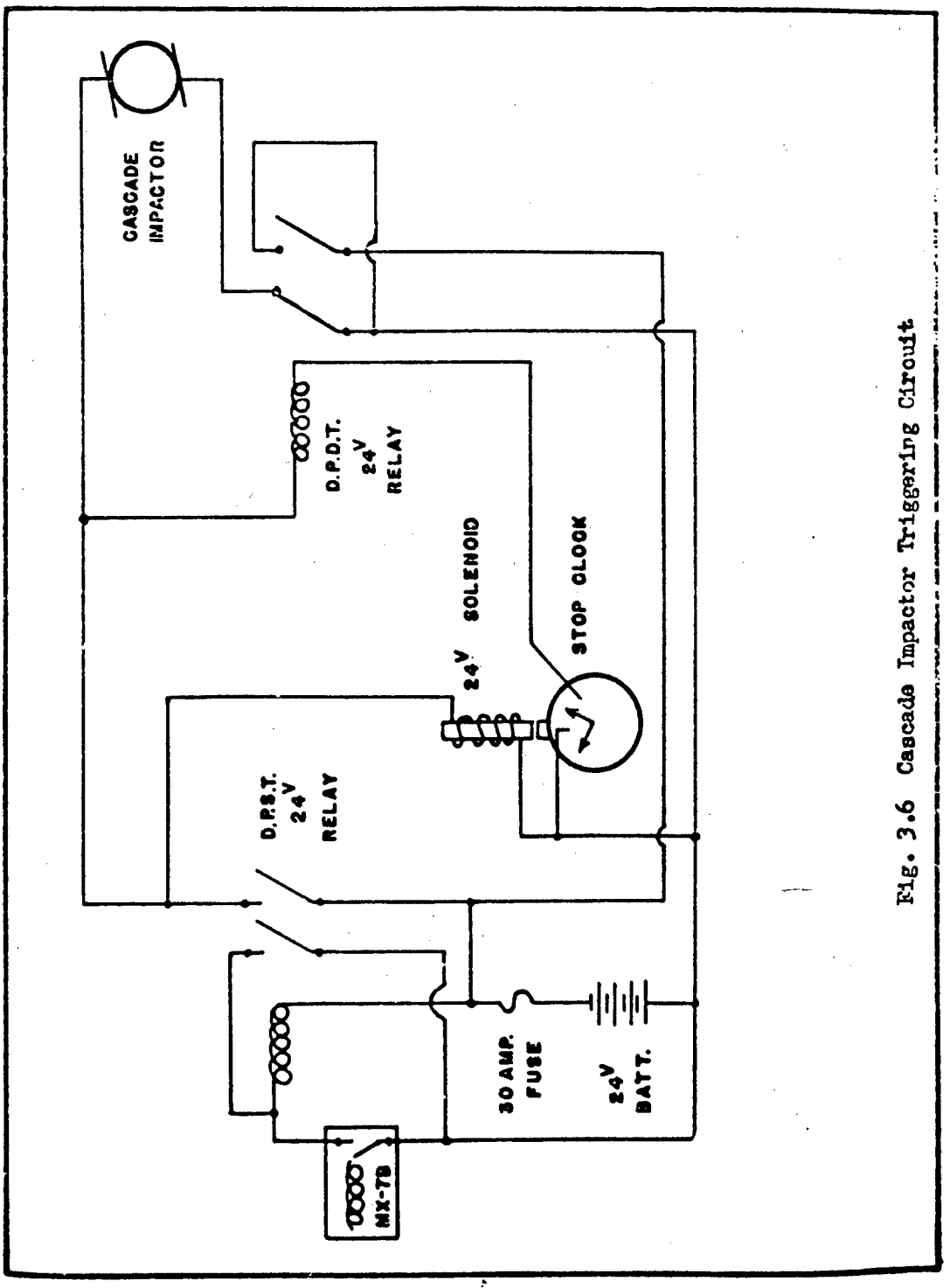

Fig. 3.6 Cascade Impactor Triggering Circuit

The triggering device was a Beckman MX-7B radiation detection alarm that was 50 per cent discharged and modified so that it would close a micro switch after being exposed to 50 milliroentgens. The alarm was placed on top of a tower and shielded in a well of lead brick, 8 inches thick and open at the top, thus it would presumably only be discharged by the radiation from the cloud.

After the cloud radiation discharged the MX-7B and closed the micro switch, the power relay was closed and supplied power from the 24 volt battery. The left pole of the relay upon closing shunted the MX-7B micro switch out of the circuit thus eliminating the possibility of its opening due to low current capacity and causing the circuit to function improperly. The right pole of the relay performed two functions upon closing; it connected one side of the battery to the cascade impactor motor and started the cascade impactor since the other side of the battery was connected to the motor through the left pole of the relay, and it also placed the clock solenoid coil across the battery. When this solenoid was placed across the battery it drove the plunger against the start button of the mechanical stop clock and started the clock. The sweep hand of the clock was arranged so that after one minute it came in contact with a terminal connected to one side of the battery and thus placed the coil of the relay across the battery through the sweep hand and threw the relay to the position opposite of that shown in Fig. 3.6. This action opened the cascade impactor circuit and at the same time shorted the terminals of the battery across the 30 ampere fuse; the fuse blew, and the battery was removed from the circuit eliminating the chance of the circuit recycling.

3.3 COLLECTION AND SHIPMENT OF SAMPLES

3.3.1 Surface Shot

Sample collections started after 4 hours and were completed within 30 hours after detonation. Rapid collection was possible due to the fact that all stations were lightly contaminated with the exception of those stations in the north-north east sector. Collections along these "legs" were deferred for approximately 20 hours to permit the area to "cool off". No pick-up team accumulated more than a 1 roentgen for the test; the maximum allowable dose for each test being 3 roentgens.

The collection of samples was accomplished by 8 groups; each consisting of a group leader, assistant, and a radiological safety

monitor; and each responsible for approximately 6 stations. Individuals wore protective clothing furnished by the radiological safety organization at the test site. This consisted of cotton-khaki coveralls, white skull cap, gloves, booties, respirator, and masking tape to seal the trouser-bootie opening. Personnel handled the sampling instruments with gloves. Filter sampler papers and portable air samplers were placed in wooden boxes and returned to the project office at the test site. The National Institute of Health (NIH) laboratory at the test site started activity measurements on filter sampler papers approximately 12 hours after shot time and completed measurements within approximately 48 hours.

Cascade impactors, conifuges, and particle separators were removed from the towers and the impactor slides and conifuge liners were removed in a dust-free room.

All samples were shipped in wooden boxes by military air to either the Army Chemical Center, Md. or Tracerlab, Inc., Boston, Mass., and analytical work was started approximately 5 days after shot time.

3.3.2 Underground Shot

Sample collections were started 6 hours after shot time and were completed 4 days later. Slow collection was necessitated by the fact that many stations were heavily contaminated. As in the surface shot, the heaviest contamination occurred in the north-north east sector, and entry into this area was delayed about 4 days.

The procedure of handling samples on this test was similar to the surface shot. Activity measurements were started 12 hours after detonation.

3.4 TREATMENT OF SAMPLES AT ACC

Shipments received at the Army Chemical Center were opened, disassembled, and distributed for analysis among the various groups in the Chemical and Radiological Laboratories according to a pre-arranged plan. Cascade impactor plates and conifuge cones were removed in a dust-free room and alalyzed for activity and particle size. Laboratory analysis started approximately 8 hours after the receipt of samples at the ACC.

CHAPTER 4

DATA AND RESULTS

4.1 CONCENTRATION OF ACTIVITY IN THE AEROSOL

4.1.1 Filter Sampler

Approximately 46 filter samplers were employed in each shot of Operation JANGLE to obtain samples of the aerosol from which activity concentration data could be derived. As described in paragraph 2.1, these instruments sampled for a period of from 5 minutes before to 115 minutes after shot time, and yielded basic data in the form of filter papers upon which was deposited a measurable amount of radioactivity.

The average concentration of activity at each station over the interval H/0 to H/115 minutes could be computed by dividing the measured activity (corrected for decay) by the volume of air sampled in 115 minutes. However, in order to obtain the concentration of activity in the cloud, it was necessary to know when and how long the instrument actually sampled the cloud, information not obtainable from the filter sampler itself. It was originally planned to determine these quantities by an examination of aerial photographs and the NBS gamma intensity data (Project 2.1a), but after careful study of records from both these sources the conclusion was reached that this determination would be possible for only five stations, all in the Underground shot. The difficulty arose in defining the "edge" of the complicated cloud structure either visually, or in terms of the gamma intensity. This was particularly true for times later than about 15 minutes after either shot, and for directions other than downwind. For example, from the photographs, it appeared that many crosswind stations never sampled the cloud, even though fair amounts of radioactivity were found on the filter papers from these stations.

To estimate the concentration of activity in the cloud, then, it was first necessary to estimate when and how long each filter sampler sampled the cloud proper. This has been done by assuming a reasonable model of the cloud, based upon the data obtained from aerial photographs, and calculating when this cloud arrived and departed from each station. The elapsed time and length of sampling time were then calculated and compared with the figures used to calculate the 115 minute concentrations, resulting in factors which could be applied to the latter to give the concentration in the cloud

proper. These factors were employed in order to emphasize the effect of these calculations. It should be noted that the cloud model, because of the restrictive assumptions regarding its size, was applied only to the downwind stations.

The following is a description of the cloud model:

At zero time a cloud of diameter d_0 is rapidly created. This cloud drifts downwind in a straight line, the velocity of the center of the cloud V being a constant 5 mph, or 440 feet per minute. The subsequent cloud diameter d increases with time, and hence with distance from ground zero r according to the equation:

$$d = d_0 + 0.1(r)$$

The arrival time of the front edge of the cloud at station whose distance from ground zero is r is:

$$t_1 = \frac{r - d/2}{V}$$

and the arrival time of the rear edge of the cloud

$$t_2 = \frac{r + d/2}{V}$$

The length of time of sampling is

$$t_2 - t_1 = \frac{d}{V}$$

The elapsed time between zero time and the time at which this sampling took place has been chosen as

$$H + \sqrt{t_1 t_2}$$

The observed initial diameter of the cloud was:

Surface Shot = 880'
Underground Shot = 3750'

Table 4.1 presents the results of these calculations for the appropriate distances from ground zero. The factor f_1 in column 5 is the ratio of the 115 minute sampling period to the sampling period determined on the basis of the model:

$$f_1 = \frac{115}{t_2 - t_1}$$

The factor f_2 in column 7 is the activity correction that must be applied to correct the activity from H/60 min. (see next paragraph) to $H / \sqrt{t_1 t_2}$ minutes. The product $f_1 f_2$, therefore, is the correction factor that must be applied to the 115 minute concentration data to obtain the approximate concentration on the cloud proper. Table 4.1 also gives the arrival of the front and rear edges, respectively, of the cloud at the only stations where these could be observed from the aerial photographs.

Tables 4.2 and 4.3 present the average concentration of activity over the 115 minute sampling period, (col. 3) together with the data required for this determination (Cols. 1 and 2). It will be noted that the selection of H/60 minutes as the time to which the activity for all stations is corrected is an arbitrary selection. The 115 minute concentrations have been plotted on a station layout in Figs. 4.1 and 4.2. From these plots stations were selected at which the concentration of the activity in the cloud was calculated. The latter concentrations and the factors which produced them are listed in cols. 4 and 5 in Tables 4.2 and 4.3.

Activity measurements were made on Chemical Corps type 6 filter paper initially by NIH at the Nevada Test Site within 100 hours after each shot, using a Model PC-1 proportional counter made by the Nuclear Measurement Corporation. Second and third papers were radioautographed in many cases and found to be free from activity. In the few cases where activity was observed, it was attributed to leakage through the edges of the filter paper package since the filter paper is 99.97 per cent efficient for 0.3 micron particles at a flow rate of 32 liters per minute through 100 square centimeters area.

TABLE 4.1

Calculation of Sampling Interval and Elapsed Time on the Basis of Cloud Model

r (feet)	t_1 (min)	t_2 (min)	t_2-t_1 (min)	f_1	$\sqrt{t_1 t_2}$ (min)	f_2	$f_1 f_2$
			Surface Shot				
2,000	3.3	5.8	2.5	46	4.3	24	1.1×10^3
3,000	5.5	8.2	2.7	43	6.7	14	6.0×10^2
4,000	7.6	10.5	2.9	39	8.9	10	3.9×10^2
6,000	11.9	15.3	3.4	34	13.5	6.1	2.1×10^2
8,000	16.3	20.1	3.8	30	18.1	4.2	1.3×10^2
11,000	22.8	27.3	4.5	26	25.0	2.9	7.5×10^1
14,000	29.2	34.4	5.2	22	31.7	2.2	4.8×10^1
20,000	42.1	48.7	6.6	17	45.4	1.4	2.4×10^1
30,000	63.7	72.5	8.8	13	68.0	.86	1.1×10^1
50,000	107.	120.	13.	8.8	113.0	.45	3.9
			Underground Shot				
2,000	.9*	9.2*	8.3	13.9	3.0	37	5.2×10^2
3,000	2.3	11.4*	9.1	12.6	5.1	19	2.4×10^2
	2.1*	11.5					
4,000	4.4	13.7	9.3	12.4	7.8	12	1.5×10^2
	4.1*	13.7*					
6,000	8.8	18.5	9.7	11.8	12.8	6.5	7.7×10^1
	8.5*	18.3*					
8,000	13.1	23.3	10.2	11.3	17.5	4.4	5.0×10^1
11,000	19.6	30.5	10.9	10.5	24.5	2.9	3.0×10^1
14,000	26.0	37.6	11.6	9.9	31.3	2.2	2.2×10^1
20,000	39.0	51.9	12.9	8.9	45.0	1.4	1.2×10^1
30,000	60.6	75.7	15.1	7.6	67.8	.86	6.5
50,000	102.	123.	21.0	5.5	112.0	.47	2.6

* Values observed from aerial photographs.

TABLE 4.2

Filter Sampler Concentration of Activity, Surface Shot

Station	Activity at H + 60 minutes μc	Volume Sampled Between Zero and H + 115 min. $cm^3 \times 10^6$	Average Conc. of Activity over 115 min. $\frac{\mu c}{cm^3}$	Factor $f_1 f_2$	Conc. of Activity in Cloud $\frac{\mu c}{cm^3}$
1	4.3×10^{-1}	4.1	1.0×10^{-5}	1.1×10^{3}	1×10^{-2}
2*	8.1	4.6	1.7×10^{-6}	1.1×10^{3}	2×10^{-3}
3	2.1	4.4	4.4×10^{-7}		
4*	1.0	2.5	4.1×10^{-7}		
5	7.8×10^{-3}	2.8	2.7×10^{-9}		
6*	1.9×10^{-2}	4.6	4.2×10^{-9}		
7	3.3	4.2	7.9×10^{-7}	6.0×10^{2}	5×10^{-4}
8	2.5	4.8	5.2×10^{-7}	6.0×10^{2}	3×10^{-4}
9	5.6×10^{-1}	4.3	1.3×10^{-7}		
10	5.6×10^{-1}	2.0	2.7×10^{-7}		
11	6.9×10^{-4}	4.1	1.6×10^{-10}		
12	1.2×10^{-3}	4.7	2.7×10^{-10}		
13		3.8		3.9×10^{2}	
14	2.2	4.1	5.3×10^{-7}	3.9×10^{2}	2×10^{-4}
15*	9.9×10^{-1}	4.0	2.5×10^{-7}		
16	9.1×10^{-1}	3.1	3.0×10^{-7}		
17	0	4.3	0		
18	4.9×10^{-4}	4.5	1.1×10^{-10}		
19	1.6	11.1	1.4×10^{-7}		
20		9.7		2.1×10^{2}	
21	4.4	11.0	3.9×10^{-7}		
22	4.8	11.7	4.1×10^{-7}		
23	1.4×10^{1}	10.6	1.4×10^{-6}	1.3×10^{2}	2×10^{-4}
24	4.7	9.3	5.1×10^{-7}		
25*	1.3×10^{-1}	9.6	1.4×10^{-8}		
26	4.1	12.1	3.4×10^{-7}		
27	1.6×10^{-1}	11.6	1.4×10^{-6}	7.5×10^{1}	1×10^{-4}
28	6.6×10^{-3}	11.0	6.0×10^{-10}		
29	2.6×10^{1}	11.3	2.3×10^{-6}	4.2×10^{1}	1×10^{-4}
30	4.7	7.7	6.1×10^{-7}		
31*	6.6×10^{-3}	8.9	7.4×10^{-10}		
32	7.8×10^{-3}	12.0	6.5×10^{-10}		
33		11.9			
34	3.6	10.2	3.5×10^{-7}		
35	4.5	10.6	4.3×10^{-7}		
36	4.7	11.9	3.9×10^{-7}	1.1×10^{1}	4×10^{-6}
37*	2.6×10^{-1}	12.0	2.2×10^{-8}		

* Instrument did not function properly.

PROJECT 2.5a

TABLE 4.2 (Contd)

Station	Activity at H + 60 minutes μc	Volume Sampled Between Zero and H + 115 min. $cm^3 \times 10^6$	Average Conc. of Activity over 115 min. $\frac{\mu c}{cm^3}$	Factor $f_1 f_2$	Conc. of Activity in Cloud $\frac{\mu c}{cm^3}$
38	1.8	8.6	2.1×10^{-7}		
39	4.1	10.6	3.8×10^{-7}	3.9	1×10^{-6}
40	1.3	8.3	1.6×10^{-7}		
41*	2.8×10^{-2}	10.2	2.7×10^{-9}		
42	5.1×10^{-1}	9.0	5.7×10^{-8}		
43	0	8.1	0		
44	4.7×10^{-3}	8.2	5.7×10^{-10}		
45	3.2×10^{-3}	11.4	2.8×10^{-10}		
46	2.8×10^{-1}	10.2	2.8×10^{-8}		

* Instrument did not function properly.

TABLE 4.3

Filter Sampler Concentration of Activity, Underground Shot

Station	Activity at H + 60 minutes μc	Volume Sampled Between Zero & H + 60 Min $cm^3 \times 10^6$	Average Conc. of Activity over 115 min. $\frac{\mu c}{cm^3}$	Factor $f_1 f_2$	Conc. of Activity in Cloud $\frac{\mu c}{cm^3}$
101				5.2×102	
102	3.6×10^2	4.6	7.7×10^{-5}	5.2×102	4×10^{-2}
103		4.4			
104	5.5×10^{-1}	2.5	2.1×10^{-7}		
105	8.5×10^{-1}	2.8	3.0×10^{-7}		
106	4.0	4.6	8.6×10^{-7}		
107	4.4×10^2	4.2	1.0×10^{-4}	2.4×10^2	2×10^{-2}
108	4.6×10^3	4.8	9.5×10^{-4}	2.4×10^2	2×10^{-1}
109	2.9×10^2	4.3	6.8×10^{-5}		
110	5.2×10^{-1}	2.0	2.5×10^{-7}		
111	1.2×10^2	4.0	2.9×10^{-5}		
112	2.8	4.6	6.1×10^{-7}		
113		3.8		1.5×10^2	
114	1.1×10^2	4.1	2.8×10^{-5}	1.5×10^2	4×10^{-3}

TABLE 4.3 (Contd)

Station	Activity at H + 60 minutes μc	Volume Sampled Between Zero & H + 60 Min $cm^3 \times 10^6$	Average Conc. of Activity over 115 min. $\frac{\mu c}{cm^3}$	Factor $f_1 f_2$	Conc. of Activity in Cloud $\frac{\mu c}{cm^3}$
115	6.7×10^{-1}	4.0	1.6×10^{-8}		
116	7.3×10^{-2}	3.0	2.4×10^{-8}		
117	2.2	4.2	5.1×10^{-7}		
118	1.2	4.4	2.6×10^{-7}		
119	1.2×10^{1}	11.1	1.1×10^{-6}		
120	4.5×10^{2}	9.7	4.7×10^{-5}	7.7×10^{1}	4×10^{-3}
121	4.3×10^{2}	11.0	3.9×10^{-5}		
122	2.6×10^{-2}	11.7	2.2×10^{-9}		
123	1.1×10^{4}	10.6	1.0×10^{-3}	$50. \times 10^{-1}$	5×10^{-2}
124	4.0×10^{2}	9.2	4.3×10^{-5}		
125	2.9×10^{1}	9.6	3.0×10^{-6}		
126		12.1			
127	7.4×10^{3}	11.6	6.4×10^{-4}	3.0×10^{1}	2×10^{-2}
128	1.4×10^{2}	11.0	1.3×10^{-5}		
129	8.8×10^{3}	11.3	7.8×10^{-4}	2.2×10^{1}	2×10^{-2}
130	7.5×10^{1}	7.6	9.8×10^{-6}		
131		8.9			
132	2.8	12.0	2.3×10^{-7}		
133		11.8		1.2×10^{1}	
134	2.9	10.1	2.8×10^{-7}		
135		10.6			
136		11.9		6.5	
137	4.6	12.0	3.8×10^{-7}		
138		8.5			
139	1.0×10^{2}	10.6	9.9×10^{-6}	2.6	3×10^{-5}
140	9.2	9.2	1.1×10^{-6}		
141		10.1			
142	2.1	9.0	2.4×10^{-7}		
143	7.9	8.0	9.8×10^{-7}		
144	2.2×10^{1}	8.2	2.6×10^{-6}		
145	3.7×10^{-1}	11.4	3.2×10^{-8}		
146	9.6×10^{-3}	10.1	9.4×10^{-10}		
147	9.9×10^{-1}	11.0	9.0×10^{-8}		

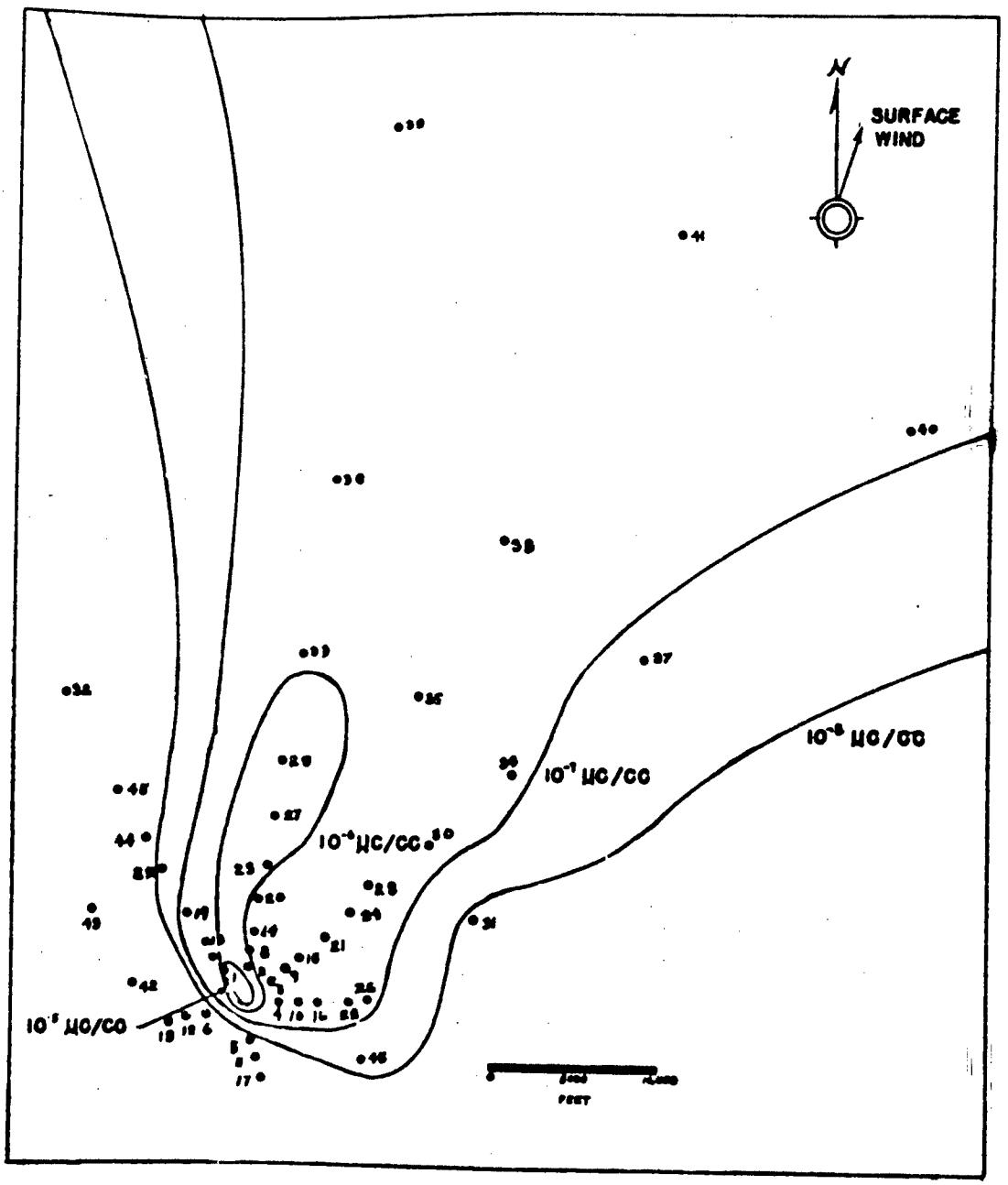

Fig. 4.1 Lines of Equal Concentration of Activity, Surface Shot Activity Corrected to H + 1 Hours, Sampling Time 115 Minutes.

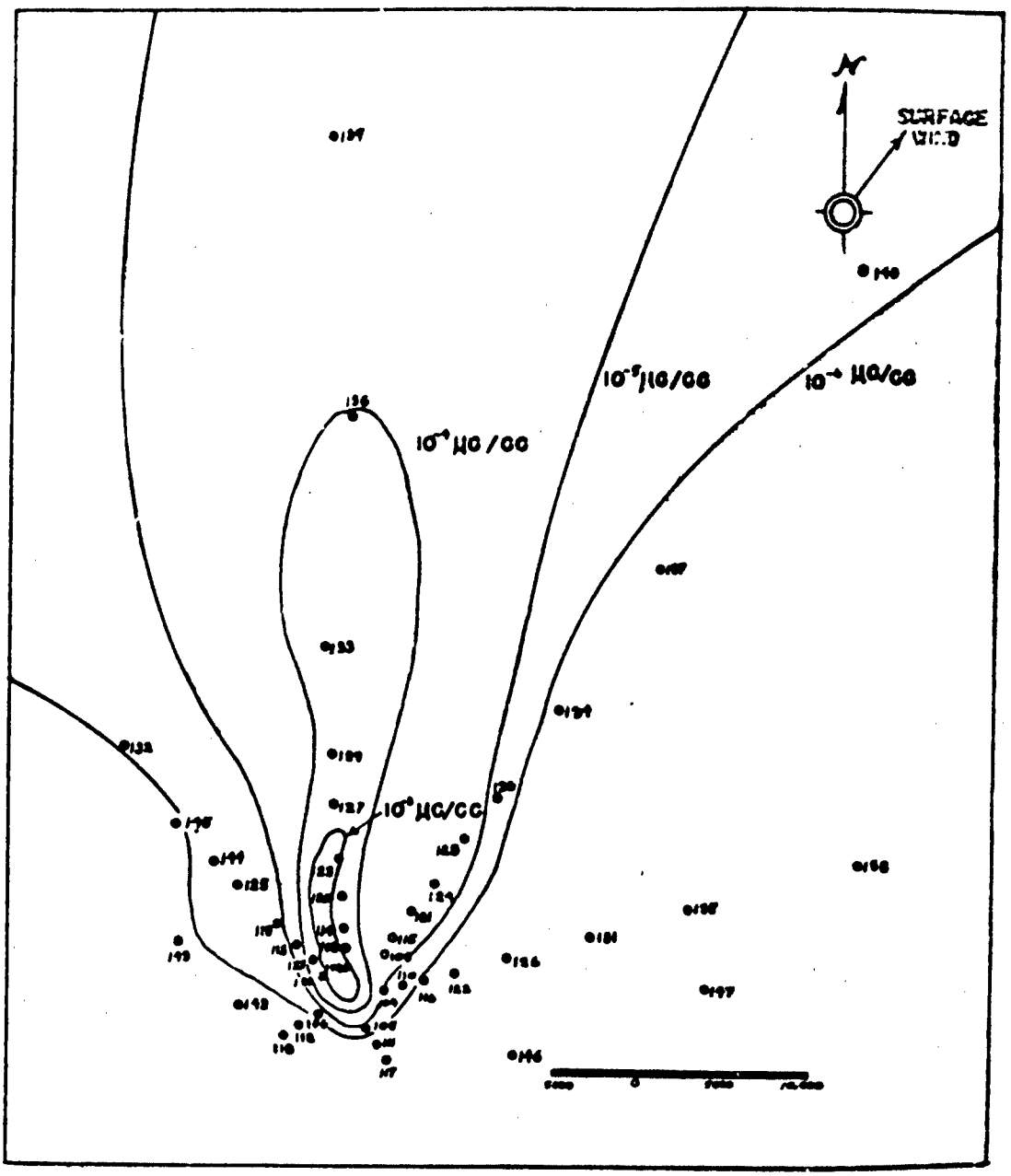

Fig. 4.2 Lines of Equal Concentration of Activity, Underground Shot. Activity Corrected to H + 1 Hours, Sampling Time 115 Minutes.

PROJECT 2.5a-1

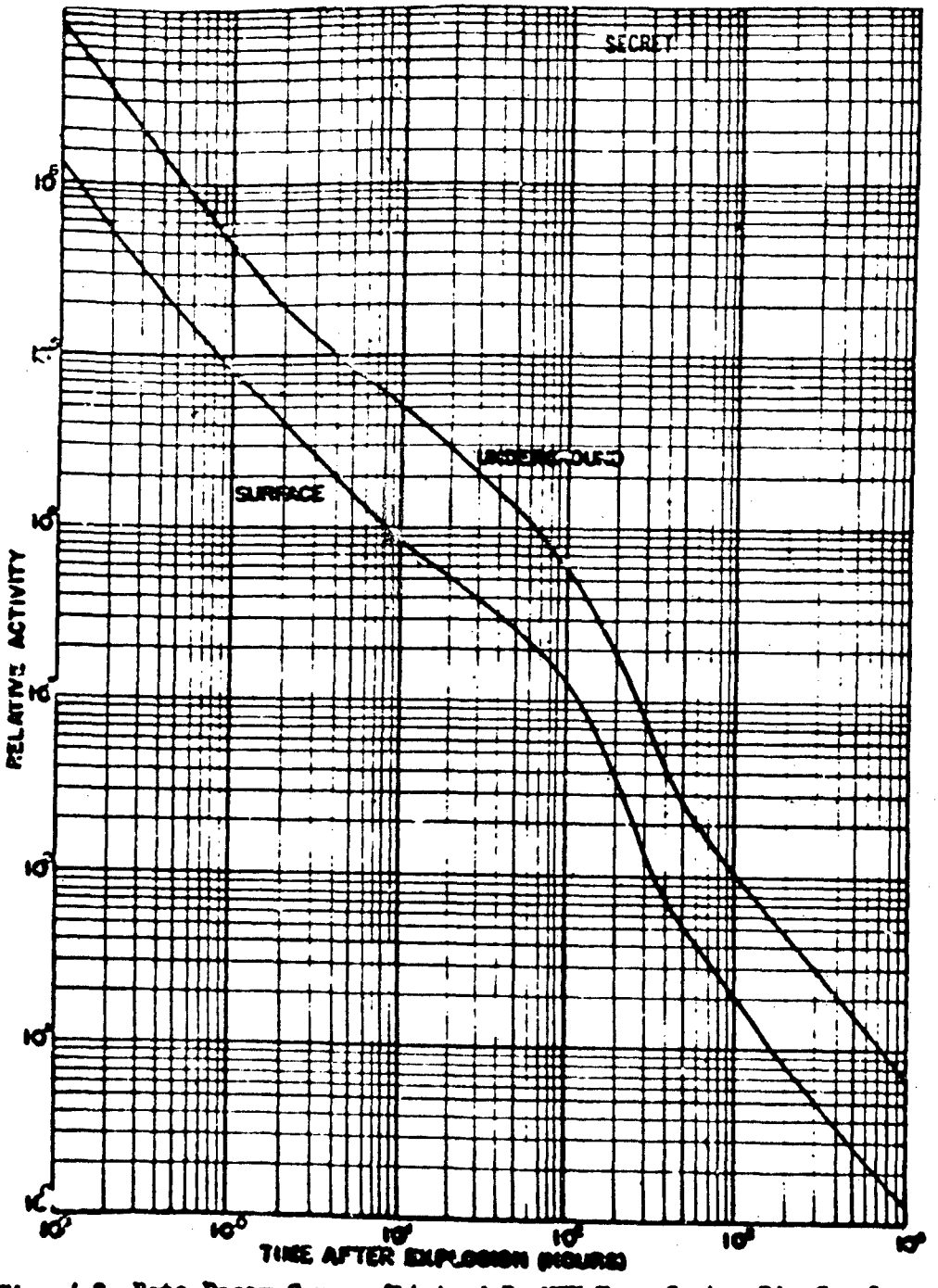

Fig. 4.3 Beta Decay Curves Obtained By NIH From Crater Lip Samples.

All activities were corrected to a common time by means of a decay curve obtained from a single station. Unfortunately approximately 40 per cent of the filter papers from both shots were too active to be counted by NIH; these were sent by military aircraft either to Tracerlab or to ACC, where they were counted between 120 and 600 hours after the shot. At these two laboratories activity measurements were corrected to a common time (ACC, H/400 hours, Tracerlab, H/600 hours) by means of the decay curves from the individual filter samplers.

Extrapolation of activity data back to very early times, was accomplished by use of the decay curves obtained by NIH[1] from crater and lip samples. These are presented in Fig. 4.3. The experimental data from which these curves were derived began at approximately H/4 hours and continued to about H/2000 hours. Extrapolations have been made to H/0.1 and H/10,000 hours.

Wherever possible the decay slopes from these "master" curves were compared with the decay slopes obtained at various time intervals from several filter samplers and various other equipment and agreement was considered satisfactory. Exact agreement is not achieved because of fractionation (See Par. 4.1.3) which influences the decay slope of samples taken at various distances from ground zero. The use of a single decay curve for all the filter sampler data thus introduces an error in the extrapolated activities.

4.1.2 Air Monitors

Three Brookhaven continuous air monitors (BCAM) and six Tracerlab continuous air monitors (TCAM) were employed to measure the radioactivity of the aerosol for both shots of Operation JANGLE. Table 4.4 summarizes their operation. It can be seen that a large number of failures occurred which were attributed either to failure of the 110 volt motor generator set[2], or mechanical failures of the instruments themselves. These latter difficulties were largely due to the delicate nature of the monitors under the severe conditions of the Nevada Test Site and the receipt of the TCAMs only a week prior to the surface shot.

For the surface shot, the BCAM at station 38 (30,000 ft. NE and defiladed by a ridge from the zero point) furnishes an interesting record as shown in the "raw" data plotted in Fig. 4.4. Of particular interest is the occurrence of a "pip" approximately 5 minutes after

[1] Letter from NIH, dated 7 February 1952.

[2] The large quantities of fine dust at the Test Site tended to rapidly foul the spark plugs.

TABLE 4.4

Air Monitor Operation for Surface and Underground Shots

Station Number	Instrument	Operation
36	BCAM	Defective rate meter prior to test
37	BCAM	Motor generator failure
38	BCAM	Vacuum leak, qualitative data
29	TCAM	Satisfactory
30	TCAM	Shear pin failure, data obtained
31	TCAM	Motor generator failure
39	TCAM	Satisfactory although off scale
40	TCAM	Mechanical failure
41	TCAM	Motor generator failure
136	BCAM	Motor generator failure
137	BCAM	Capstan frozen to sampling port
138	BCAM	Imperfect filter paper
129	TCAM	Mechanical failure
130	TCAM	" "
131	TCAM	" "
139	TCAM	Recorder broken, replay data obtained
140	TCAM	Satisfactory
141	TCAM	Satisfactory but low concentration

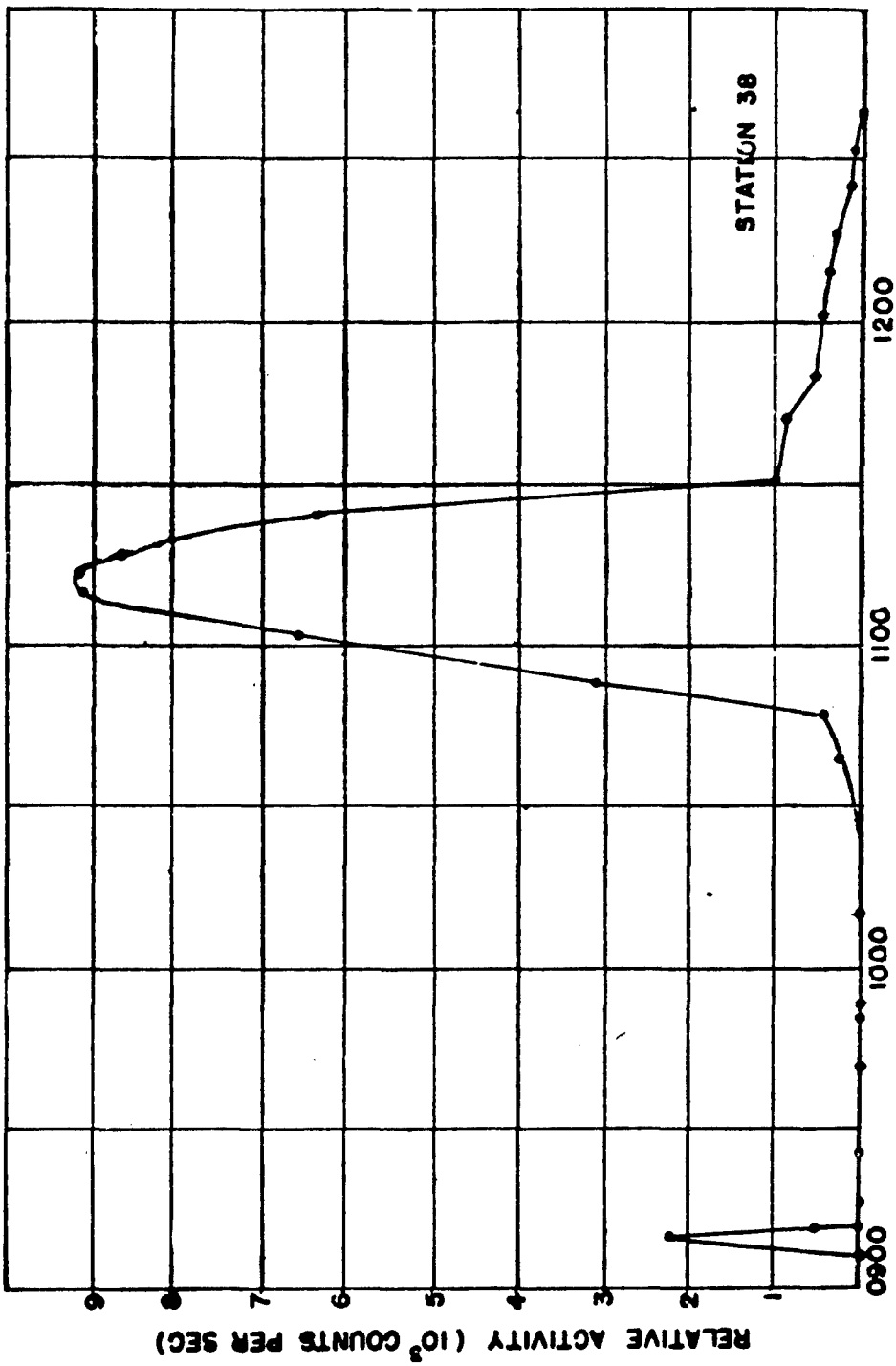

Fig. 4.4 Raw Counting Data from a BCAM at Station 38.

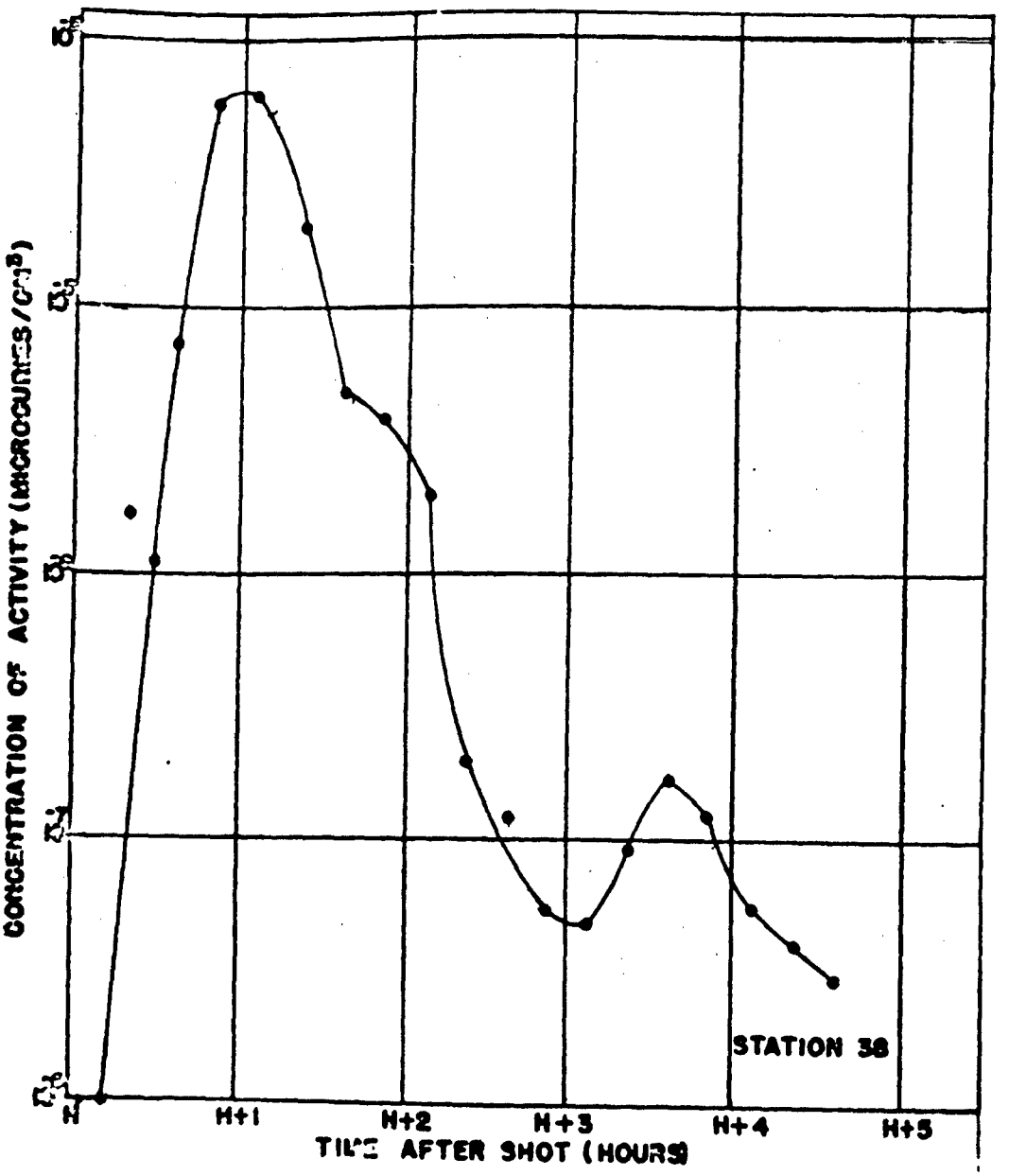

Fig. 4.5 Approximate Concentration of Activity at Station 38.

zero time (0900 hours PST). This "pip" appears to be identifiable only as external gamma radiation from an overhead cloud whose average speed was about 20 mph[3]. Fig. 4.5 presents the same data converted to microcuries per cubic centimeter by the methods described in Appendix B together with appropriate allowances to instrument time lag. The maximum at 1000 hours corresponds to a ground-level cloud speed of about 5 mph. Unfortunately the exact flow rate through the instrument is in doubt due to damage to the vacuum line right angle bend which could not be repaired prior to the zero hour so that the data of Fig. 4.5 must be regarded as approximate. It is interesting to note that the rate of change of the ground-level cloud activity concentration appears to have been as rapid as the BCAM was able to measure. It would thus appear that the BCAM in its present form is not well suited to monitor such rapidly changing concentrations.

For the surface shot, the Tracerlab Continuous Air Monitor (TCAM) at station 29 furnished a record of events which are plotted in Fig. 4.6. The cloud apparently arrived about an hour after shot time and either remained there for a number of hours, or as appears more likely, gamma radiation from local fall-out contributed a significant count rate to the instrument.

The TCAM at station 30 failed when a shear pin in the paper drive mechanisms broke, causing the monitor to sample on one spot of filter paper. However, the beta activity concentrations were readily obtained by graphical differentiations[4] of the recorded counts per minute, dividing by the volumetric flow rate, and applying the efficiency factor for a uniformly contaminated tape as derived in Appendix C. This record is presented in Fig. 4.7. The sharp changes of activity concentrations in the ground-level cloud can be especially well seen here since no instrument time lag or averaging error exists for these data.

Due to a pre-shot estimate that the 20,000 c/m beta scale was most desirable for a distant station, the TCAM at surface shot station 39 went off scale ($> 44 \times 10^{-7}$ uc/cc) at about H/1.5 hours and remained there until the record was retrieved by the pick-up crew on 20 November. The count rate record obtained is shown in Fig. 4.8. Of especial interest

[3] A ground-level cloud could not have been sampled on the tape and register as early as 0915. See paragraph 2.6.2 for time lag discussion.

[4] It may be noted that while a moving air monitor filter tape furnishes an averaged concentration directly, the derivative of the record obtained from a stationary tape gives instantaneous concentrations.

PROJECT 2.5a-1

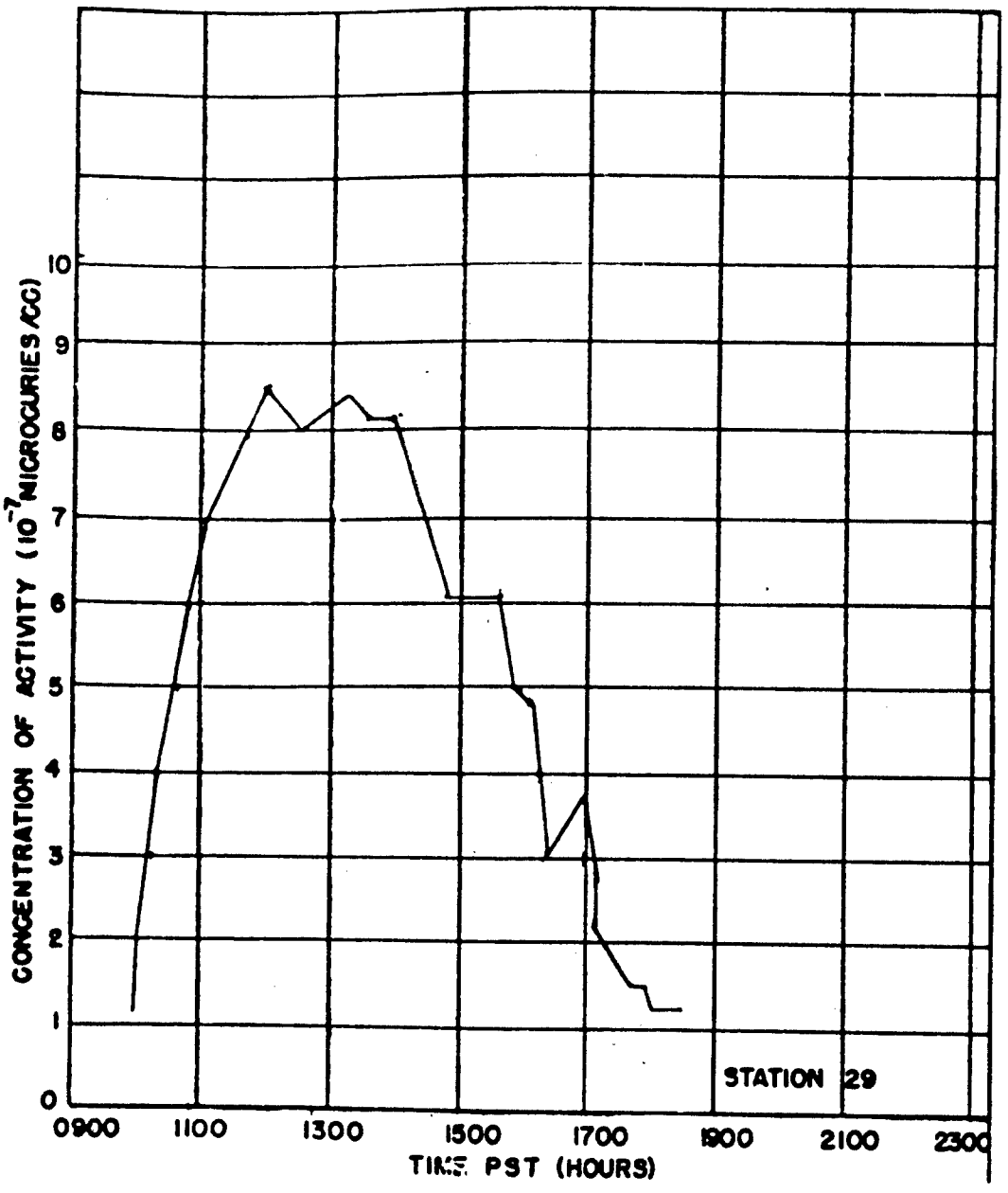

Fig. 4.6 Concentration of Activity at Station 29, Surface Shot, TCAM Data.

PROJECT 2.5a-1

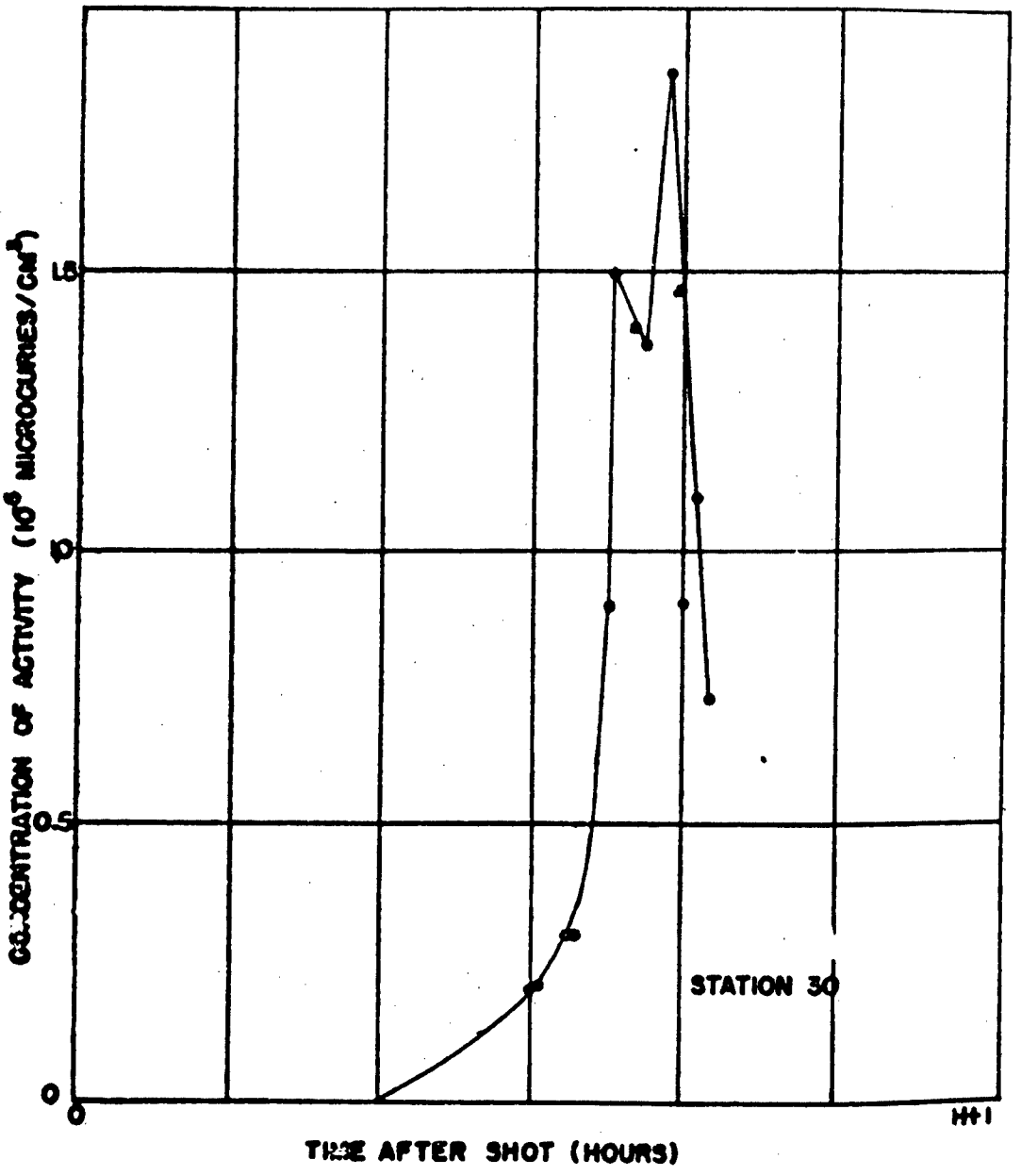

Fig. 4.7 Concentration of Activity at Station 30, Surface Shot, TCAM Data.

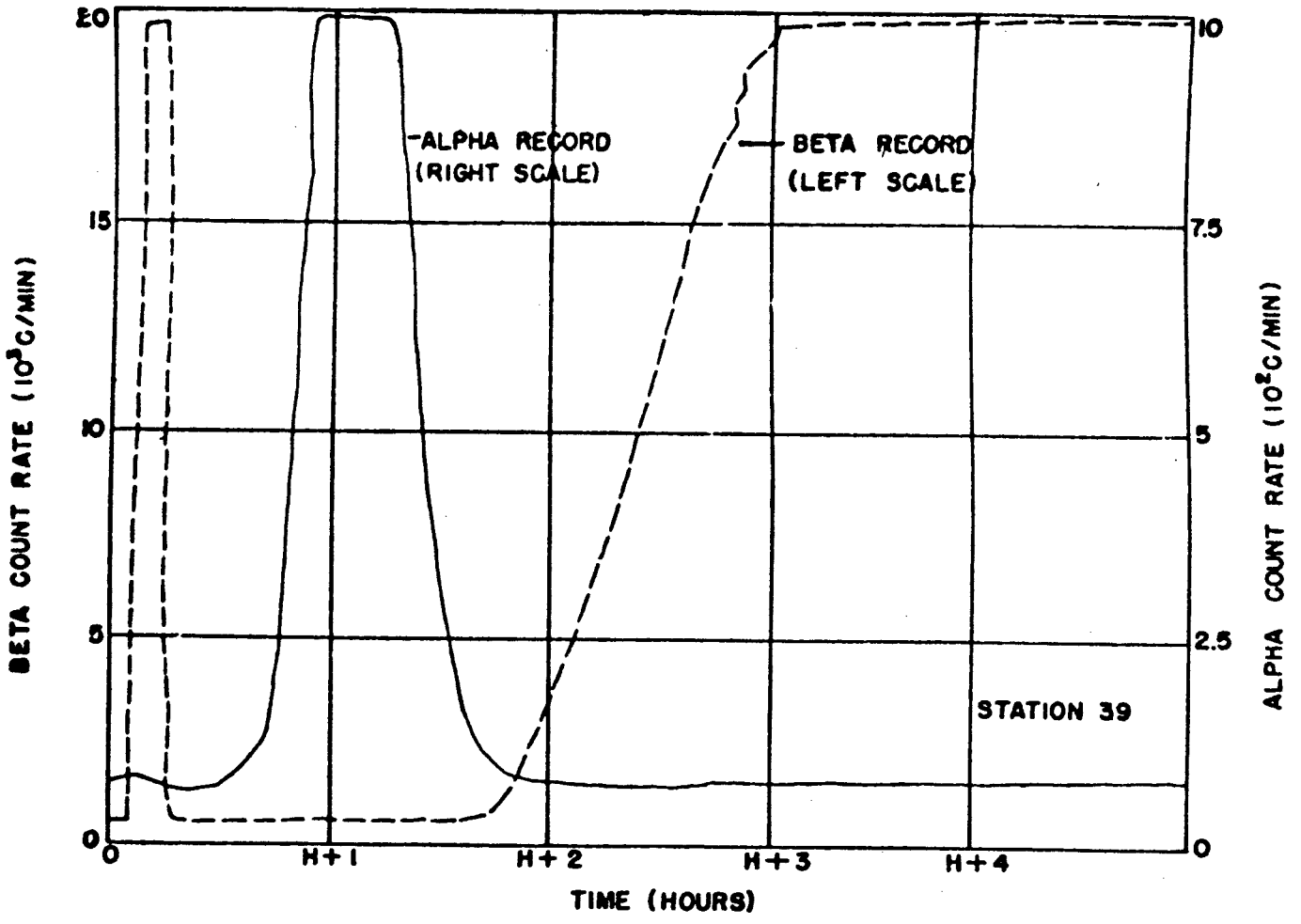

Fig. 4.8 Relative Activity Record Obtained from TCAM at Station 39, Surface Shot

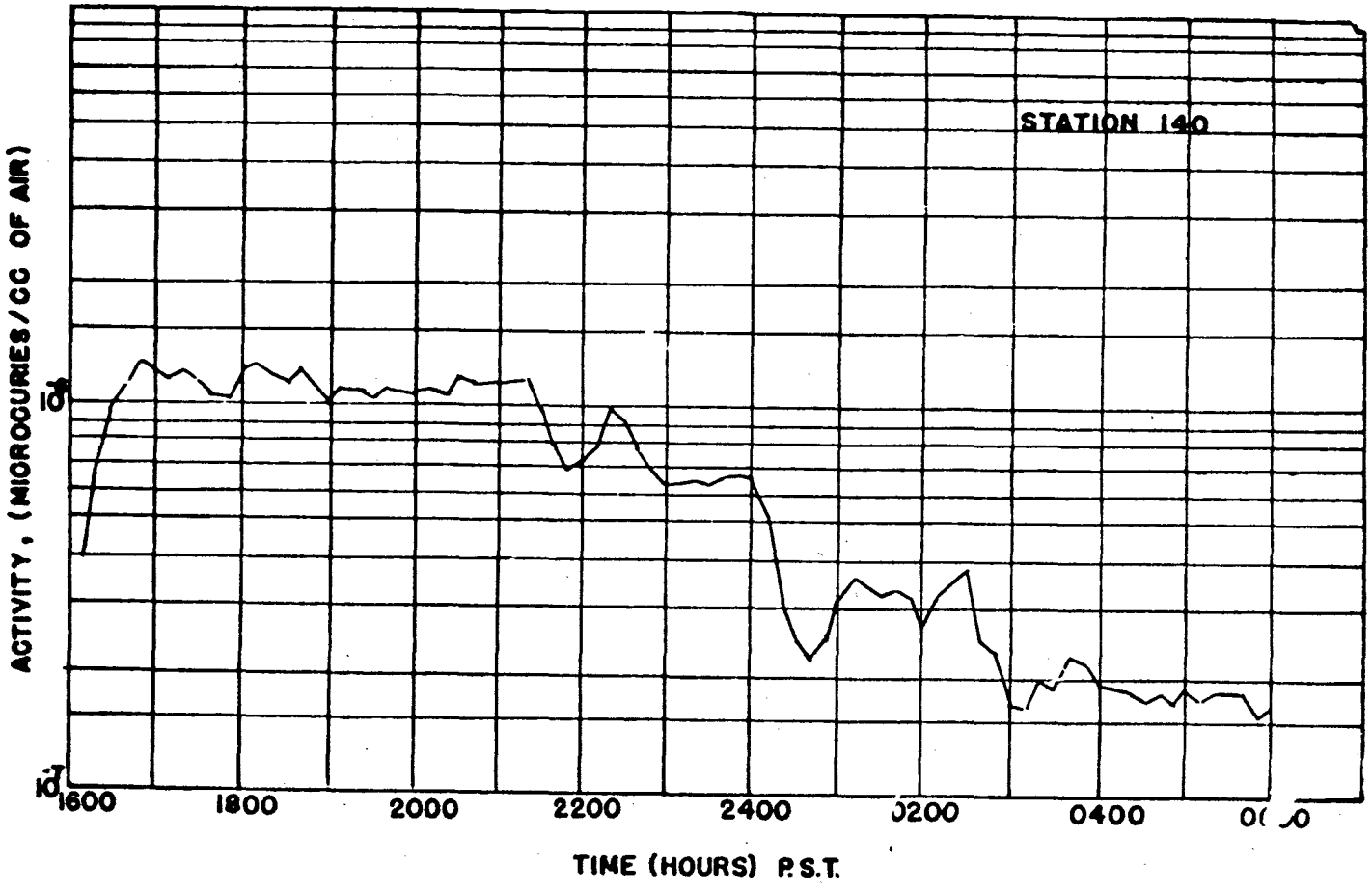

Fig. 4.9 Concentration of Activity at Station 140, Underground Shot, TCAH Data

is the alpha count rate pip which occurred at about H/2 hours. This pip occurred after cessation of a shot time beta pip (see discussion of BCAM 38) and prior to the hump due to the ground-level cloud. Since the beta record at this time shows nothing it is difficult to explain this effect.

A more regular record was obtained from the TCAM at station 140, in the Underground Shot. Fig. 4.9 presents the concentration of activity derived from the instrument at this station.

4.1.3 Particle Separator

Concentration data were obtained from particle separators used in each shot of Operation JANGLE by summing the activities measured on all the sampling elements of the particle separator, correcting for decay, and dividing by the volume of air sampled in the 115 minute sampling time. These data, of course, represent the average concentration in the air over the 115 minute sampling time. Concentration of activity in the cloud was computed using the sampling time and elapsed time as determined from the cloud model described in paragraph 4.1.1, for selected particle separators. These data are presented in Table 4.5.

The eleven screens, the metal disc, and the molecular filter of each particle separator were counted in a Nuclear Measurement Corporation PC-1 proportional counter. It was necessary to use two rings, one plastic and one aluminum, to prevent excessive contamination, hold the screen in place in the chamber, and yet insure suitable contact with the piston. In counting the surface shot samples it was found that the screens, metal disc, and molecular filters caused disturbances in the counting chamber; namely, the counting rate of any individual sample decreased with time. The surface shot samples had essentially no loose particles so colloidal graphite was sprayed on each sample before counting. After this treatment, reproducible measurements were obtained. The underground shot samples presented a more difficult problem since there was a large deposit of loose granular particles on most of the screens except the molecular filters. These screens were covered on both the influent and effluent sides with scotch tape. In this way it was possible to achieve reproducible results without seriously effecting the beta counting rates.

These activity measurements were made between 150 and 400 hours after the Surface Shot, and in two series, 400 to 800 hours and 1000 and 1200 hours after the underground shot, due to the extremely high activities encountered. Decay corrections were made to H/200, 400, and 1000 hours respectively by means of the individual decay curves for each

TABLE 4.5

Particle Separator Concentration of Activity

Station	Activity Corrected to H + 60 min. (μc)	Volume of Air Sampled in 115 minutes ($cm^3 \times 10^6$)	Average Conc. of Activity Over 115 min. $\mu c/cm^3$	Factor $f_1 f_2$	Conc. of Activity in Cloud $\mu c/cm^3$
			Surface Shot		
8	6.1	3.0	2.0×10^{-6}	6.0×10^{2}	1×10^{-3}
9	1.1	2.1	5.3×10^{-7}		
14	10.2	2.8	3.6×10^{-6}	3.9×10^{2}	1×10^{-3}
15	0.64	2.8	2.3×10^{-7}		
20	4.6	2.9	1.5×10^{-6}	2.1×10^{2}	3×10^{-4}
21	2.4	3.0	8.1×10^{-7}		
23	4.2	3.0	1.4×10^{-6}	1.3×10^{2}	2×10^{-4}
24	1.6	3.2	4.9×10^{-7}		
28	0.91	3.2	2.8×10^{-7}		
29	0.93	3.3	2.8×10^{-7}	4.8×10^{1}	1×10^{-5}
			Underground Shot		
108	1.6×10^{3}	3.0	5.5×10^{-4}	2.4×10^{2}	1×10^{-1}
109	4.2×10^{2}	1.5	2.7×10^{-4}		
114	2.7×10^{3}	2.7	1.0×10^{-3}	1.5×10^{2}	2×10^{-1}
115	6.9×10^{1}	2.7	2.5×10^{-5}		
120	3.3×10^{3}	3.1	1.2×10^{-3}	7.7×10^{1}	9×10^{-1}
121	3.8×10^{2}	2.9	1.3×10^{-4}		
123	3.8×10^{3}	3.4	1.1×10^{-3}	5.0×10^{1}	6×10^{-2}
124	4.4×10^{2}	3.2	1.4×10^{-4}		
128	4.2×10^{2}	3.2	1.3×10^{-4}		
129	2.9×10^{2}	3.5	8.6×10^{-5}	2.2×10^{1}	2×10^{-3}
130	2.9×10^{2}	3.1	9.7×10^{-5}		

sampling screen. The NIH decay curves (Fig. 4.3) were used to correct all activities to earlier times.

4.1.4 Cascade Impactor

Concentration data was also obtained from seven cascade impactors in the surface shot and ten cascade impactors in the underground shot. As discussed in paragraph 2.2.1, these instruments contained five slides and a molecular filter. By summing the measured activities on these elements, correcting for decay, and dividing by the volume sampled, the concentration of activity was determined. Since some of these instruments sampled for only a minute, and were initiated by a radiation alarm upon arrival of the cloud, the concentrations derived from these instruments should represent the concentration of activity in the cloud proper. The balance of the cascade impactors sampled for the usual 115 minutes, and their concentration data should represent the average concentration over that interval. The data from selected impactors of this latter group have been corrected by the methods described in paragraph 4.1.1 to produce the concentration of activity in the cloud. The entire data are presented in Table 4.6.

The measurements of activity on the cascade impactor slides were made in a gas flow proportional counter (Nuclear Measurements Model PC-1) in which the brass piston forming the base of the counting chamber was milled out in such a manner that the surface of the slide was flush with the surface of the piston. Calibration was accomplished with a UXIIB standard mounted with the same geometry as the sample geometry. No corrections were made for absorption or scattering. The measurements were completed by about H/200 hours and were corrected to H/100 hours by means of individual decay curves. Use was made of the NIH decay curves (Fig. 4.3) to connect back to H/1 hours.

4.1.5 Radiological Air Sampler

The Radiological Air Sampler which consisted basically of twelve small filter samplers sampling in succession, was designed to produce concentration data as a function of time. The decision to use these instruments was made a short time prior to Operation Jangle, and was based upon a desire to evaluate the instrument. Although time did not allow construction of a device to afford protection of the filter assembly, it was planned that the first filter assembly, which sampled from H-5 minutes to H/5 minutes, be used as a control for the balance of the filter assemblies. The assumption was made that the fall-out would uniformly contaminate all the filter assemblies, and that the first assembly, which had ceased sampling before the arrival of the cloud, would contain only fall-out activity. This activity would be subtracted from the activities on succeeding assemblies.

PROJECT 2.5a-1

TABLE 4.6

Cascade Impactor Concentration of Activity

Station	Activity at H + 60 min. (μc)	Sampling Interval (mins)	Volume Sampled (cm^3)	Concentration of Activity ($\mu c/cm^3$)	Factor f_2	Conc. of Act in Cloud ($\mu c/cm^3$)
Surface Shot						
13	2.8×10^{-3}	1	1.3×10^4	2.1×10^{-7}	10	2×10^{-6}
23	1.9×10^{-3}	1	1.3×10^4	1.5×10^{-7}	4.2	6×10^{-7}
25	2.1×10^{-4}	115	1.6×10^6	1.3×10^{-10}		
26	1.1×10^{-2}	115	1.5×10^6	7.2×10^{-9}		
30	2.9×10^{-2}	115	1.5×10^6	1.9×10^{-8}		
35	2.5×10^{-2}	115	1.6×10^6	1.6×10^{-8}		
40	6.0×10^{-3}	115	1.5×10^6	4.1×10^{-9}		
Underground Shot						
113	1.7×10^{-3}	1	1.3×10^4	1.3×10^{-7}	12	2×10^{-6}
114	7.5×10^{-3}	1	1.2×10^4	6.2×10^{-7}	12	7×10^{-6}
115	3.5×10^{-3}	1	1.3×10^4	2.7×10^{-7}		
119	1.8×10^{-3}	1	1.3×10^4	1.3×10^{-7}		
124	1.8×10^{-3}	115	1.5×10^6	1.2×10^{-9}		
125	1.1×10^{-3}	115	1.6×10^6	7.0×10^{-10}		
126	5.6×10^{-4}	115	1.5×10^6	3.7×10^{-10}		
132	8.0×10^{-5}	115	1.5×10^6	5.3×10^{-11}		
135	3.8×10^{-4}	115	1.6×10^6	2.4×10^{-10}		
140	2.3×10^{-3}	115	1.5×10^6	1.6×10^{-9}		

However, it was found that the activities on the various filter assemblies varied widely; in many cases there was more activity on the first filter assembly than on succeeding assemblies. A particularly good example of this variability was afforded by the two RAS at station 120. Both instruments failed to be initiated, and consequently all 24 filter assemblies were subjected only to fallout. On one of these instruments the most active filter assembly was more than three times as active as the least active filter assembly, and the standard deviation, percentagewise, of the 24 from the mean activity (computed by summing the activities and dividing by the number of filter assemblies) was found to be 25 per cent. Probably a reasonable explanation for this effect is that the small filter assembly offers a poor target, statistically, for large highly radioactive particles, or that in the various stages of transportation of the samples, these particles were lost.

Since the variability in fall-out activity was sufficiently large to mask the activity due to the sampled aerosol, it has not been possible to determine the concentration of activity in the aerosol with this instrument.

4.2 PARTICLE SIZE DISTRIBUTION

4.2.1 Cascade Impactor

The slides of twelve cascade impactors in each shot were examined by optical and electron microscopic methods to determine the size distribution of particles in the aerosol. A summary of the data from each shot is presented in Tables 4.7 and 4.8. The measuring and computing methods by which these data were obtained are described in the following paragraphs.

The particles on the first and second jets were counted and measured by examining the projected image of 1000 diameters from a light microscope. The particles on the 3rd and 4th jets were examined from projected images of 50,000 diameters. All measurements were made with transparent rules with millimeter divisions. Particles which measured between 14 and 15 mm were recorded as 15 mm, particles which measured between 15 and 16 mm were recorded as 16 etc. An attempt was made to measure the equivalent diameter of each particle (i.e., the diameters of a circle of area equal to the area of the particle). Since most of the particles had a rather circular projection, little difficulty was encountered. In most cases, the 2nd, 3rd, and 4th jet samples were relatively homogeneous and a particle count of 300-600 particles appeared satisfactory. The 1st and 5th jet samples were rather heterogeneous and particle counts of 400-1000 were made. The area represented

PROJECT 2.5a-1

TABLE 4.7

Cascade Impactor Particle Size Distribution
Surface Shot

	NMD (μ)	D^2MD (μ)	MMD (μ)	σ_g	Davg (μ)	Total No.	Total Surface	Total Mass
Cascade Impactor 13								
Jet 1	2.02	17.0	41.5	2.97	4.45	1.61×10^{5}	7.73×10^{6}	1.34×10^{8}
Jet 2	0.67	11.4	51.8	3.99	2.19	1.18×10^{5}	1.47×10^{6}	3.17×10^{7}
Jet 3	0.458	1.39	4.04	2.36	0.72	1.72×10^{5}	1.83×10^{5}	5.87×10^{5}
Jet 4	0.335	2.94	8.18	2.98	0.68	9.40×10^{5}	1.17×10^{5}	4.78×10^{5}
Jet 5								
Comp.Imp.	0.998	17.1	47.7	3.28	2.15	5.45×10^{5}	1.02×10^{7}	1.87×10^{8}
Cascade Impactor 14								
Jet 1	0.71	11.8	42.0	3.59	2.14	1.25×10^{6}	1.63×10^{7}	3.46×10^{8}
Jet 2	0.87	25.7	101.3	4.20	2.82	6.72×10^{5}	3.07×10^{7}	4.22×10^{8}
Jet 3	0.91	16.0	66.0	3.79	2.27	2.30×10^{5}	4.11×10^{6}	4.58×10^{8}
Jet 4	0.83	7.45	8.80	2.23	2.72	4.39×10^{4}	6.48×10^{5}	5.11×10^{6}
Jet 5								
Comp.Imp.	0.75	15.6	75.5	3.63	2.42	2.2×10^{6}	5.31×10^{7}	1.88×10^{9}
Cascade Impactor 15								
Jet 1 Jet 2 Jet 3 Jet 4 Jet 5 Comp.Imp.	Insufficient Sample.							
Cascade Impactor 19								
Jet 1	0.96	17.9	69.5	3.90	2.84	1.50×10^{5}	3.99×10^{6}	8.46×10^{7}
Jet 2	1.92	22.9	84.2	2.86	4.10	7.49×10^{4}	5.08×10^{6}	1.96×10^{8}
Jet 3 Jet 4 Jet 5 Comp.Imp.	Insufficient Sample.							
Cascade Impactor 23								
Jet 1	0.19	9.90	59.50	1.96	1.84	4.56×10^{6}	3.71×10^{7}	5.23×10^{8}
Jet 2	1.65	39.0	42.0	3.96	8.35	3.24×10^{4}	8.12×10^{6}	3.27×10^{8}
Jet 3	2.07	5.30	7.50	1.88	2.53	1.40×10^{5}	1.90×10^{5}	1.38×10^{6}
Jet 4	1.13	3.69	8.18	2.26	2.07	2.81×10^{4}	1.97×10^{5}	1.52×10^{6}
Jet 5								
Comp.Imp.	0.606	7.65	31.6	3.47	1.93	4.63×10^{6}	4.87×10^{7}	9.35×10^{3}

PROJECT 2.5a-1

TABLE 4.7 (cont'd)

	NMD (μ)	D^2MD (μ)	MMD (μ)	σ_g	Davg (μ)	Total No.	Total Surface	Total Mass
Cascade Impactor 24								
Jet 1 Jet 2 Jet 3 Jet 4 Jet 5 Comp.Imp.	Insufficient Sample.							
Cascade Impactor 25								
Jet 1	2.72	15.3	31.2	2.50	5.03	2.09×10^5	1.09×10^7	1.49×10^8
Jet 2	2.17	5.35	8.40	2.05	3.26	2.11×10^5	3.28×10^6	2.34×10^7
Jet 3	.97	3.44	6.78	2.22	1.44	3.58×10^5	1.38×10^6	6.87×10^6
Jet 4	1.15	2.31	3.13	1.74	1.29	3.68×10^5	9.63×10^5	2.56×10^6
Jet 5	0.438	1.16	1.76	2.01	.50	8.45×10^5	4.12×10^5	5.41×10^5
Comp.Imp.	0.84	9.15	20.7	2.83	1.65	1.99×10^8	1.79×10^7	2.12×10^8
Cascade Impactor 26								
Jet 1	6.25	16.7	25.6	1.91	7.30	2.2×10^4	2.19×10^6	5.01×10^7
Jet 2	1.03	5.25	10.3	2.76	2.19	4.13×10^5	3.54×10^6	3.24×10^7
Jet 3	.495	2.19	4.03	2.40	.776	9.24×10^5	1.10×10^6	2.84×10^6
Jet 4	.519	1.48	2.25	1.98	.66	7.47×10^5	6.22×10^5	1.10×10^6
Jet 5	.095	.778	1.38	2.97	.182	1.88×10^6	1.49×10^5	1.05×10^5
Comp.Imp.	.302	6.00	19.4	3.44	.678	4.04×10^6	8.14×10^6	8.39×10^7
Cascade Impactor 30								
Jet 1	.94	6.0	18.7	2.67	2.18	1.29×10^6	1.29×10^7	1.65×10^8
Jet 2	1.41	3.83	6.2	2.13	2.29	1.05×10^5	8.62×10^5	4.28×10^6
Jet 3	1.01	1.87	2.32	1.62	1.10	4.59×10^5	8.21×10^5	1.70×10^6
Jet 4	.643	1.27	1.82	1.80	.798	3.34×10^5	3.00×10^5	5.14×10^5
Jet 5	.052	.362	.816	2.80	.099	4.80×10^5	1.10×10^4	4.00×10^3
Comp.Imp.	.89	6.11	8.75	2.60	1.50	2.67×10^6	1.56×10^7	8.05×10^7
Cascade Impactor 32								
Jet 1	1.97	9.85	21.0	2.64	3.61	1.26×10^5	3.27×10^6	4.07×10^7
Jet 2	1.70	3.72	5.15	1.94	2.44	4.67×10^4	4.05×10^5	1.93×10^6
Jet 3	.62	3.47	9.05	2.66	1.02	1.87×10^5	4.46×10^5	2.47×10^6
Jet 4	.495	1.07	1.57	1.88	.66	5.34×10^5	3.32×10^5	4.57×10^5
Jet 5	.216	.590	.967	2.11	.31	1.57×10^6	2.21×10^5	1.33×10^5
Comp.Imp.	.345	5.41	18.2	3.18	.67	2.47×10^6	4.98×10^6	4.99×10^7

TABLE 4.7 (cont'd)

	NMD (μ)	D^2MD (μ)	MMD (μ)	σ_g	Davg (μ)	Total No.	Total Surface	Total Mass
				Cascade Impactor 35				
Jet 1	3.75	11.5	18.4	2.11	5.32	3.46×10^5	1.76×10^7	2.57×10^8
Jet 2	2.08	5.85	9.20	2.14	3.23	1.88×10^5	3.14×10^6	2.31×10^7
Jet 3	1.44	2.90	3.79	1.70	1.42	2.61×10^5	9.43×10^5	3.34×10^6
Jet 4	.83	1.36	1.11	1.64	.97	4.82×10^5	5.91×10^5	9.37×10^5
Jet 5	.098	.308	.46	1.96	.072	1.14×10^7	1.72×10^5	6.44×10^4
Comp.Imp.	.592	12.5	31.4	3.82	1.44	2.42×10^6	2.43×10^7	3.16×10^8
				Cascade Impactor 40				
Jet 1	1.52	22.3	82.5	3.55	3.70	3.53×10^4	1.62×10^6	4.91×10^7
Jet 2	1.94	3.72	5.10	1.75	2.60	3.83×10^4	3.64×10^5	1.75×10^6
Jet 3	1.47	2.67	3.18	1.79	1.21	1.67×10^5	4.67×10^5	1.40×10^6
Jet 4	0.705	1.56	2.47	1.95	0.944	2.53×10^5	3.31×10^5	6.80×10^5
Jet 5	0.033	0.256	0.620	2.98	0.068	8.82×10^6	1.00×10^5	3.05×10^4
Comp.Imp.	0.030	9.25	81.5	5.36	0.138	9.31×10^5	3.09×10^6	5.63×10^7

TABLE 4.8

Cascade Impactor Particle Size Distribution
Underground Shot

				Cascade Impactor 113				
Jet 1	0.91	4.43	14.80	2.85	1.9	6.04×10^5	4.11×10^6	3.81×10^7
Jet 2	1.28	7.9	18.9	2.58	2.51	8.94×10^3	1.22×10^5	1.57×10^6
Jet 3								
Jet 4	Excessive Sample.							
Jet 5								
Comp.Imp.								
				Cascade Impactor 114				
Jet 1	1.68	12.6	30.9	2.80	3.43	1.94×10^5	5.41×10^6	8.89×10^7
Jet 2	1.42	4.75	8.58	2.22	2.44	1.40×10^4	1.50×10^5	1.02×10^6
Jet 3	1.04	2.21	2.90	1.88	1.85	3.80×10^4	1.68×10^5	4.95×10^5
Jet 4	0.74	4.37	7.55	2.57	1.76	1.38×10^4	7.69×10^4	4.34×10^5
Jet 5								
Comp.Imp.	1.41	12.3	31.5	2.99	3.15	2.61×10^5	6.32×10^6	1.02×10^8

PROJECT 2.5a-1

TABLE 4.8 (Cont'd)

	NMD (μ)	D^2_{MD} (μ)	MMD (μ)	σ_g	Davg (μ)	Total No.	Total Surface	Total Mass
				Cascade Impactor 115				
Jet 1	3.30	27.2	73.0	2.61	5.98	9.35×10^3	1.24×10^6	4.38×10^6
Jet 2	1.72	58.0	102.16	3.90	4.61	2.3×10^3	2.55×10^5	1.78×10^7
Jet 3								
Jet 4	Excessive Sample.							
Jet 5								
Comp.Imp.								
				Cascade Impactor 119				
Jet 1	1.13	10.5	25.6	3.10	2.72	1.67×10^5	3.07×10^6	4.18×10^7
Jet 2	1.00	10.8	25.7	3.60	2.52	4.78×10^3	7.93×10^4	1.09×10^6
Jet 3								
Jet 4	Excessive Sample.							
Jet 5								
Comp.Imp.								
				Cascade Impactor 123				
Jet 1	0.46	5.70	18.0	3.35	1.54	7.61×10^6	3.87×10^7	3.52×10^8
Jet 2	3.35	8.35	11.5	1.90	4.33	1.20×10^4	3.37×10^5	3.44×10^6
Jet 3	1.05	5.75	13.0	2.75	2.12	3.00×10^4	2.52×10^5	2.11×10^6
Jet 4	0.5	5.99	14.5	3.40	1.00	2.42×10^5	6.19×10^5	2.42×10^6
Jet 5	0.88	1.77	2.53	1.61	1.15	1.03×10^5	1.28×10^5	4.22×10^5
Comp.Imp.	0.473	5.65	20.4	3.47	1.28	8.00×10^6	4.26×10^7	4.15×10^8
				Cascade Impactor 124				
Jet 1	0.81	2.17	96	3.83	2.53	4.13×10^3	1.01×10^5	3.68×10^6
Jet 2	1.23	8.00	19.5	2.67	2.45	3.9×10^3	5.42×10^4	6.94×10^5
Jet 3								
Jet 4	Excessive Sample.							
Jet 5								
Comp.Imp.								
				Cascade Impactor 125				
Jet 1	1.95	5.90	9.90	2.10	2.80	1.56×10^6	2.27×10^7	1.86×10^8
Jet 2	0.68	5.50	11.80	2.96	1.76	3.73×10^4	2.32×10^5	1.79×10^6
Jet 3								
Jet 4	Excessive Sample.							
Jet 5								
Comp.Imp.								

PROJECT 2.5a-1

TABLE 4.8 (Cont'd)

	NMD (μ)	D^2MD (μ)	MMD (μ)	σ_g	D_{avg} (μ)	Total No.	Total Surface	Total Mass
Cascade Impactor 126								
Jet 1 Jet 2 Jet 3 Jet 4 Jet 5 Comp.Imp.	Excessive Sample.							
Cascade Impactor 130								
Jet 1	2.34	9.15	16.20	2.31	3.81	2.23×10^5	6.14×10^6	7.97×10^7
Jet 2	1.46	4.30	6.75	2.19	2.41	3.78×10^5	3.44×10^6	1.87×10^7
Jet 3	1.48	4.35	6.80	2.16	2.41	2.14×10^5	1.96×10^6	1.15×10^7
Jet 4	0.85	1.89	2.84	2.00	1.57	3.32×10^5	1.11×10^6	3.15×10^7
Jet 5	0.058	0.196	0.328	2.28	0.098	1.75×10^6	2.92×10^4	7.08×10^3
Comp.Imp.	0.120	8.25	20.7	3.67	0.726	2.89×10^6	1.02×10^7	1.10×10^8
Cascade Impactor 132								
Jet 1	2.5	10.5	20.5	2.44	4.10	2.35×10^4	7.51×10^5	9.57×10^5
Jet 2	1.38	4.15	5.85	2.21	2.33	1.64×10^4	1.41×10^5	7.52×10^5
Jet 3	1.55	2.41	3.01	1.62	2.08	3.05×10^4	1.68×10^5	5.44×10^5
Jet 4	0.343	1.41	2.44	2.28	0.476	1.30×10^5	7.03×10^4	1.20×10^5
Jet 5	0.18	0.304	0.376	1.63	0.201	1.62×10^6	8.72×10^4	2.94×10^4
Comp.Imp.	0.203	7.95	29.3	3.25	0.350	1.82×10^6	1.19×10^4	1.38×10^4
Cascade Impactor 135								
Jet 1	0.49	2.72	7.50	3.06	1.42	5.05×10^5	1.63×10^6	7.95×10^6
Jet 2	0.70	4.20	11.30	2.99	1.79	2.93×10^4	1.71×10^5	1.26×10^6
Jet 3	1.12	2.55	4.65	1.96	1.93	3.44×10^4	1.78×10^5	8.06×10^5
Jet 4	0.139	1.08	2.25	2.76	0.283	5.20×10^5	9.93×10^4	1.35×10^5
Jet 5	0.053	0.20	0.41	2.30	0.086	2.12×10^6	5.80×10^4	8.56×10^3
Comp.Imp.	0.104	2.39	11.7	4.04	0.339	3.37×10^6	2.34×10^6	1.15×10^7
Cascade Impactor 140								
Jet 1	1.26	7.55	19.5	2.78	2.54	1.24×10^5	1.70×10^6	2.14×10^7
Jet 2	0.81	3.72	8.40	2.74	1.84	5.34×10^4	3.10×10^5	1.87×10^6
Jet 3	0.73	1.75	2.17	2.22	1.50	1.04×10^5	3.00×10^5	8.84×10^5
Jet 4	0.184	1.44	3.17	3.10	0.31	4.02×10^5	1.43×10^5	2.01×10^5
Jet 5	0.12	0.24	0.36	1.33	0.14	3.34×10^6	7.40×10^4	2.15×10^4
Comp.Imp.	0.094	2.39	11.7	4.04	0.339	3.37×10^6	2.34×10^5	1.15×10^7

by the count was measured and recorded. Also the total impaction area was measured for each sample with the light microscope using scattered light.

A table of data and calculations was made for each jet, the completed table being similar in form to Table 4.9.

TABLE 4.9

Sample Cascade Impactor Data and Calculation Sheet

Diameter Microns	Number	Per Cent by No.	$n_i D_i^2$	Per Cent by Surface	Cum. Per Cent by Area	$n_i D_i^3$	Per Cent by Mass	Cum. Per Cent by Mass

It will be noticed that to obtain the percent by surface and percent by mass only the relative surface area and mass were computed.

Three sets of points representing cumulative per cent less than stated size by number, by surface, and by mass, were plotted on log-probability paper. Straight lines were drawn to represent the sets of points by inspection, using the following criteria:

A. The slope in best agreement with all three sets of points was used for all three lines. (If the distribution is assumed to be log-normal then this procedure is indicated by theory[5,6,7].

[5]Hatch & Choate, "Statistical Description of the Size Properties of Non-Uniform Particulate Substances", J. Franklin Inst., 207, (1929), 369

[6]T. Hatch, "Determination of Average Particle Size From the Screen Analysis of Non-Uniform Particulate Substances", J. Franklin Inst., 215, (1933), 27

[7]C. E. Lappel, "Mist and Dust", Heating and Air Cond., 18, (1946)

Also, this method gives a single average measure of the degree of homogeneity of the sample.)

B. The slope being already determined, the lines were positioned to best fit the points in the 10-90 per cent range.

C. Known difficulties in analysis, such as measuring the smallest particles, were allowed some consideration. The following parameters were obtained from the lines:

NMD = Number Median Diameter = D(50%) from No. line.

D^2MD = Surface Median Diameter = D(50%) from surface line.

MMD = Mass Median Diameter = D(50%) from mass line.

σ_g = Geometric Standard Deviation = $\frac{D(84.13\%)}{D(50\%)}$

Other values obtained are:

D_{avg} = Average Diameter = $\frac{n_i D_i}{n_i}$

Total No. of Particles Collected
Total Surface (Relative)
Total Mass (Relative)

There are many good arguments against the use of log-probability plots to represent sub-samples such as those from the jets of a cascade impactor[8,9]. However, the method is expedient and gives parameters that represent the sample to a reasonable accuracy. There are several analytic methods of curve fitting[8,9], but they would be

[8] F. Kottler, "The Distribution of Particle Sizes", Parts I and II, J. Franklin Inst., 250 (Oct & Nov, 1950), 339 and 419.

[9] F. Kottler, "The Goodness of Fit and Distribution of Particle Sizes", Parts I and II, J. Franklin Inst., 251, (May and June 1951) 499 and 617.

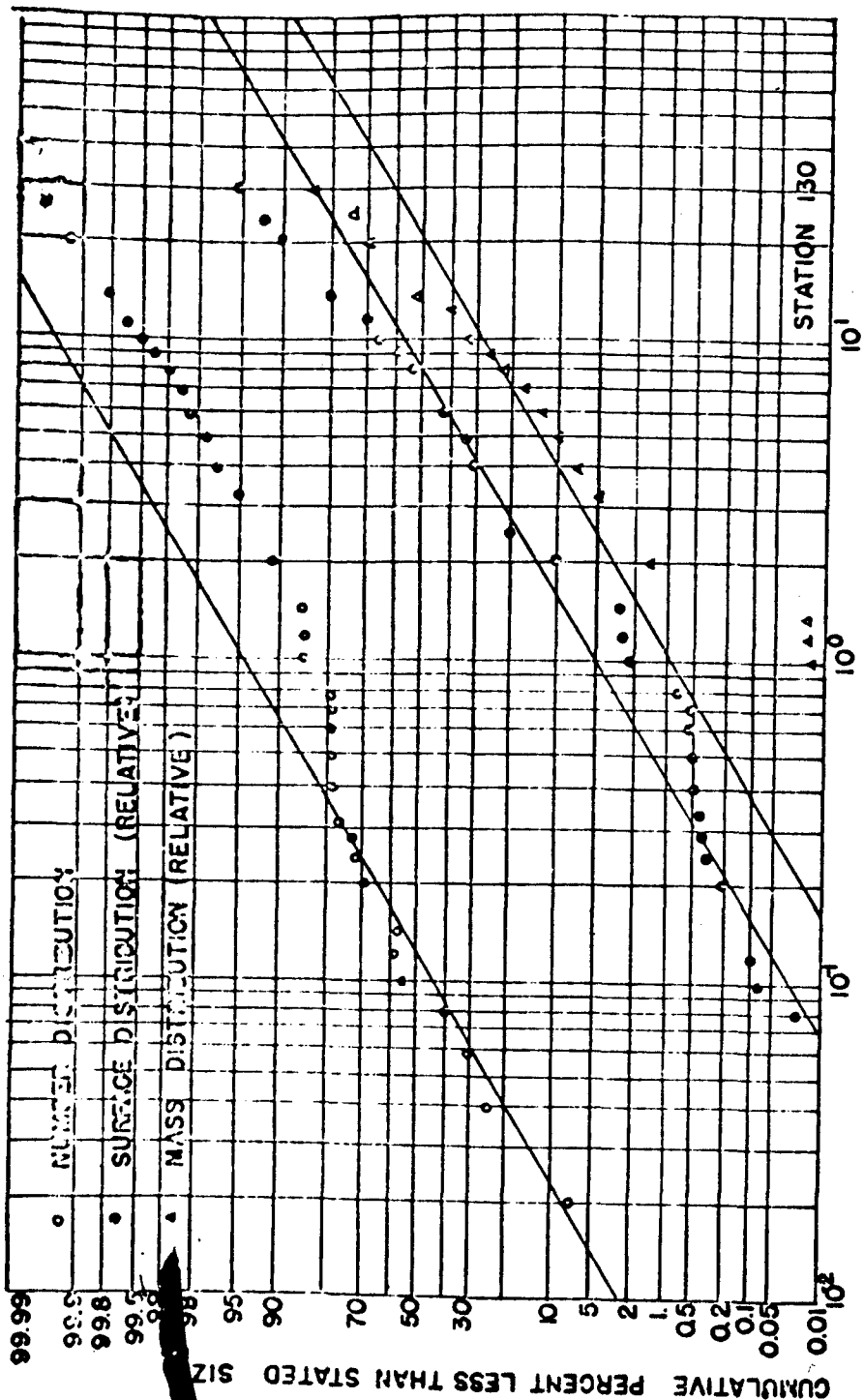

Fig. 4.10 Particle Size Distribution in the Aerosol at Station 130, Cascade Impactor Data

very difficult to use considering the large number of points involved and the fact that parallel lines are to be drawn.

Having obtained sufficient information about the individual jet samples, it was necessary to combine the data from each set of 5 jets to obtain the size distribution of the cloud. An area correction factor was obtained for each jet by dividing the impaction area of the jet by the area counted. The number of particles in each size group (class interval) was multiplied by the area factor and the resulting number represented the total number of particles in each class interval collected by the jet. An integrated set of fifth class intervals covering the entire size range studied (0.02-100 microns) had been formulated, and the individual jet data were fit to these class intervals on a sub-size basis. The number falling in each class interval was found by adding the contributions from each jet; a table of data and calculations similar to those for the individual jets was made. From the data thus obtained, four cycle log-probability plots for the entire cascade impactor were constructed, from which the parameters tabulated tabulated in Table 4.7 and 4.8 were taken. Fig. 4.10 is an example of such a graph. It should be noted that the parameters listed in the tables permit reconstruction of the straight lines in any desired plot.

4.2.2 Filter Sampler

The filter papers from the filter samplers at stations 29,30 and 129,130 were analyzed by Tracerlab for particle size distributions. The results are reported in Appendix E.

4.2.3 Fall-out Tray

Of the twenty fall-out trays employed in each shot, one tray in the surface shot and twenty in the underground shot collected a weighable sample of the fall-out material. The former and eight of the latter contained sufficient material to permit a sieve analysis, while four of the latter passed sufficient material through the last (37 micron) sieve to permit further separation by means of a Roller Analyzer. Fig. 4.11 shows the mass of the material collected on the trays plotted against distance grom ground zero, while Figs. 4.12 through 4.15 show the particle size distributions obtained from the four stations that were put through the sieve analysis and Roller Analyzer.

The sieve analysis consisted of sifting the samples through a column of U. S. standard sieves shaken by a Rotap machine. This machine was operated for 5 minutes on fractions greater than 1410 microns, and for ten minutes on smaller size fractions. In the case of four stations where more than grams of material was found to pass the last screen,

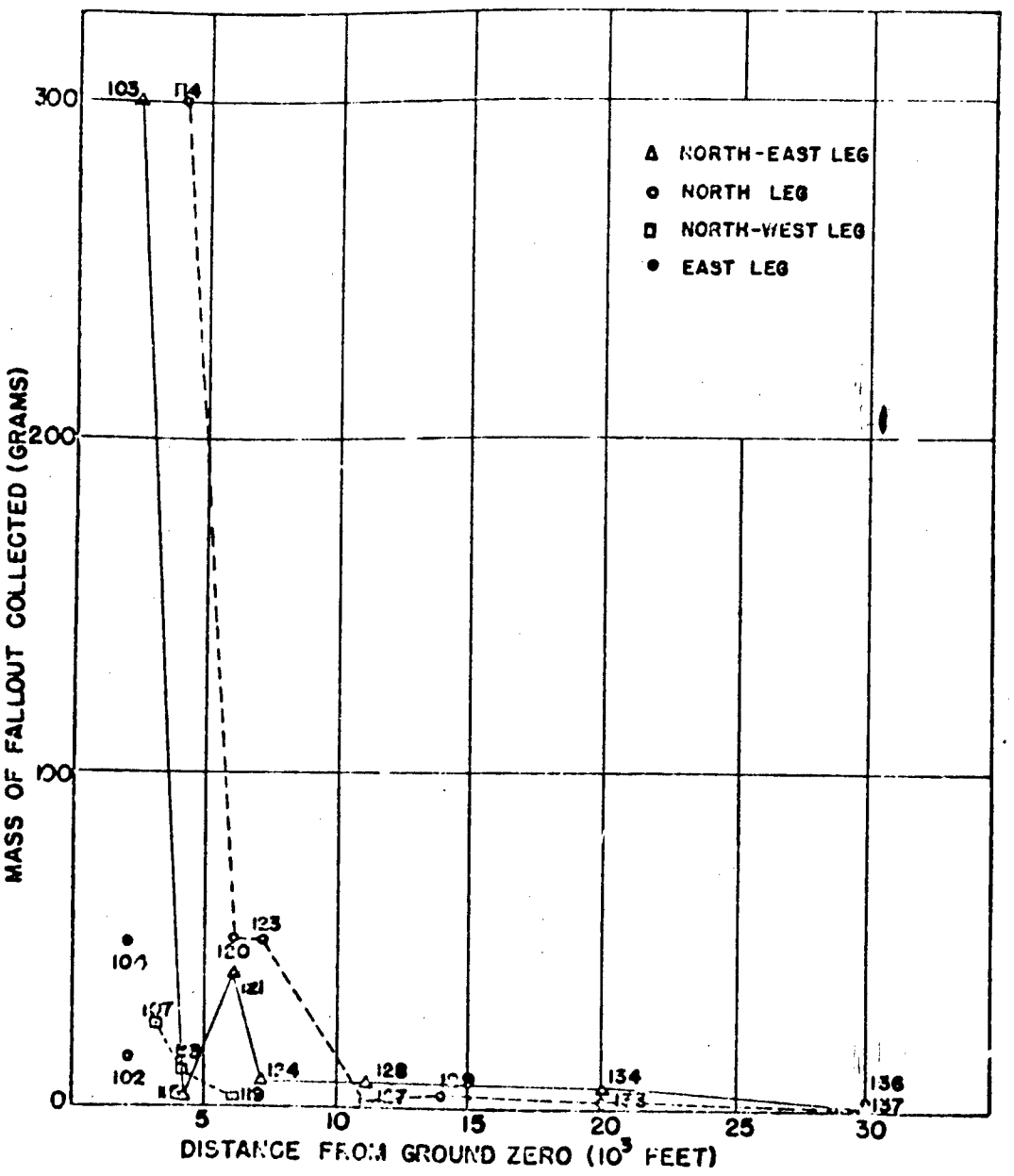

Fig. 4.11 Mass of Material Collected by the Fall-out Trays

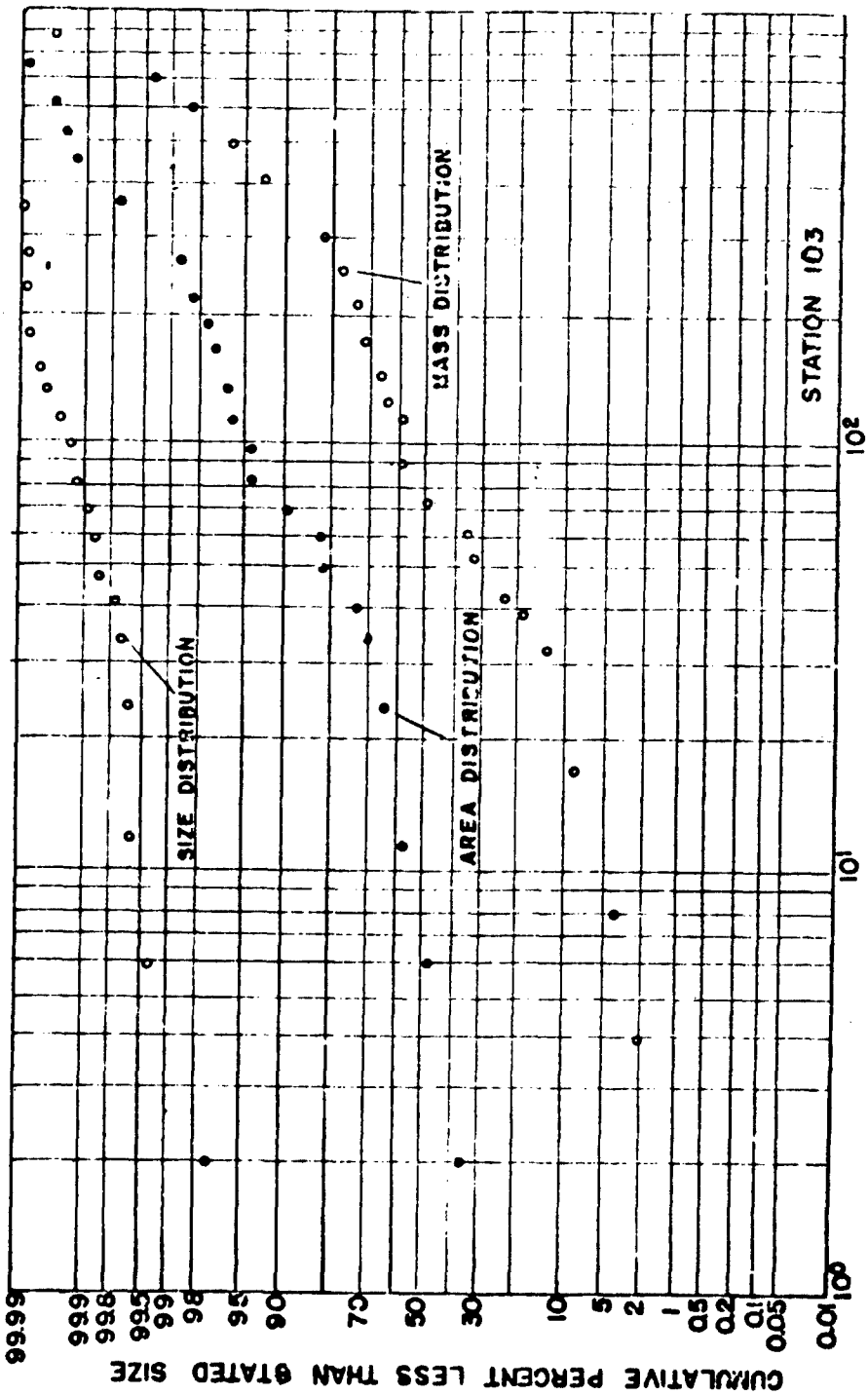

Fig. 4.12 Particle Size Distribution of Fall-out, Underground Shot, Station 103

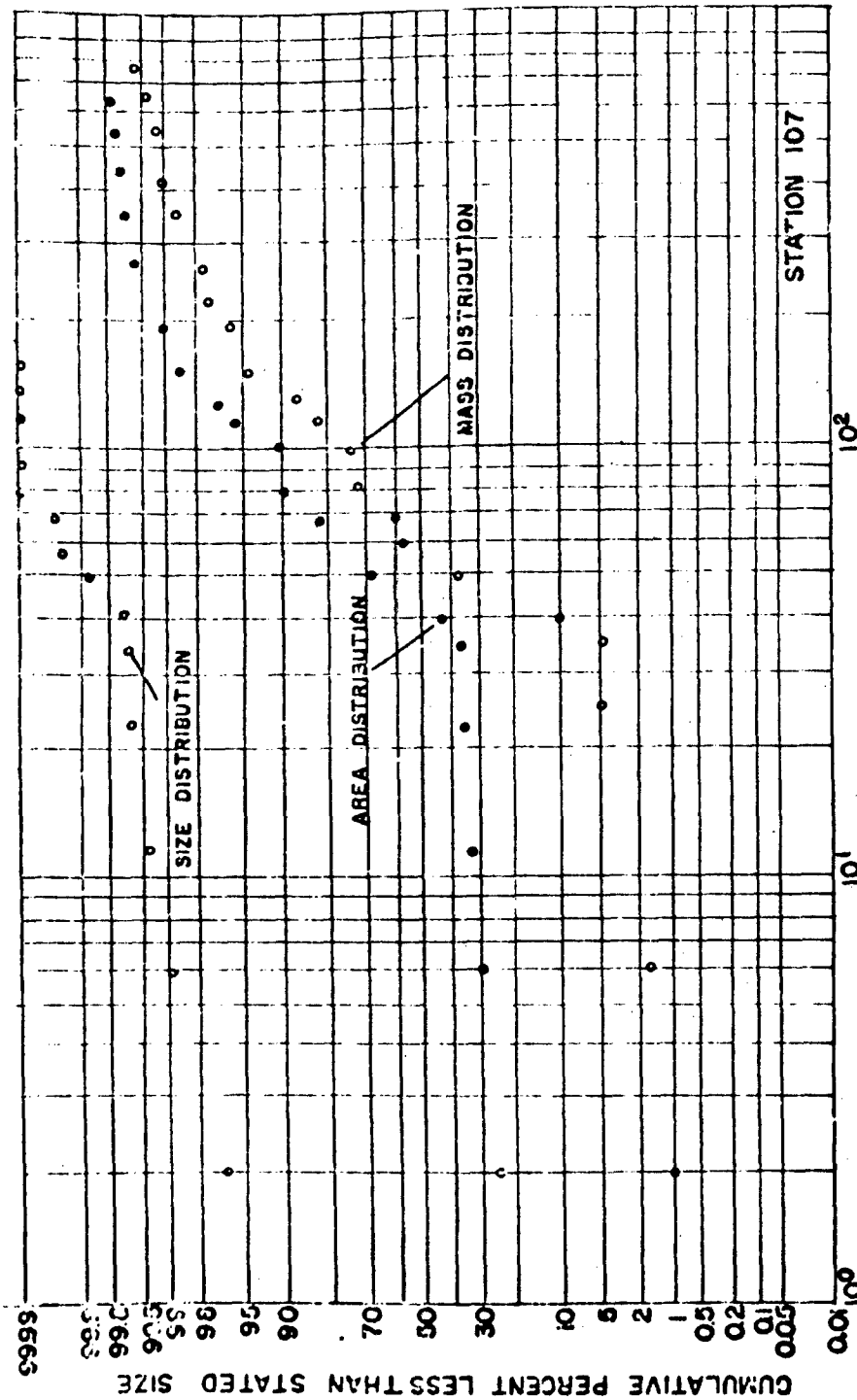

Fig. 4.13 Particle Size Distribution of Fall-out Station 107, Underground Shot

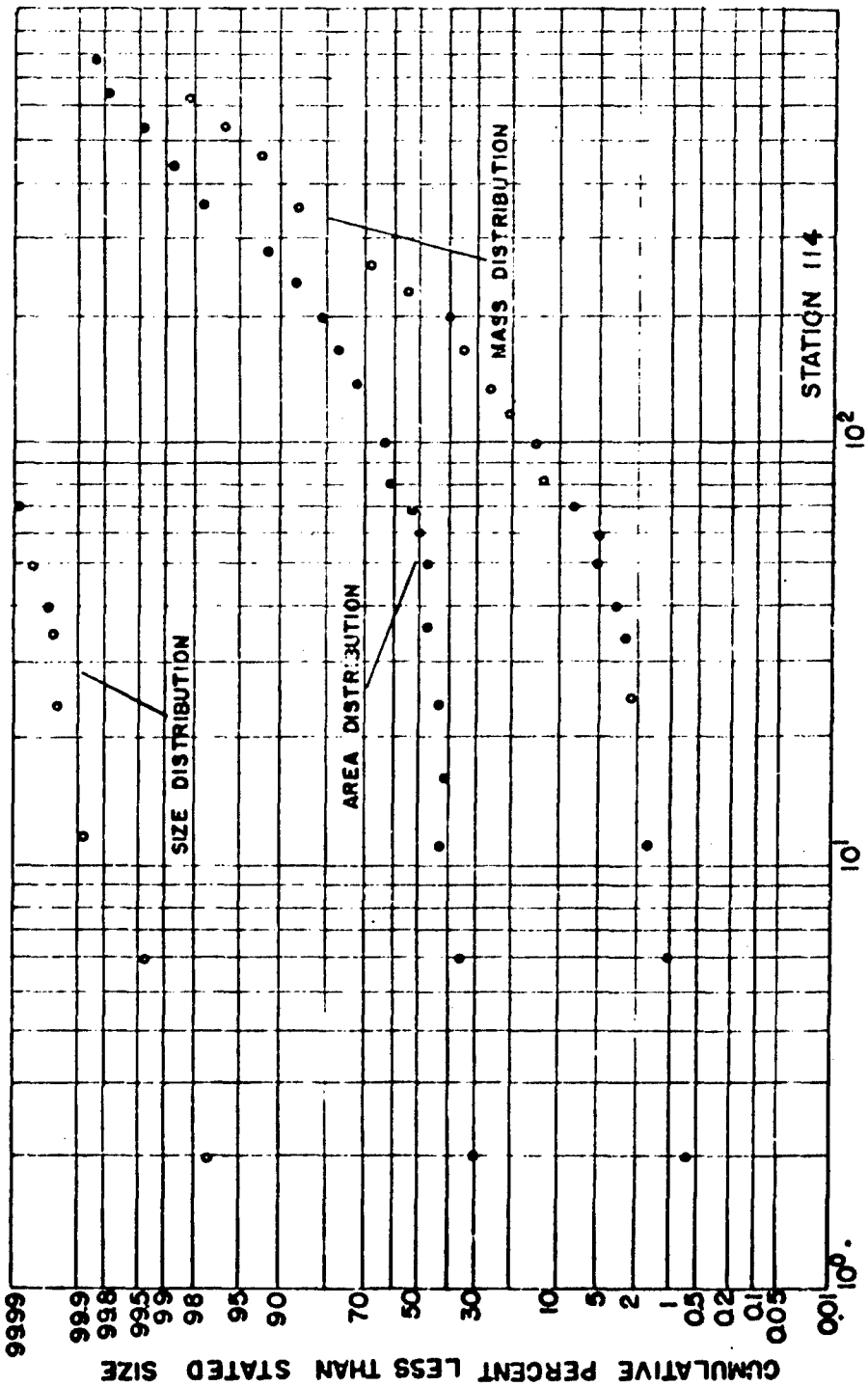

Fig. 4.14 Particle Size Distribution of Fall-out, Station 114, Underground Shot

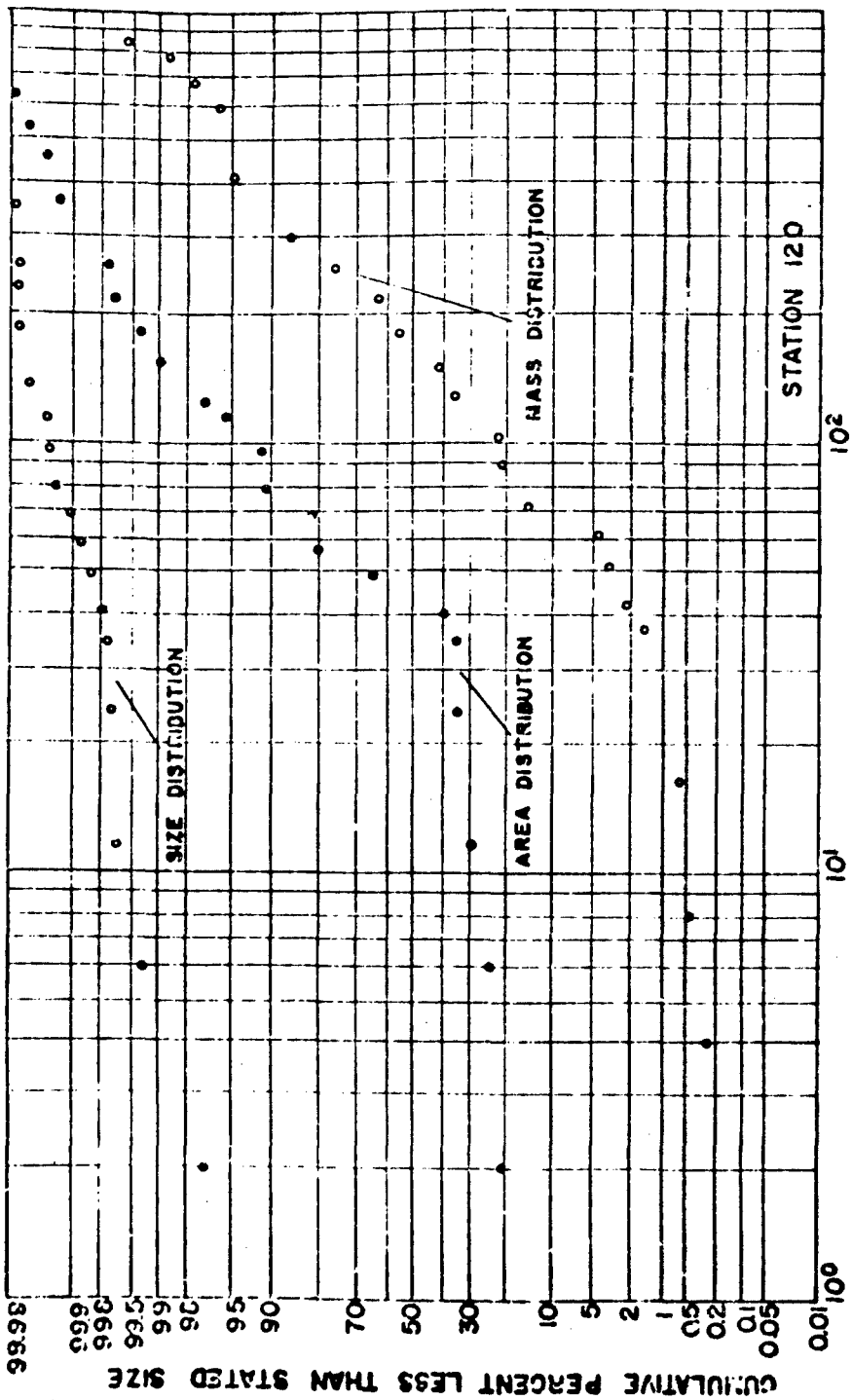

Fig. 4.15 Particle Size Distribution of Fall-out, Station 120, Underground Shot

further fractionation was accomplished with the Roller Analyzer. This machine separated the remaining sieve material into the size fractions 0-4, 4-8, 8-16, and 16-37 microns and the fractions were weighed on an analytical balance.

The basic data obtained in this technique, then, is the weight associated with the various particle size fractions, which may be termed the weight distribution of the fall-out sample. A specific gravity of 2.7 was assumed for all particles, and from the weight distribution the area distribution as well as the size distribution has been computed. It was also assumed that all particles on a given sieve were of a size equal to the average pore size of that sieve and the next higher. All particles were treated as spheres in the calculations.

4.2.4 Pre-Shot Soil Analysis

The particle size distribution of the soil at the test site was determined on six samples taken at five foot depth intervals from a location near the underground shot zero point. These samples were analyzed by the method described in par. 4.2.3; the data are presented in Figs. 4.16 and 4.17.

4.3 RADIOACTIVITY AS A FUNCTION OF PARTICLE SIZE

4.3.1 Cascade Impactor

The activity in the aerosol as a function of particle size was determined from the cascade impactors by measuring the activity on each slide and plotting these data against the particle size impacted on the slide.

The data are tabulated in Tables 4.10 and 4.11 for the surface and underground shots respectively. The activity on each slide, corrected to H/1 hours, is shown in column 4, while the NMD, the measure of the size of particles on that slide, is shown in column 3. The latter data were taken from Tables 4.7 and 4.8. Column 7 shows the specific activity of the particles on each slide as computed by dividing the activity on the slide by the mass of particles on that slide. The latter were obtained by multiplying the "total mass" on each jet in Tables 4.7 and 4.8 by $\pi \rho / 6$, where $\rho = 2.7 \times 10^{-12}$ grams per cubic micron.

A description of the procedures used in making the activity measurements is given in par. 4.1.4.

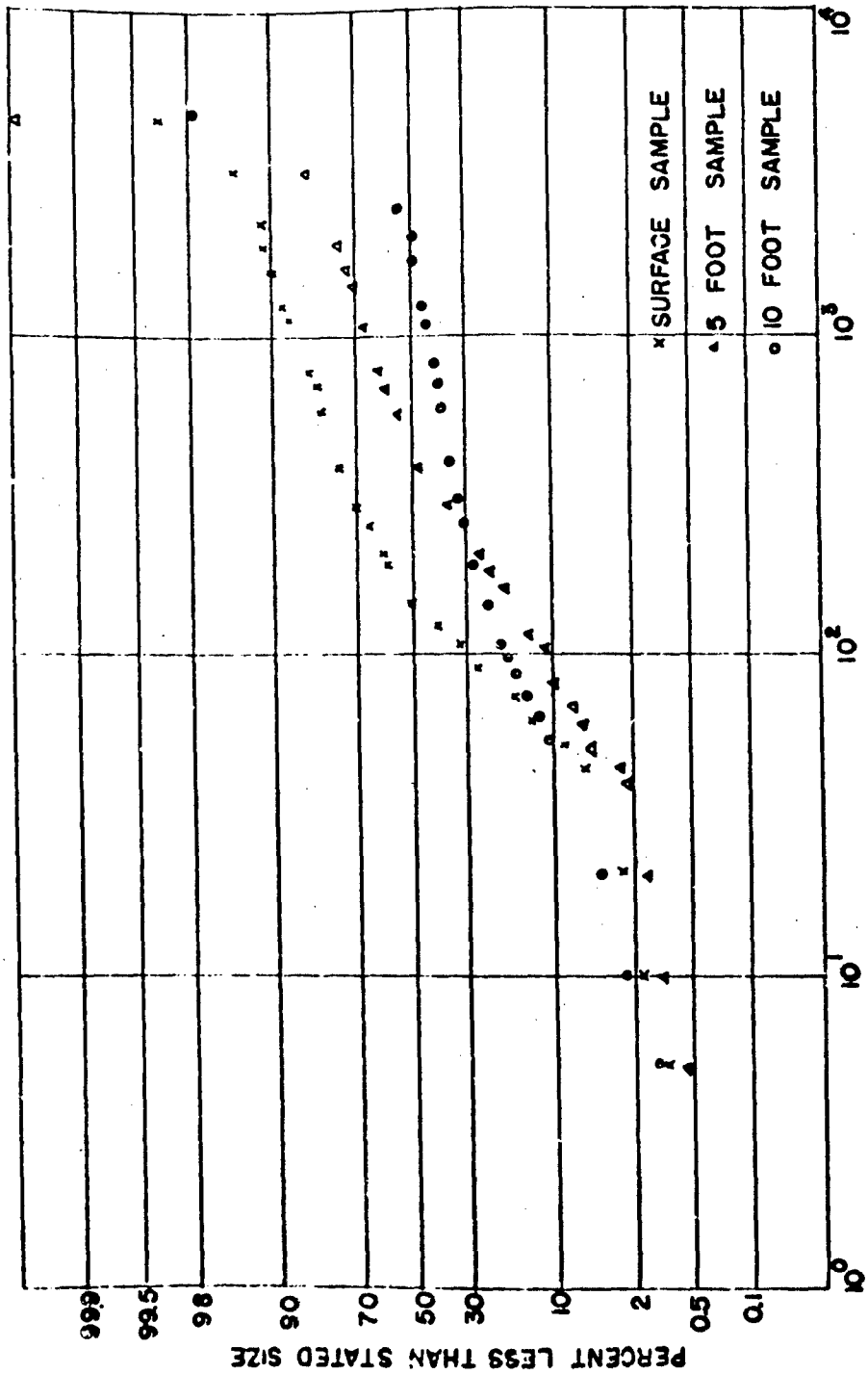

Fig. 4.16 Particle Size Distribution of Pre-shot Soil, Surface, Five and Ten Foot Depths.

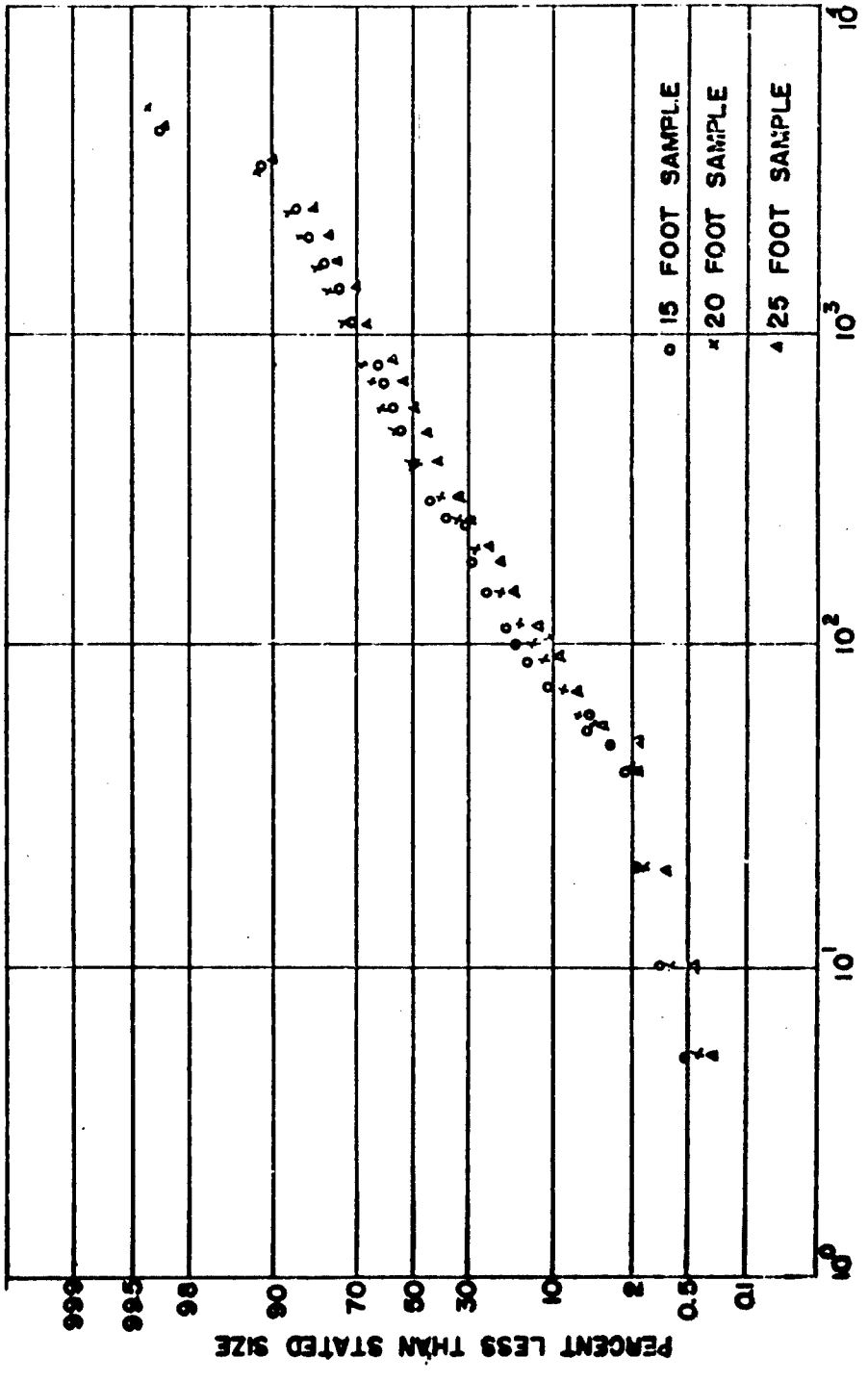

Fig. 4.17 Particle Size Distribution of Pre-shot Soil, Fifteen, Twenty, and Twenty-five Foot Depths

PROJECT 2.5a-1

TABLE 4.10

Surface Shot Activity Measurements on the Cascade Impactor

Station No.	Jet No.	Number Median Diameter (microns)	Activity on Jet at H + 1 Hrs. (μc)	Percentage of Total Cas. Imp. Activity	Mass of Particles on Jet (grams)	Specific Activity $\frac{\mu c}{gram}$
13	1	2.0	3.7×10^{-4}	13.	1.9×10^{-4}	1.9
13	2	0.67	2.2×10^{-3}	80.		
13	3	0.45	1.9×10^{-4}	7.	8.3×10^{-7}	2.3×10^{2}
23	1	0.19	7.5×10^{-4}	40.	7.4×10^{-4}	1.0
23	2	1.6	1.1×10^{-3}	59.	4.6×10^{-4}	2.4
23	4	2.1	2.5×10^{-5}	1.	2.1×10^{-6}	1.2×10^{1}
25	1	2.7	1.1×10^{-4}	51.	2.1×10^{-4}	5.2×10^{-1}
25	2	2.2	6.7×10^{-5}	32.	3.3×10^{-5}	2.1
25	5	0.44	3.6×10^{-5}	16.	7.6×10^{-7}	4.7×10^{1}
26	1	6.3	2.7×10^{-4}	3.	7.1×10^{-5}	3.8
26	2	1.0	4.4×10^{-3}	41.	3.2×10^{-6}	1.4×10^{2}
26	3	0.50	4.8×10^{-3}	44.	4.0×10^{-6}	1.2×10^{3}
26	4	0.32	7.0×10^{-4}	6.	1.6×10^{-6}	4.5×10^{2}
26	5	0.09	6.3×10^{-4}	6.	1.5×10^{-7}	4.3×10^{3}
30	1	0.94	7.0×10^{-4}	2.	2.3×10^{-4}	3.0
30	2	1.4	9.0×10^{-3}	32.	6.7×10^{-6}	1.3×10^{3}
30	3	1.0	1.4×10^{-2}	48.	2.4×10^{-6}	5.7×10^{3}
30	4	0.64	3.2×10^{-3}	11.	7.3×10^{-7}	4.4×10^{3}
30	5	0.05	1.9×10^{-3}	7.	5.6×10^{-9}	3.4×10^{5}
35	1	3.8	1.6×10^{-3}	6.	3.6×10^{-4}	4.4
35	2	2.1	5.5×10^{-3}	22.	3.3×10^{-5}	1.7×10^{2}
35	3	1.4	1.2×10^{-2}	48.	4.7×10^{-6}	2.6×10^{3}
35	4	0.83	5.2×10^{-3}	21.	1.3×10^{-6}	3.9×10^{3}
35	5	0.10	7.0×10^{-4}	3.	9.1×10^{-8}	7.7×10^{3}
40	1	1.5	1.8×10^{-4}	3.	6.9×10^{-5}	2.6
40	2	1.9	2.1×10^{-3}	35.	2.5×10^{-6}	8.5×10^{2}
40	3	1.5	1.8×10^{-3}	30.	1.9×10^{-6}	9.1×10^{2}
40	4	0.71	1.2×10^{-3}	20.	9.7×10^{-7}	1.2×10^{3}
40	5	0.03	7.0×10^{-4}	12.	1.4×10^{-8}	1.6×10^{4}

PROJECT 2.5a-1

TABLE 4.11

Underground Shot Activity Measurements on the Cascade Impactor

Station No.	Jet No.	Number Median Diameter (microns)	Activity on Jet at H +1Hrs. (μc)	Percentage of Total Cas. Imp. Activity	Mass of Particles on Jet (grams)	Specific Activity $\frac{\mu c}{gram}$
113	1	0.91	1.4×10^{-4}	8.	5.4×10^{-5}	2.6
113	2	1.3	5.4×10^{-4}	32.	2.2×10^{-6}	2.4×10^{2}
113	3		3.5×10^{-4}	20.		
113	4		3.5×10^{-4}	20.		
113	5		3.4×10^{-4}	20.		
114	1	1.7	9.9×10^{-4}	13.	1.3×10^{-4}	7.9
114	2	1.4	2.9×10^{-3}	39.	1.4×10^{-6}	2.0×10^{3}
114	3	1.0	1.5×10^{-3}	19.	6.9×10^{-7}	2.1×10^{3}
114	4	0.74	1.3×10^{-3}	17.	6.1×10^{-7}	2.1×10^{3}
114	5		8.5×10^{-4}	12.		
115	1	3.3	2.8×10^{-3}	78.	6.2×10^{-6}	4.4×10^{2}
115	2	1.7	2.3×10^{-4}	7.	2.5×10^{-5}	9.1
115	3		1.2×10^{-4}	3.		
115	4		1.7×10^{-4}	5.		
115	5		2.5×10^{-4}	7.		
119	1	1.1	7.8×10^{-4}	44.	5.9×10^{-5}	1.3×10^{1}
119	2	1.0	2.8×10^{-4}	16.	1.5×10^{-6}	1.8×10^{2}
119	3		4.4×10^{-4}	24.		
119	4		2.2×10^{-4}	12.		
119	5		7.0×10^{-5}	4.		
124	1	0.81	1.7×10^{-4}	9.	5.2×10^{-6}	3.3×10^{1}
124	2	1.2	8.5×10^{-4}	46.	9.3×10^{-7}	8.7×10^{2}
124	3		6.2×10^{-4}	34.		
124	4		1.9×10^{-4}	10.		
124	5		2.2×10^{-5}	1.		

TABLE 4.11

Underground Shot Activity Measurements on the Cascade Impactor (Contd)

Station No.	Jet No.	Number Median Diameter (microns)	Activity on Jet at H + 1 Hrs. (μc)	Percentage of Total Cas. Imp. Activity	Mass of Particles on Jet (grams)	Specific Activity $\frac{\mu c}{gram}$
125	1	1.9	5.6×10^{-4}	50.	2.6×10^{-4}	2.1
125	2	0.68	9.5×10^{-5}	8.	2.5×10^{-6}	3.8×10^{1}
125	3		6.7×10^{-5}	6.		
125	4		3.2×10^{-4}	29.		
125	5		8.3×10^{-5}	7.		
126	1		3.1×10^{-5}	5.		
126	2		3.2×10^{-5}	6.		
126	3		7.7×10^{-5}	14.		
126	4		7.2×10^{-5}	13.		
126	5		3.5×10^{-4}	62.		
132	1	2.5	1.9×10^{-5}	24.	1.3×10^{-5}	1.4
132	2	1.4	1.8×10^{-5}	22.	1.1×10^{-6}	1.7×10^{1}
132	5	0.18	4.3×10^{-5}	54.	4.2×10^{-8}	1.0×10^{3}
135	1	0.49	9.5×10^{-5}	25.	1.1×10^{-5}	8.5
135	2	0.70	6.1×10^{-5}	16.	1.8×10^{-6}	3.4×10^{1}
135	3	1.12	1.8×10^{-5}	5.	1.1×10^{-6}	1.6×10^{1}
135	4	0.14	1.5×10^{-4}	39.	1.9×10^{-7}	7.8×10^{2}
135	5	0.053	6.0×10^{-5}	15.	1.2×10^{-8}	5.0×10^{3}
140	1	1.26	1.7×10^{-4}	7.	3.0×10^{-5}	5.6
140	2	0.81	9.5×10^{-5}	4.	2.6×10^{-6}	3.6×10^{1}
140	3	0.73	1.4×10^{-3}	60.	1.2×10^{-6}	1.1×10^{3}
140	4	0.18	4.9×10^{-4}	22.	2.8×10^{-7}	1.7×10^{3}
140	5	0.12	1.6×10^{-4}	7.	3.0×10^{-8}	5.3×10^{3}

4.3.2 Conifuge

By means of a radioautograph technique, it was possible to determine the activity in the aerosol as a function of particle size (subject to the limitations of the conifuge). Unfortunately, of all the conifuge cones employed, only the one from station 133, located 20,000 feet north of the underground zero point, exhibited what could be considered a good radioautograph pattern. The majority were not sufficiently active to produce a definite film darkening while most of those that were sufficiently active produced irregular patterns, indicating improper operation of the instrument.

The technique consisted of placing the plastic conifuge cone over a matching conical mandrel upon which was fitted a fan-shaped piece of DuPont dosimeter film, type 552. After an exposure of approximately one month, the cones were removed and the film processed. This radioautograph (Fig. 4.18) was scanned along several radii with an Ansco optical densitometer (after standardizing on the clear film) at a number of distances from the inner edge of the fan shaped film. The averaged optical densities were plotted versus r, the distance from the inner edge of the film. This plot was graphically integrated and normalized to a fractional density and plotted versus r as shown in Fig. 4.19. Assuming that the density of the film was proportional to the radioactivity deposited upon the conifuge cone, and the density of the aerosol was similar to glass, the percent activity of the aerosol as a function of particle size can be obtained by use of the data of Table 2.5. In addition, these data were plotted on log probability paper as shown in Fig. 4.20.

Upon the basis of the results from this conifuge, it may be concluded that the median radioactive particle size of the aerosol at station 133 was of the order of two microns.

4.3.3 Particle Separator

Although a determination of the activity of the aerosol as a function of particle size from the particle separator would have been a relatively easy matter and, indeed, the necessary activity measurements were made, no results are reported because the instrument failed to separate particles satisfactorily according to their size.

Microscopic examination of the particle separator screens revealed that the larger screens collected a considerable amount of fine ($< 37\,\mu$) airborne particles while the larger material ($> 37\,\mu$) behaved normally in passing through the various meshed screens. This effect can be seen by examination of Figs. 4.21 and 4.22, which are photomicrographs of the first screen of the particle separator at station 123, taken at different magnifications. Figure 4.21 shows the large particles which

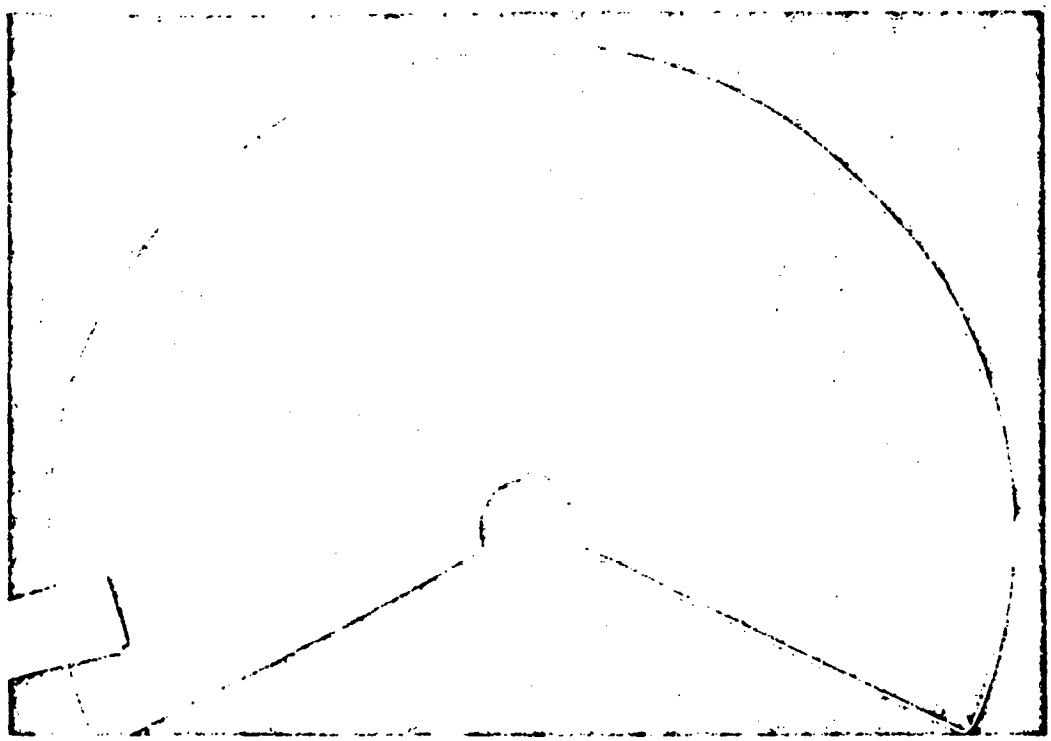

Fig. 4.18 Radioautograph of Conifuge Cone, Station 133, Underground Shot. This is Actually a Positive Print. The Dark Radial Lines Were Caused By the Use of Scotch Tape to Obtain Samples of the Collected Particles. The Dark Dots Were Caused By the Electron Microscope Screens.

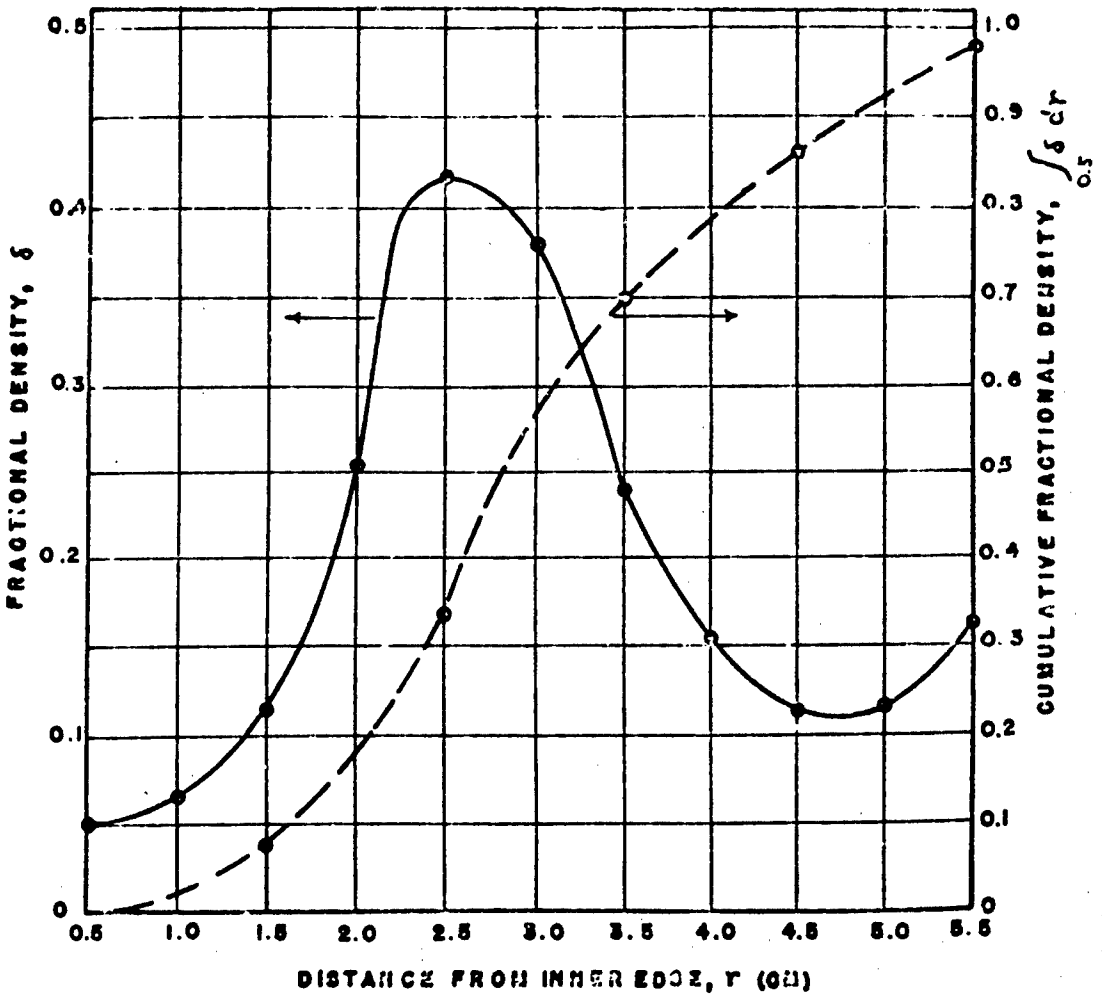

Fig. 4.19 Fractional Density and its Integral, Station 133, Underground Shot, Conifuge Data.

PROJECT 2.5a-1

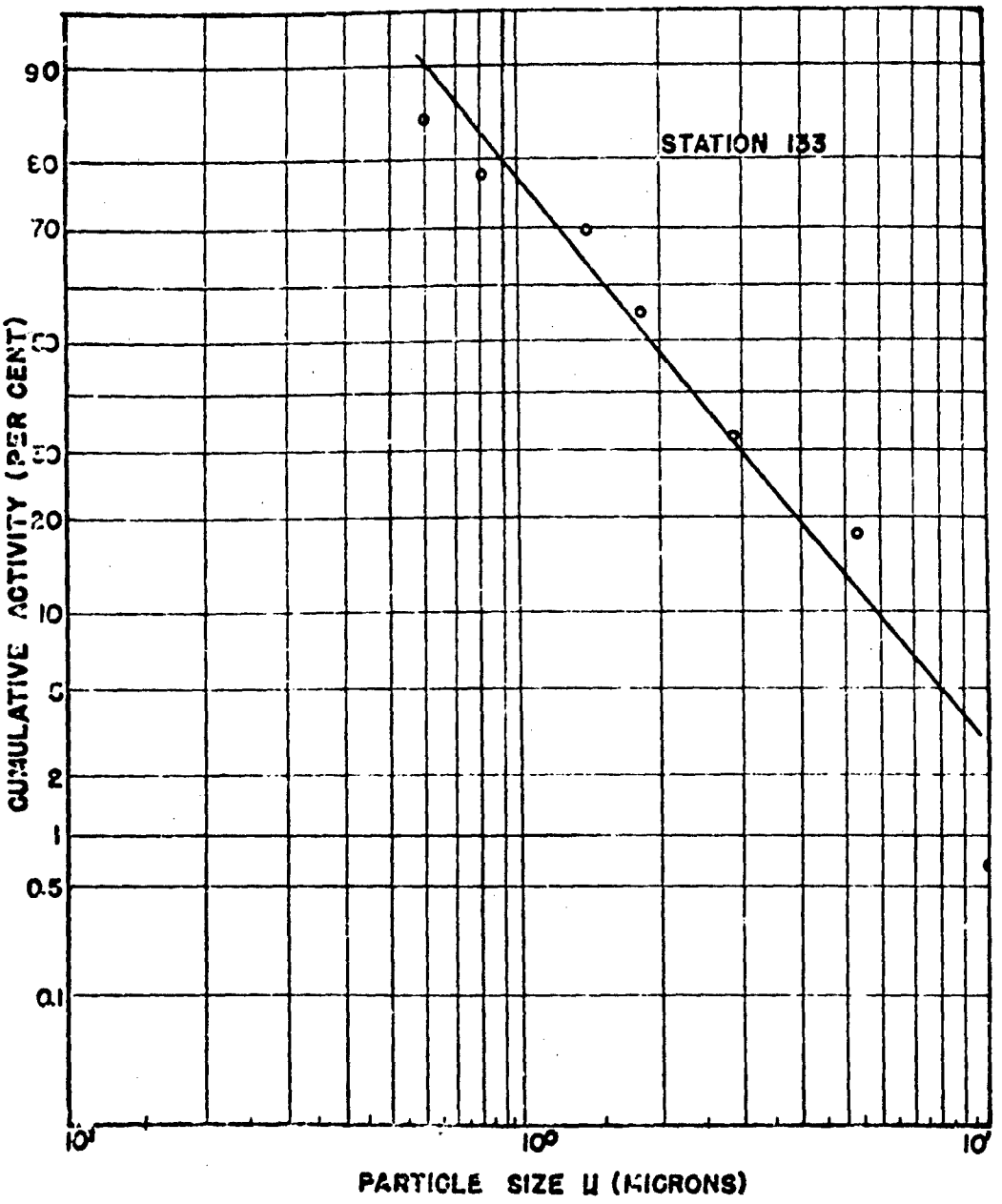

Fig. 4.20 Cumulative Percent Activity as a Function of Particle Size, Station 133, Underground Shot, Conifuge Data.

Fig. 4.21 Photomicrograph of the First Screen of the Particle Separator at Station 123, at 20x Magnification. The Large Particles are Apparent.

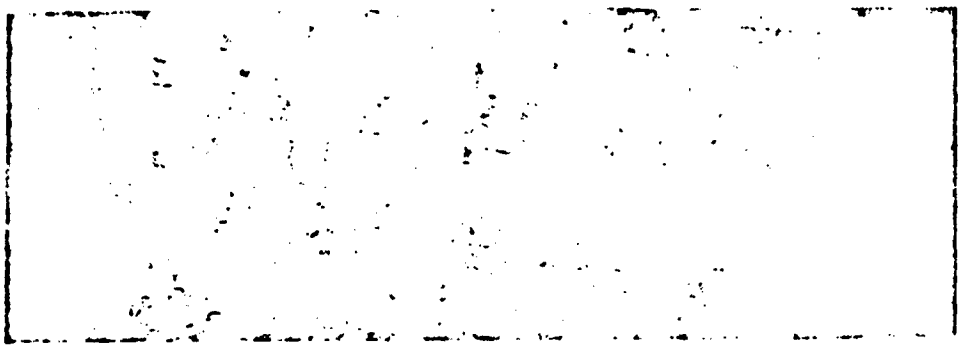

Fig. 4.22 Photomicrograph of the First Screen of the Particle Separator at Station 123, at 50x Magnification. The Small Particles May be Seen Adhering to the Screen Wires.

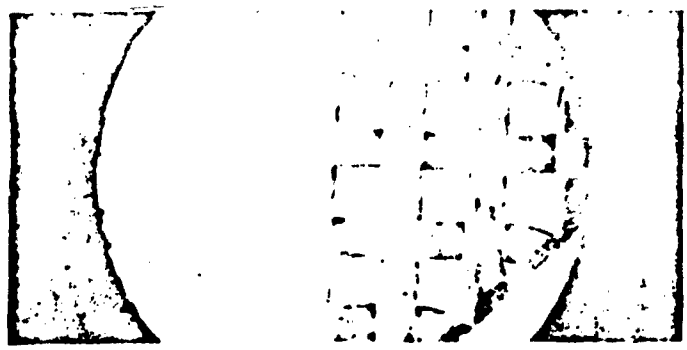

Fig. 4.23 Photomicrograph of a Clean Particle Separator Screen.

were stopped by the screen, while Fig. 4.22 shows the small particles that also adhered to the screen. For comparison purposes a photomicrograph of a clean screen has been included in Fig. 4.23. It was noted that the large mesh screens were densely covered, front and rear, by a layer of the order of one to ten microns, while the smaller mesh screens were almost entirely free of particulate matter. Activity measurements and microscopic examination of the porous stainless steel back-up filters indicated, however, that a considerable number of particles passed all screens.

The only plausible explanation of this anomaly so far advanced is that the air passing through the screens builds up an electrostatic charge on the well insulated metal screens sufficient to attract and remove from the air stream those particles with suitable charge and inertia values while permitting the neutral and oppositely charged particles to pass through the screens until mechanically stopped by the back-up filter.

In order to test this hypothesis, attempts were made in this laboratory to measure electrostatic charge built up by the particle separator screens while air passed through at the correct rate. A charge of the order of a volt was indicated by an oscilloscope after several minutes of air flow. While it is conceivable that in the drier climate at the Nevada Test Site a somewhat higher electrostatic potential might be attained, it would appear that the electrostatic theory is untenable unless the particulate matter in the JANGLE aerosols was highly charged.

4.3.4 Fall-out Tray

Activity measurements were made on the particle size fractions obtained in the sieve analysis (see par. 4.2.3) of one fall-out tray from the surface shot and eight trays from the underground shot, and from these data the activity of the fall-out as a function of particle size has been determined. Figs. 4.24 through 4.29 show in cumulative fashion the percentage of activity associated with each particle size fraction, the data from stations at the same radial distance being shown on the same graph. Table 4.12 shows the specific activity, corrected to H/1 hour, of the particle size fractions of four stations from the underground shot.

The activity measurements were made by means of a Tracerlab SC-5a automatic sample changer and associated equipment. Aliquots of each particle size fraction were transferred to the counting planchets and coated with collodion to prevent loss in handling. A Tracerlab TBC-1 Geiger tube having a window thickness of 2.48 mg/cm^2 was

PROJECT 2.5a-1

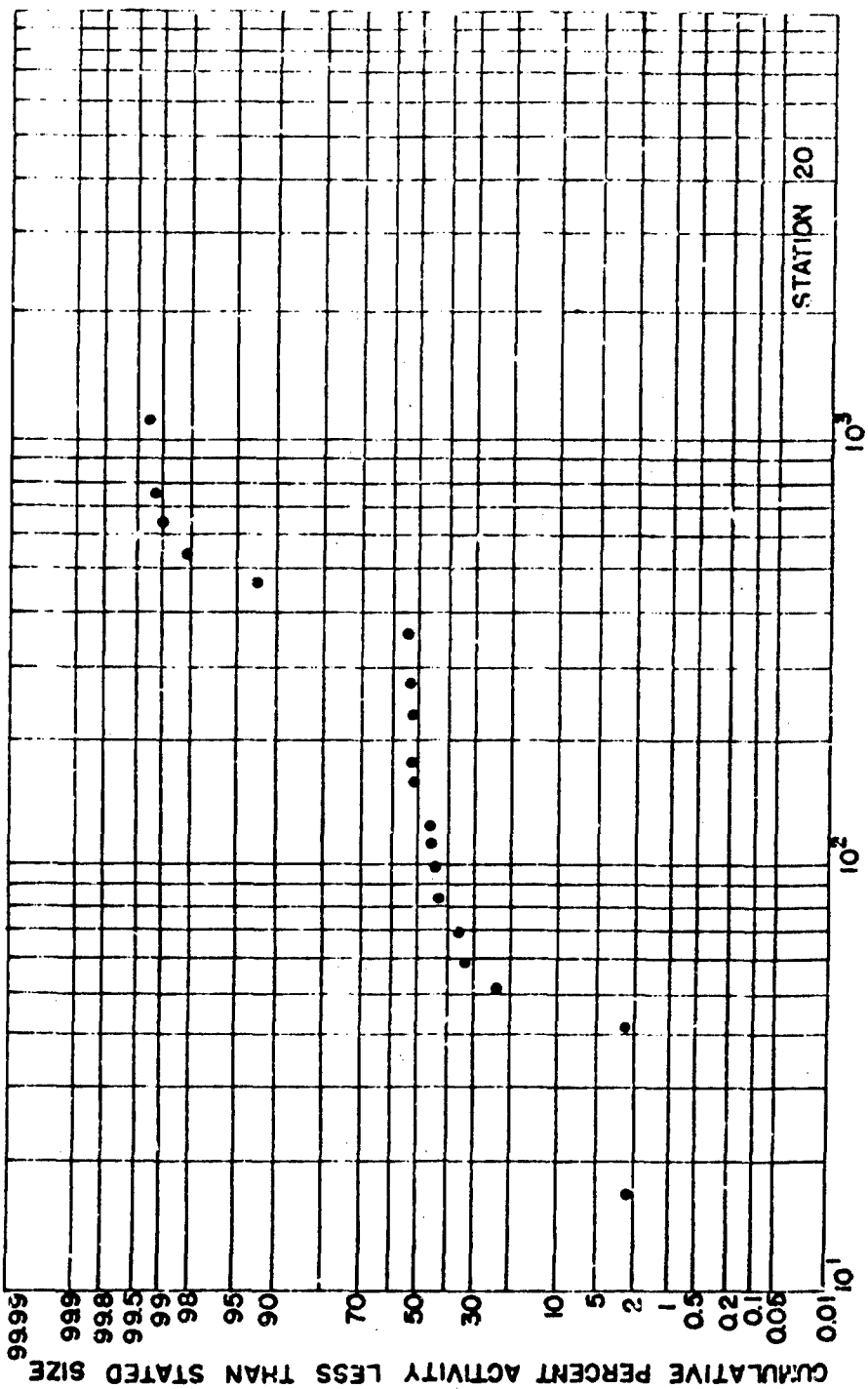

Fig. 2.24 Fall-out Activity as a Function of Particle Size, Station 20, Surface Shot.

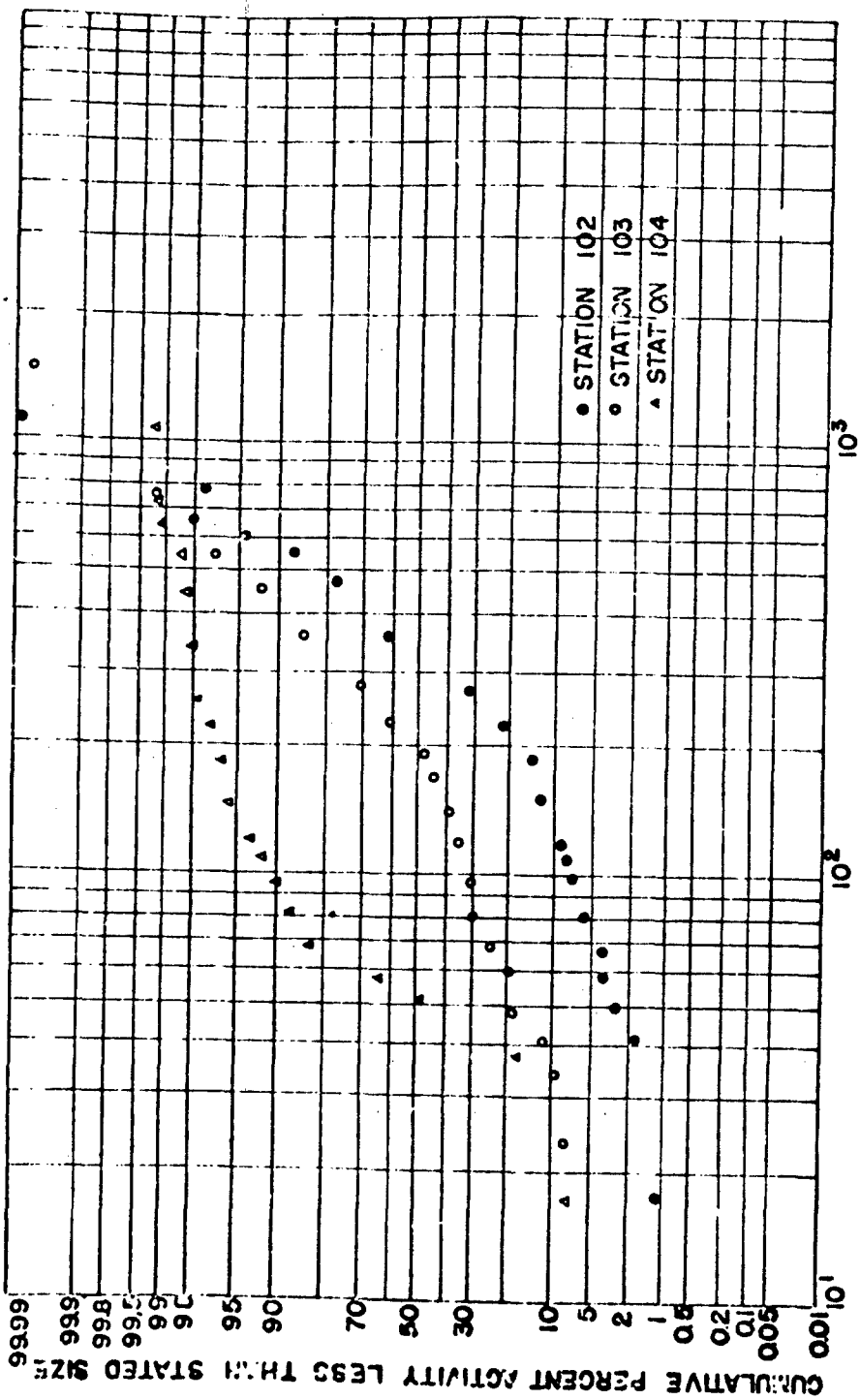

Fig. 4.25 Fall-out Activity as a Function of Particle Size, 2000 Foot Radius, Underground Shot.

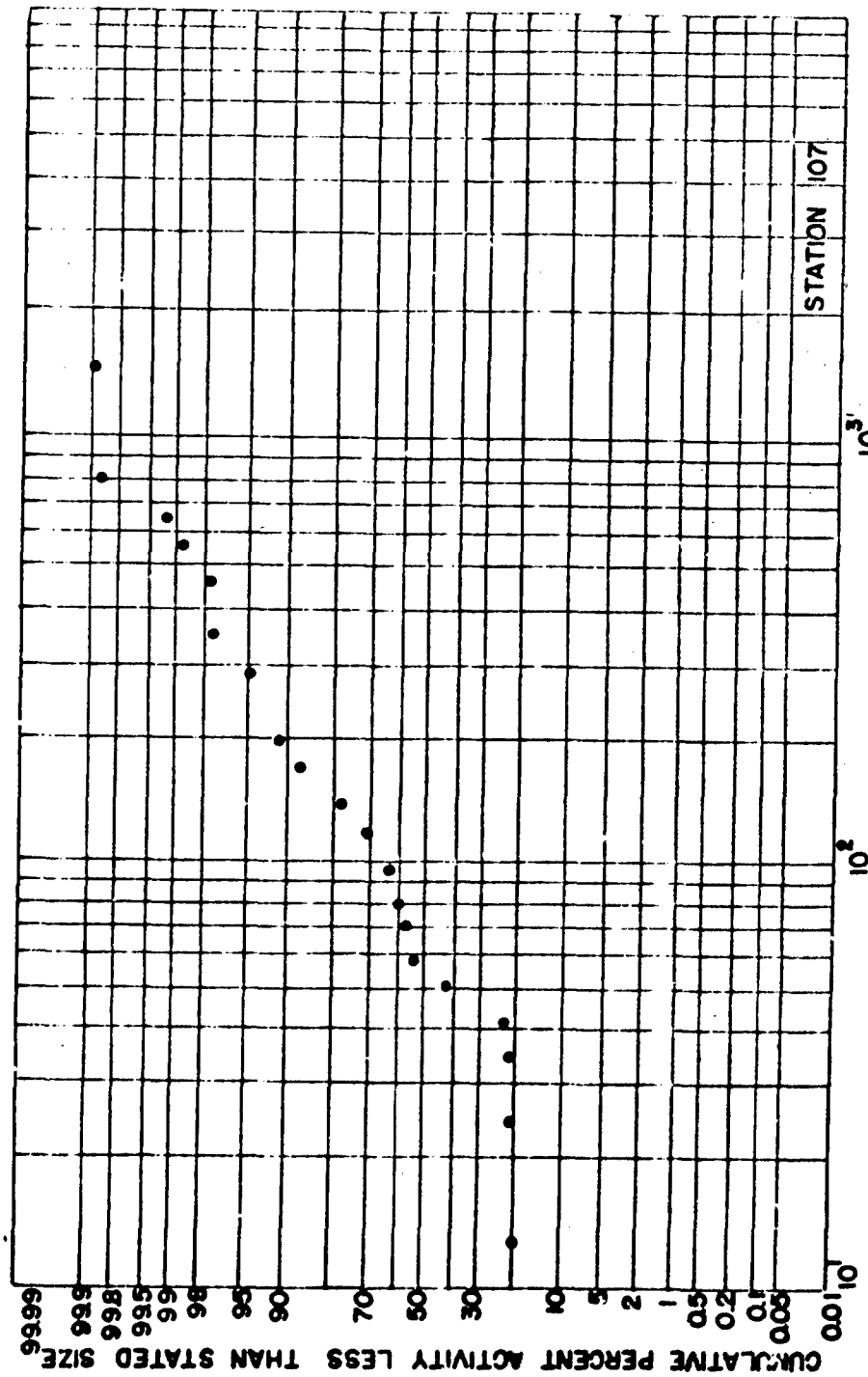

Fig. 4.26 Fall-out Activity as a Function of Particle Size, 3000 Foot Radius, Underground Shot.

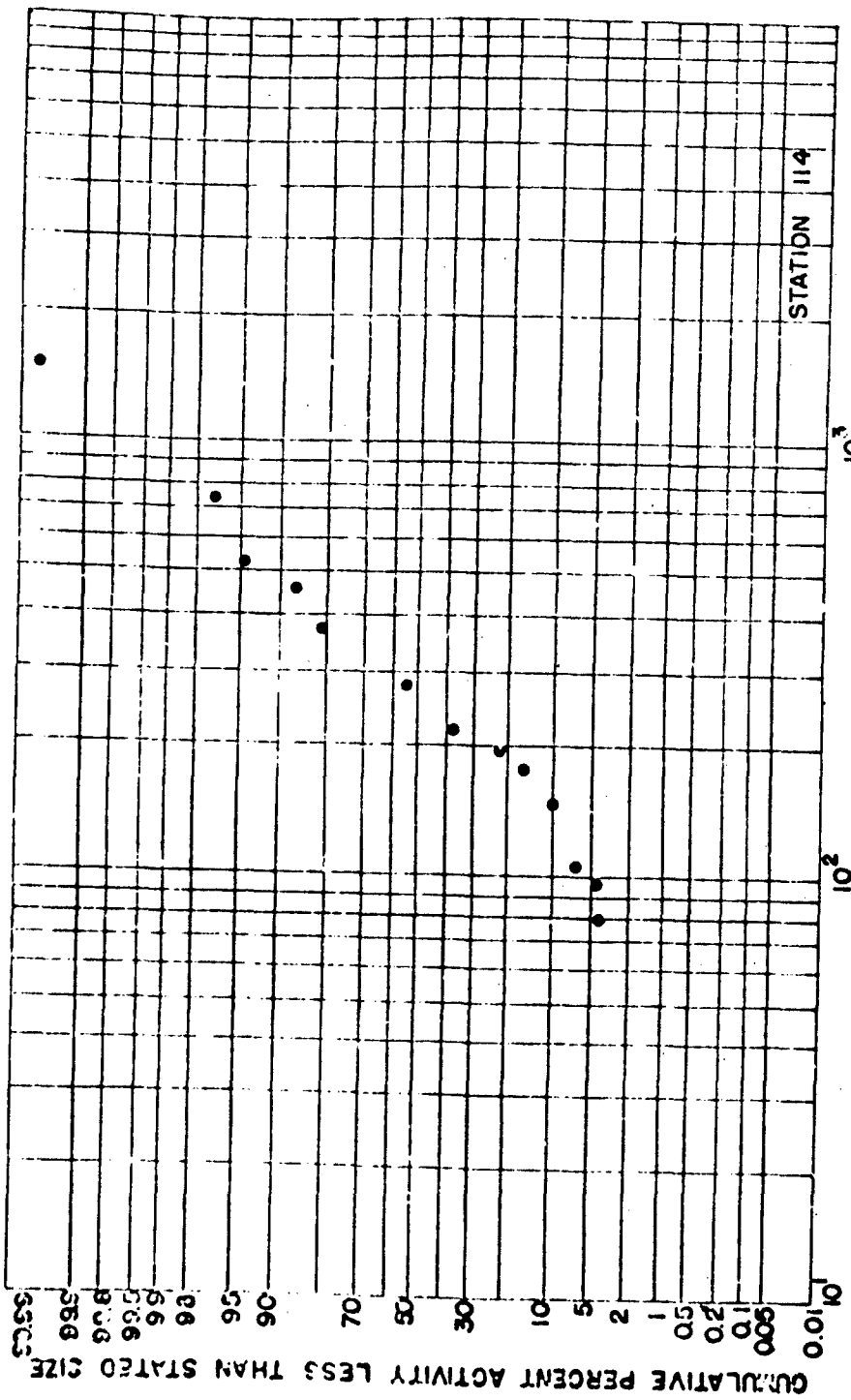

Fig. 2.27 Fall-out Activity as a Function of Particle Size, 4000 Foot Radius, Underground Shot.

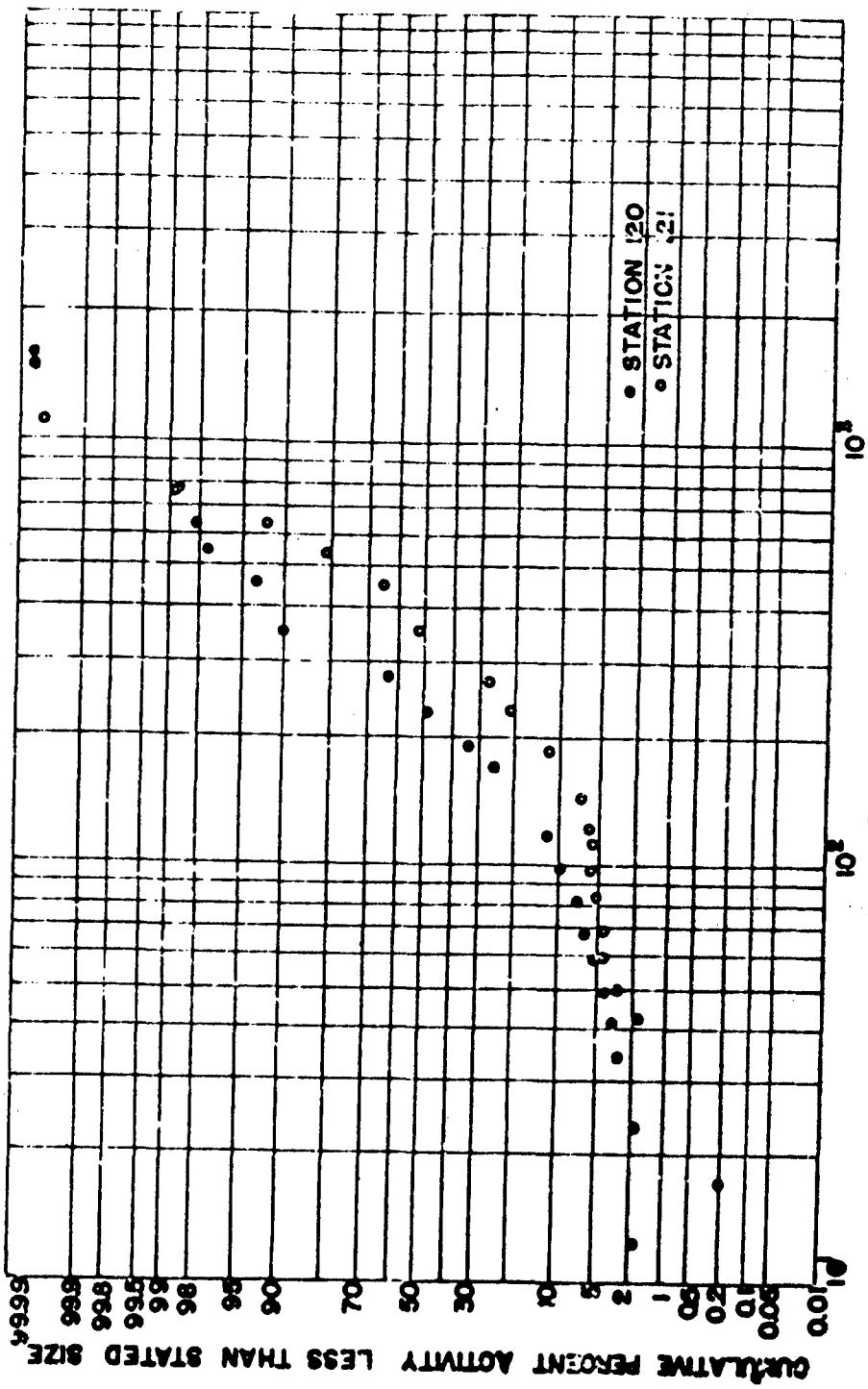

Fig. 4.28 Fall-out Activity as a Function of Particle Size, 6000 Foot Radius, Underground Shot.

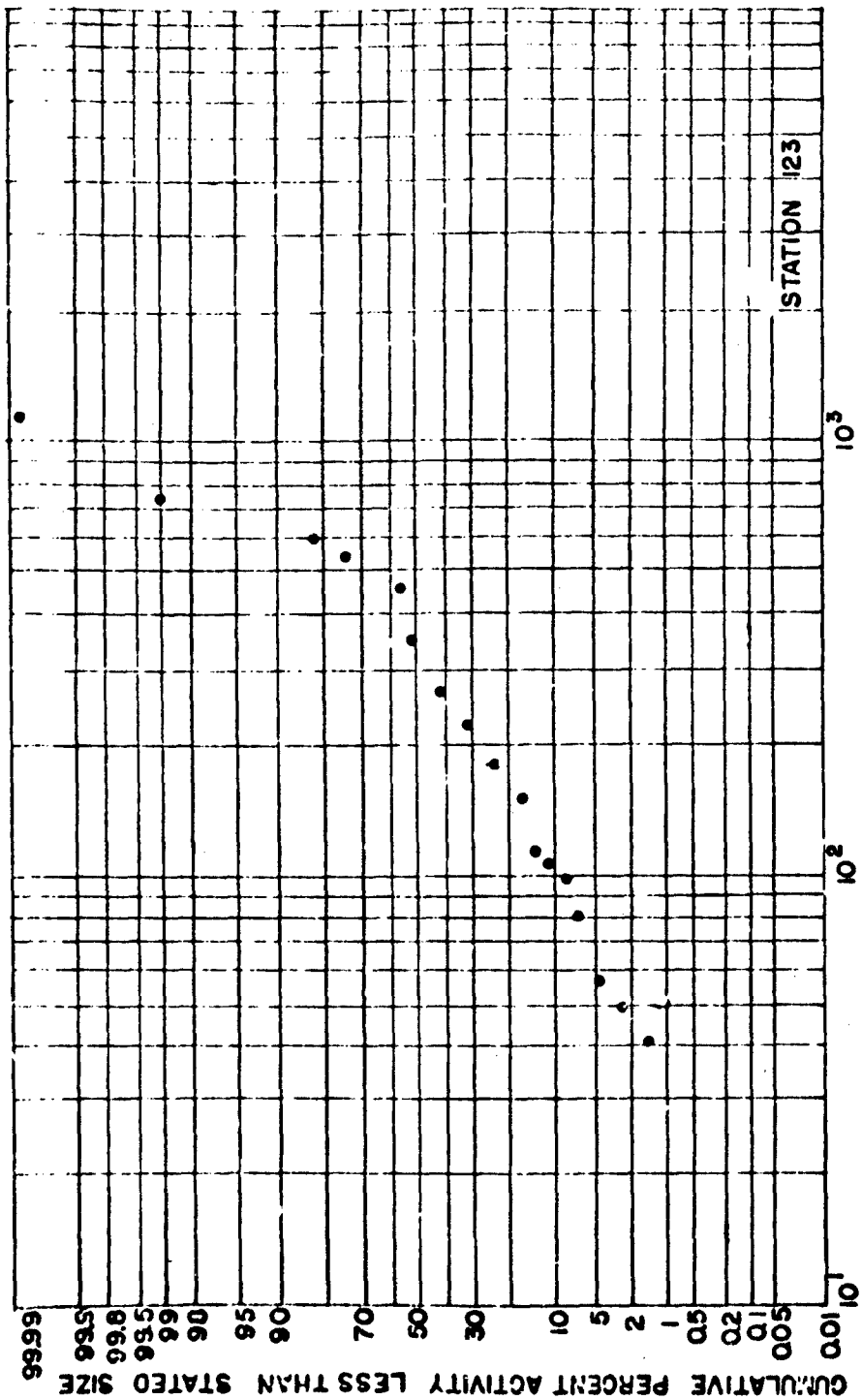

Fig. 4.29 Fall-out Activity as a Function of Particle Size, 8000 Foot Radius, Underground Shot.

PROJECT 2.5c-1

TABLE 4.12

Specific Activity Corrected to H+1, of Fall-out,
Underground Shot

Particle Size (microns)	Station 103 (10^{-1} uc/gm)	Station 107 (10^{-1} uc/gm)	Station 114 (10^{-1} uc/gm)	Station 120 (10^{-1} uc/gm)
2	51.	36.	28.	48.
6	30.	26.	19.	24.
12	14.	19.	10.	19.
24	10.	12.	8.5	17.
34	7.5	8.7	8.6	11.
40	16.	10.	12.	16.
48	17.	10.	8.8	11.
58	24.	8.4	6.2	11.
68	12.	9.1	7.6	8.3
81	13.	7.2	7.8	5.7
96	11.	15.	1.0	6.5
115	26.	13.	13.	11.
137	42.	17.	22.	14.
163	44.	23.	22.	16.
194	48.	25.	32.	19.
230	48.	27.	34.	30.
274	71.	115.	35.	32.
358	77.	33.	41.	39.
460	43.	32.	39.	22.
545	69.	43.	46.	30.
650	80.	64.	40.	43.
775	38.	72.	44.	52.
1500	360.	18×10^{-2}	51.	25.

employed, and the scaler was preset for a cumulative count of 4096 for each sample. A Tracerlab R-11a simulated P^{32} source was used as a reference standard for absolute beta counting. Range curves in aluminum were run for the standard and several fall-out samples to determine correction factors for air path and window losses. Back scattering and possible collodion absorption corrections were not attempted. All activity measurements were made between 1000 and 2000 hours after the shot and were corrected to H-1000 by means of individual decay curves obtained on each sample. The NIH decay curves described in par. 4.1.1 were used to correct all fractions from H/1000 hours to H/1 hour.

4.4 PERCENTAGE OF RADIOACTIVE PARTICLES

4.4.1 Cascade Impactor

The number of active particles on each of the five slides from the cascade impactors at stations 123 and 130 was determined by means of a radioautograph technique. Since the particle size analysis of the cascade impactors (par. 4.2.1) yielded the total number of particles per slide, the percentage of radioactive particles could be determined. The data are presented in Figure 4.30.

The radioautographs were made after the particle size measurements were completed since the emulsion on the slides would have interfered with the electron microscope particle size analysis. Eastman Kodak Company type NTB stripping film was cut to size and cemented over the sample area of the slide. Development of the film was carried out as recommended by Eastman Kodak Company. The radioautographs were then examined by means of a microscope to determine the number of particles with associated activity. The slides from station 123 were exposed from H/1704 to H/2208 hours; station 130 slides from H/1704 to H/2016. Although other slides were exposed for an even greater length of time, too few of the particles on each slide were sufficiently active to provide reliable results.

4.4.2 Fall-out Tray

The size fractions of the fall-out from stations 103 and 120 of the underground shot were analyzed by a radioautograph technique to determine the percentage of radioactive particles. The data are presented in Fig. 4.31. The size fractions were obtained from the sieve analysis described in par. 4.2.3, and the radioautograph technique is described below.

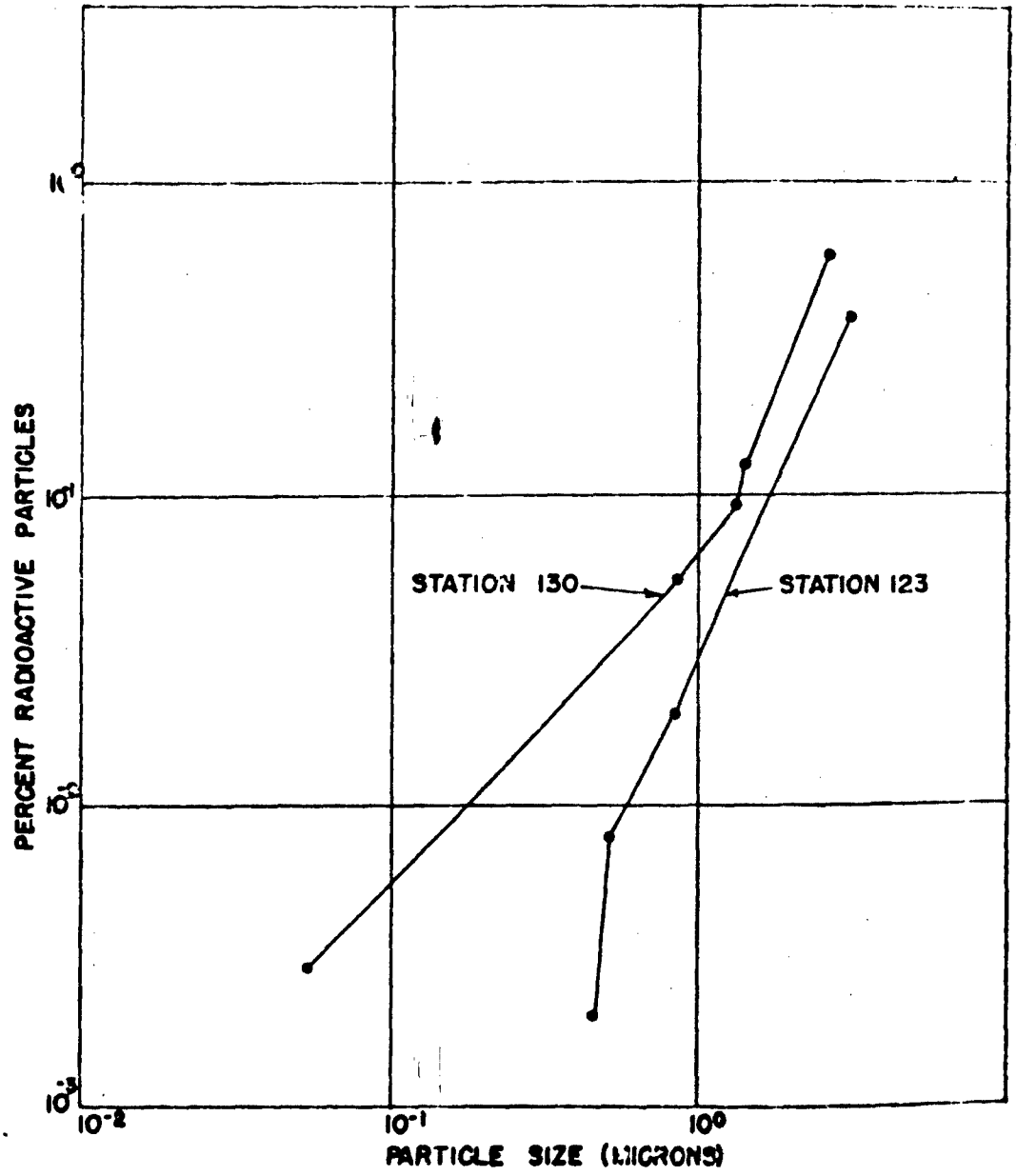

Fig. 4.30 Percentage of Active Particles in the Aerosol as a Function of Particle Size, Underground Shot, Cascade Impactor Data.

PROJECT 2.5a-1

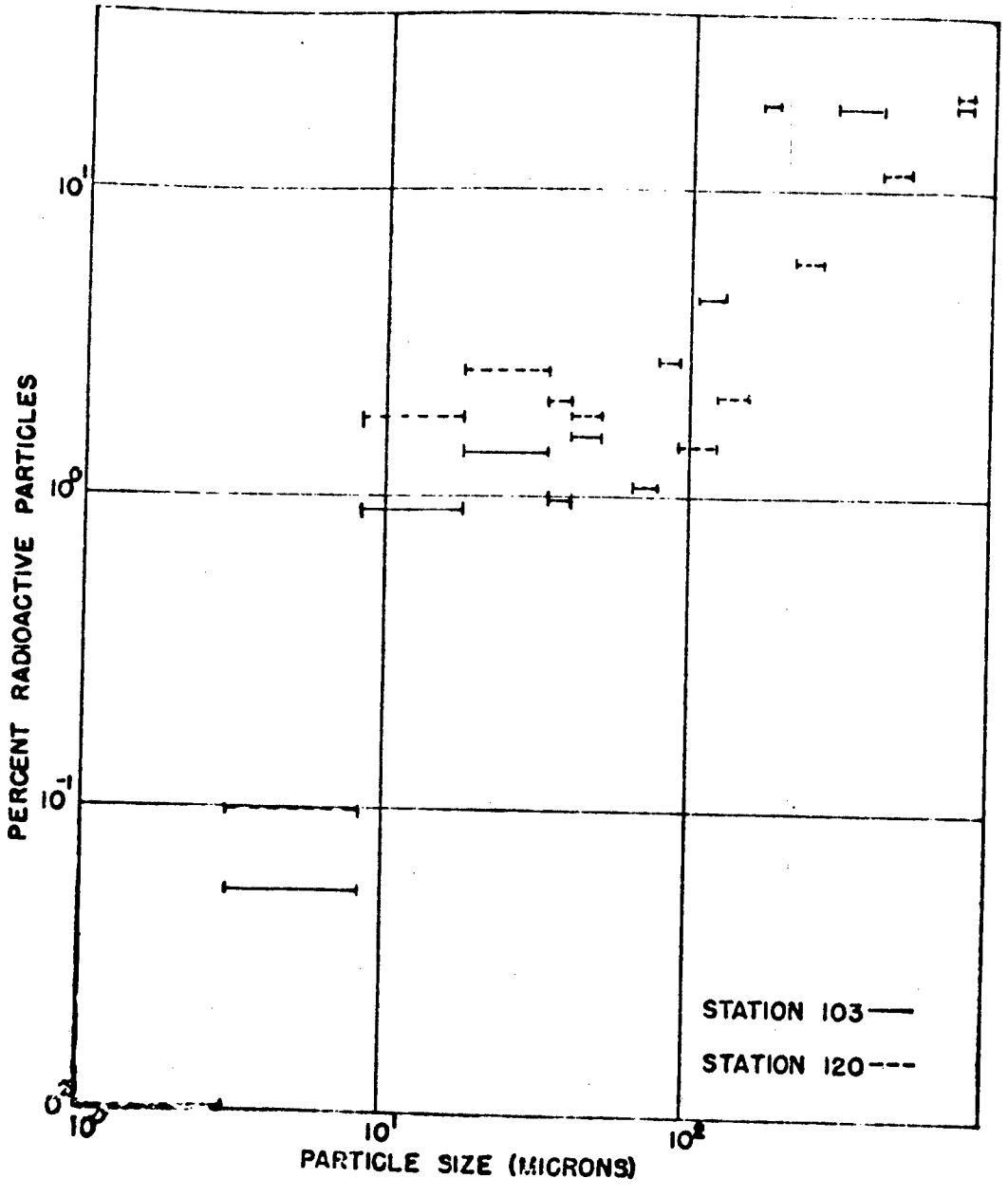

Fig. 4.31 Percentage of Active Particles in the Fall-out as a Function of Particle Size, Underground Shot.

After some experimentation, a number of procedures for determining the percentages of radioactive particles were developed[10] for various size ranges. These were as follows: Method No. 1 approximately 150 to 850 microns. In this method, Kodak NTB Autoradiographic Stripping Film was employed to distinguish active particles. This emulsion was stripped from its cellulose backing, relaid emulsion side down on its backing and lightly fastened to it with strips of tape. The fractionated sample was distributed over the back side of the emulsion by means of a spatula and the particles were affixed by covering with a Duco cement solution (one volume of cement to four of acetone). After drying, the strip film was reversed and retaped to the support. The film was stored in a light-tight box for a three to four day exposure. The exposed film was developed with DuPont x-ray developer, fixed, washed, and dried and again removed from its support and fastened to a clean glass slide over millimeter graph paper for examination and counting with a stereomicroscope. Black areas were observed above each radioactive particle while the inactive ones did not effect the emulsion. The intensity of blackening appeared somewhat variable and occasional difficulty was experienced when only a small spot was evident or when only a portion of the particle appeared to be active or when the emulsion appeared fogged or grey rather than intense black. In doubtful cases the particle was considered to be radioactive. A number of these "doubtful" active particles were picked up and were found in every case to be radioactive when held in front of the window of a G-M tube counter. Thus the assumption that all "doubtful" particles were active appears to be justified. Considerable wrinkling of the strip film was experienced but this does not interfere with the method. Below approximately 150 microns the method becomes impractical due to difficulties in ascertaining the nature of many particles.

Method No. 2, approximately 16 to 150 microns. Kodak NTB Nuclear Track plates softened for 10 to 15 seconds in warm water (50 C) were utilized in this procedure. The size-fractionated particles were distributed over the moist plates in the same manner as in the first method and the plates with their adhering particles were allowed to dry and expose for two to three days in a light-tight box. The plates were developed with careful agitation so as to avoid displacement of the imbedded particles. Examination of the plate with a stereomicroscope revealed the radioactive particles over their associated darkened area on the film. (See Fig. 4.32)

[10] Malcolm G. Gordon and Benjamin J. Intorre, "Some Techniques Applicable to the Study of ABD Fall-out", CRL Interim Report No. 137, 14 Mar 1952.

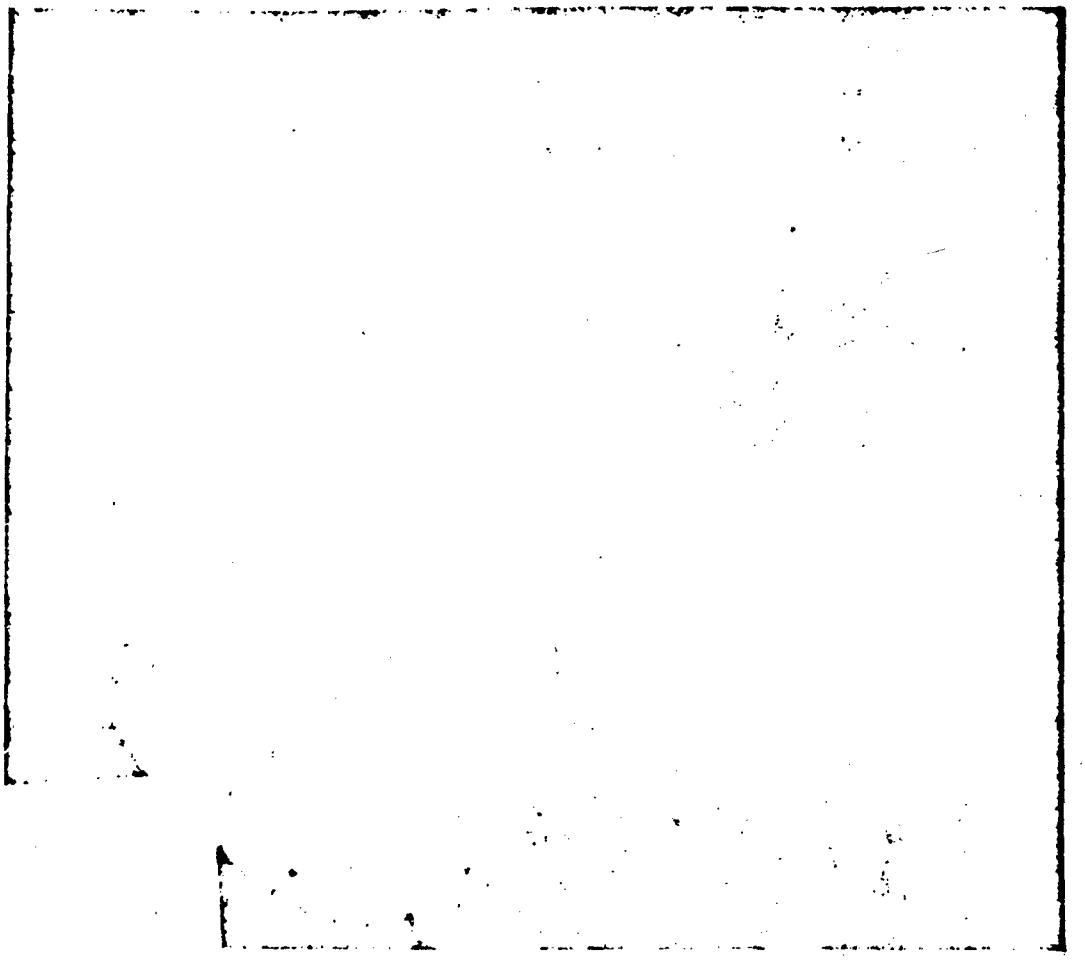

Fig. 4.32 Station 103 Fall-out Particles (74-88 u) on an NTB plate showing the film darkening around two radioactive particles.

As a check upon the agreement of the two methods, the percentage of radioactive particles in a 240 to 420 micron range sample was determined. Results of 16.7 and 17.7 per cent were obtained for the strip-film and the plate methods respectively.

Method No. 3, approximately 8 to 40 microns. Inasmuch as the smaller particles tended to agglomerate, the second method was modified for the lowest particle size ranges so that the sample was dropped into a swirling inch of hot water (50°C) in a battery jar. After suspension of the particles an NTB plate was submerged and after approximately 30 seconds removed, dried, exposed for four or five days and then processed in the usual manner. Particle counting was most easily accomplished in the range of 8 to 40 microns by visually counting the radioactive particles in a given area with a light background and then photographing the same area with a dark background. The total number of particles could be conveniently counted on the print.

4.5 STUDY OF FRACTIONATION

4.5.1 Radiochemistry

The study of fractionation included radiochemical analysis of many JANGLE samples obtained from various types of instruments which were located at a number of different stations. Sr^{89}, Zr^{95}, Mo^{99}, Ag^{111}, Cd^{115}, Ba^{140}, Ce^{141}, and Ce^{144}, were determined on four filter papers from the underground shot, and Zr^{95} and Mo^{99} were determined on a horizontal ointment plate from the surface shot. These data are tabulated in Table 4.13 as counting rate ratios (at zero time) with respect to Mo^{99} (an allegedly non-fractionating nuclide). Ag^{111}/Ba^{140} and Ag^{111}/Cd^{115} ratios have also been tabulated because of their special interest.

In addition, the large quantities of fall-out collected from the underground shot at Operation JANGLE provided a unique opportunity to perform radiochemical analyses upon size-graded particles. Sr^{89}, Zr^{95}, Ba^{140}, and Ce^{144} were determined on a number of different particle size fractions of fall-out collected at stations 103,107,114, and 120. These data are tabulated in Table 4.14. Mo^{99} was not determined because the decision to make the fall-out analysis was not made until some weeks after the shot. The nuclide activity per unit mass of radioactive material was calculated by dividing the nuclide activity by the mass of active particles in each fraction. The latter was determined by applying the data of par. 4.3.3 to the measured mass of each fraction. These data are tabulated in Table 4.15 and will be used in the discussion in par. 5.5.

PROJECT 2.5a-1

The fission products separations were carried out essentially by the methods compiled by Coryell and Sugarman[11] as modified by J-11 Group, Los Alamos Scientific Laboratory. The only important modification was the determination of silver as iodate rather than iodide. The fall-out samples were run in duplicate, the others in quadruplicate.

In order to provide a basis for comparison with other laboratories, radiochemical analyses were performed on an irradiated U^{235} sample for each of the fission products listed above with the exception of Cd^{115} and Ce^{141}. The sample consisted of 14.8 milligrams of enriched uranium foil irradiated to 9.3×10^{13} fissions in the Brookhaven pile.

Filter paper samples were digested by treatment with fuming nitric, perchloric, and hydrofluoric acids by the procedure described by Spence and Bowman[12]. The M-5 ointment was removed from the aluminum plate with facial tissue and digested by the same procedure. It was necessary to repeat the digestion to effect complete solution. The fall-out samples were fumed successively with perchloric and hydrofluoric acids and taken up with hydrochloric acid.

Samples were mounted in a reproducible geometry system on 3-1/4x2-1/2x1/16 inch aluminum cards. In the case of Mo, Cd, Ag, Ba, and Sr the final precipitation was carried out by the glass chimney and Hirsch funnel technique, which confined the precipitate to a defined area on the filter paper. Ce and Zr precipitates were tapped out of the ignition crucibles into counter ores in the aluminum cards. Samples were covered with either 3.8 mg/cm^2 of cellophane or 0.45 mg/cm^2 of rubber hydrochloride. Ce^{144} was counted face down and hence through 217 mg/cm of aluminum.

Each mounted sample was counted for decay with a thin mica end-window G-M tube and conventional scaler unit until a satisfactory curve was obtained or the activity became too low, whichever occurred first. The counting rates were measured to 0.95 errors[13] of 2-5% for the

---

[11] C. D. Coryell and N. Sugarman, Radiochemical Studies: The Fission Products, McGraw-Hill Book Co., New York, N. Y. 1951

[12] R. W. Spence and M. G. Bowman, "Radiochemical Efficiency Results of Operation SANDSTONE", SANDSTONE Report 10, Appendix A, Los Alamos Scientific Laboratory, March 25, 1949

[13] i.e., We are 95% certain that the statistical error in counting is not greater than the listed per cent.

pp. 108-110 deled

plate. Spreads[14] for repeated analyses on the size-graded fall-out were within 5% for the Ba^{140} and Sr^{89} and from 10-20% for Ce^{144} and Zr^{95}. The spreads for the filter paper and ointment plate work were also 10-20%

The activity was read from the smoothed decay curve at an arbitrary time and corrected to zero time. Four different G-M tubes, cross-calibrated with samples of each fission product, were used, and all data were corrected to the same tube. Data were further corrected to 100% chemical yield, first shelf and zero added absorber. No corrections for coincidence were required nor were corrections made for self-absorption and self-scattering since time did not permit preparation of correction curves. This error was insignificant except in the case of some strontium samples where the chemical yields were extremely high. The correction even here would be less than 5%. The aluminum mounting cards provided saturation backscattering. Corrections to zero added absorber were based on absorption curves in Coryell and Sugarman[15]. Barium activities were corrected for growth of lanthanum activity as indicated by Finkle and Sugarman[16].

4.5.2 Activity of the Radioactive Particles as a Function of Particle Size

In the study of fractionation it is of interest to determine the activity of the radioactive particles as a function of their size, surface area, and mass. The analysis of the size-graded fallout samples at stations 103 and 120 of the underground shot for activity and per cent active particles offered an opportunity to determine these quantities indirectly. The results are presented in Figures 4.33 through 4.35.

The following procedure was employed: The percent active particle data (par. 4.4.2) in each fraction were applied to the

[14] The spread was obtained by dividing the difference between the extremes by the mean.

[15] Coryell and Sugarman, op. cit., Book 2

[16] Ibid., p. 1123

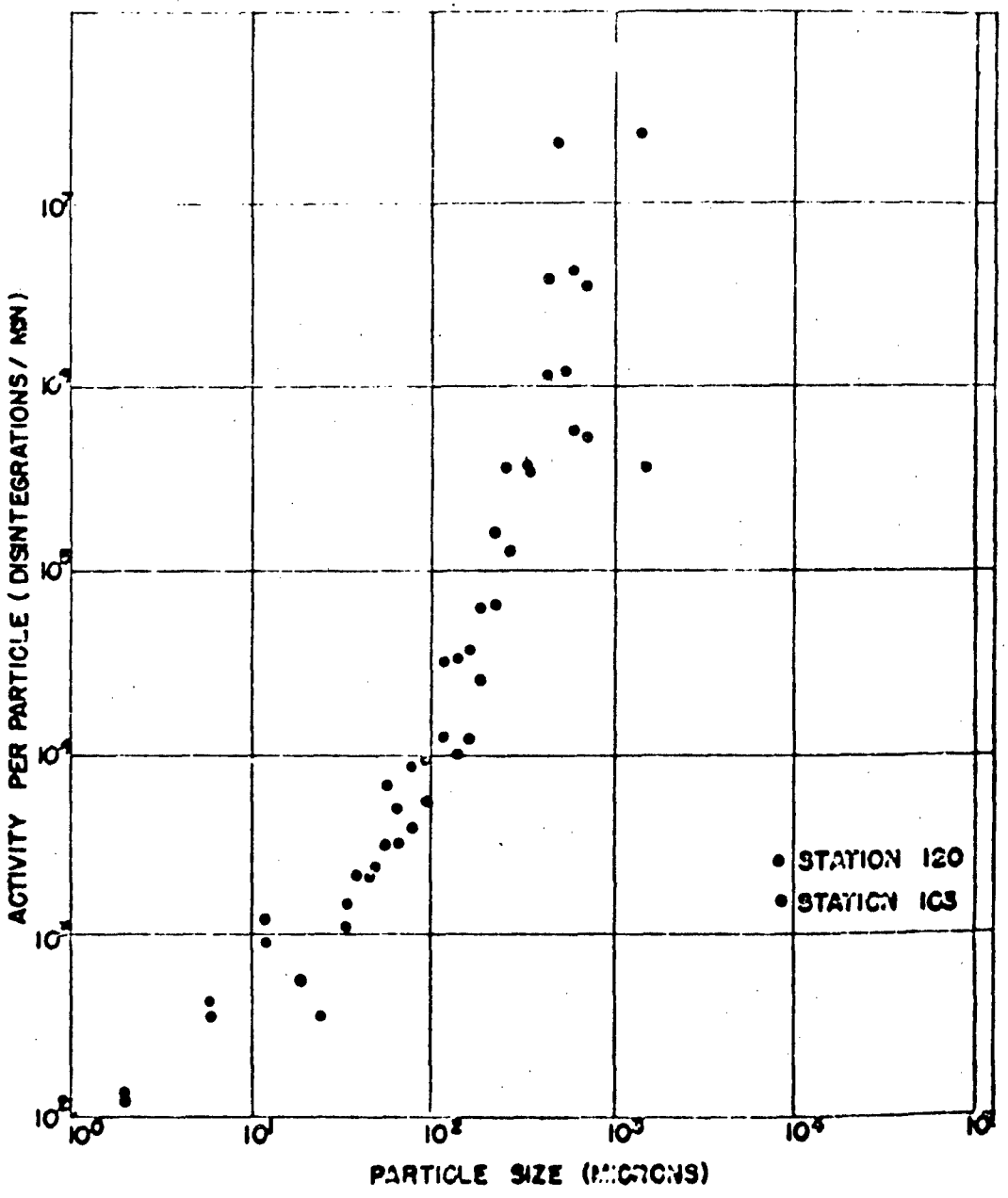

Fig. 4.33 Activity per Radioactive Particle as a Function of Particle Size.

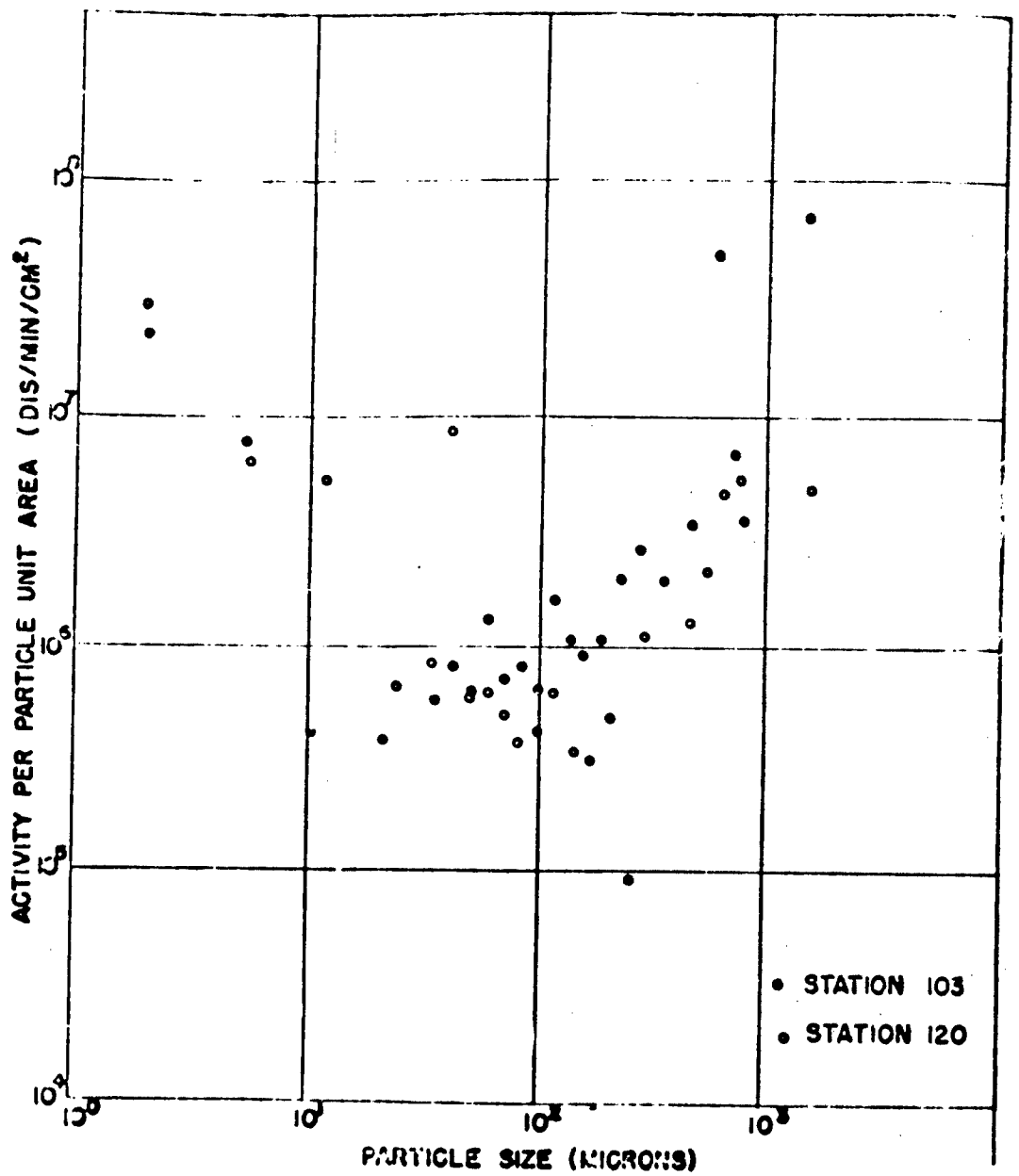

Fig. 4.34 Activity per Unit Area of Radioactive Particles as a Function of Particle Size.

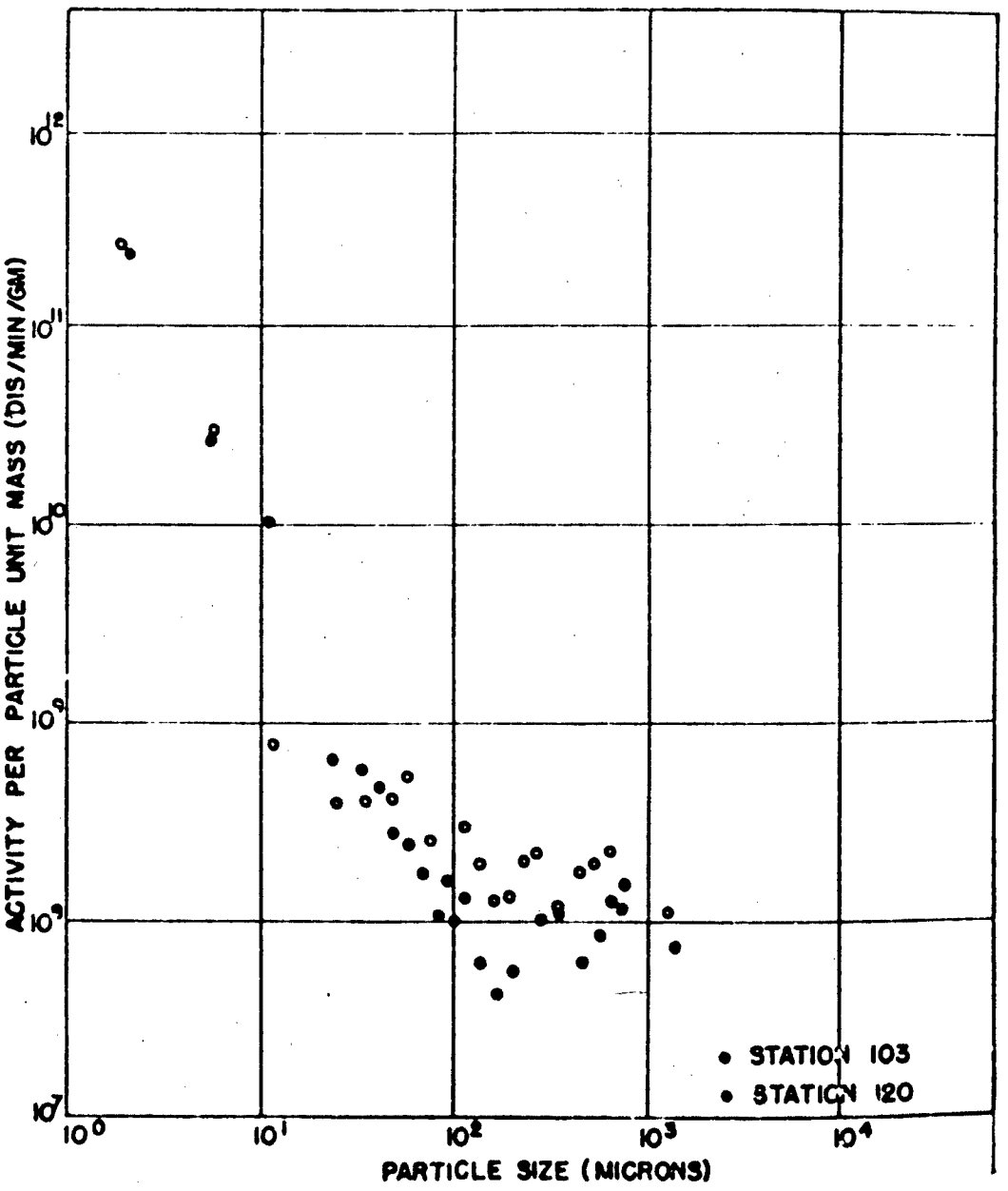

Fig. 4.35 Activity per Unit Mass of Radioactive Particles as a Function of Particle Size.

specific activity of that fraction (par. 4.3.4), giving the specific activity of the active particles of the fraction (assuming all particles in the fraction had the same weight). Making the further assumption that all particles in the fraction had the same density and shape, the activity per unit active particle surface area, and the activity per active particle were calculated. A specific gravity of 2.7 was assumed, and all particles were assumed to be spherical in shape. The size of particles in a given size fraction was taken to be the average of the pore size of the sieve on which the particles were found and the pore size of the sieve directly above.

4.5.3 Decay Rates

It was expected that fractionation would manifest itself by a variation in decay rate with particle size. To investigate this possibility, the activity measurements on the size fractions of fallout at stations 103, 107, 114, and 120 were continued from about H/1000 hours to approximately H/2000 hours. The resulting activities were plotted as a function of time on log-log paper and a straight line was fitted to them by the method of least squares. The slopes of these lines are presented in Table 4.16. The data for station 120 is presented in graphical form in Figure 4.36.

TABLE 4.16

Decay Slopes (Between H/1000 and 2000 Hours) of Size Graded Fall-out Samples

Particle Diameter (microns)	Decay Slope*			
	Station 103	Station 107	Station 114	Station 120
1500	-1.110	/0.127	-1.217	-1.225
775	-1.238	-0.448	-1.205	-1.124
650	-1.291	-1.417	-1.058	-1.221
545	-1.162	-0.613	-1.177	-1.203
460	-1.424	-0.587	-1.165	-1.105
358	-1.128	-1.252	-1.247	-1.066
274	-1.284	-0.796	-1.241	-1.154
230	-1.244	-0.878	-1.241	-1.279
194	-1.308	-0.943	-1.229	-1.140
163	-1.349	-0.913	-1.253	-1.165
137	-1.302	-0.687	-1.241	-1.211
115	-1.331	-0.856	-1.329	-1.228
96	-1.354	-0.883	-1.288	-1.229
81	-1.331	-1.204	-1.247	-1.186
68	-1.430	-0.987	-1.300	-1.244
58	-1.337	-0.843	-1.215	-1.321
48	-1.436	-1.170	-1.312	-1.261
40	-1.343	-0.836	-1.394	-1.294
18	-1.424	-0.738	-1.429	-1.331

*The decay slope is defined as n in the equation

$$A = kt^n$$

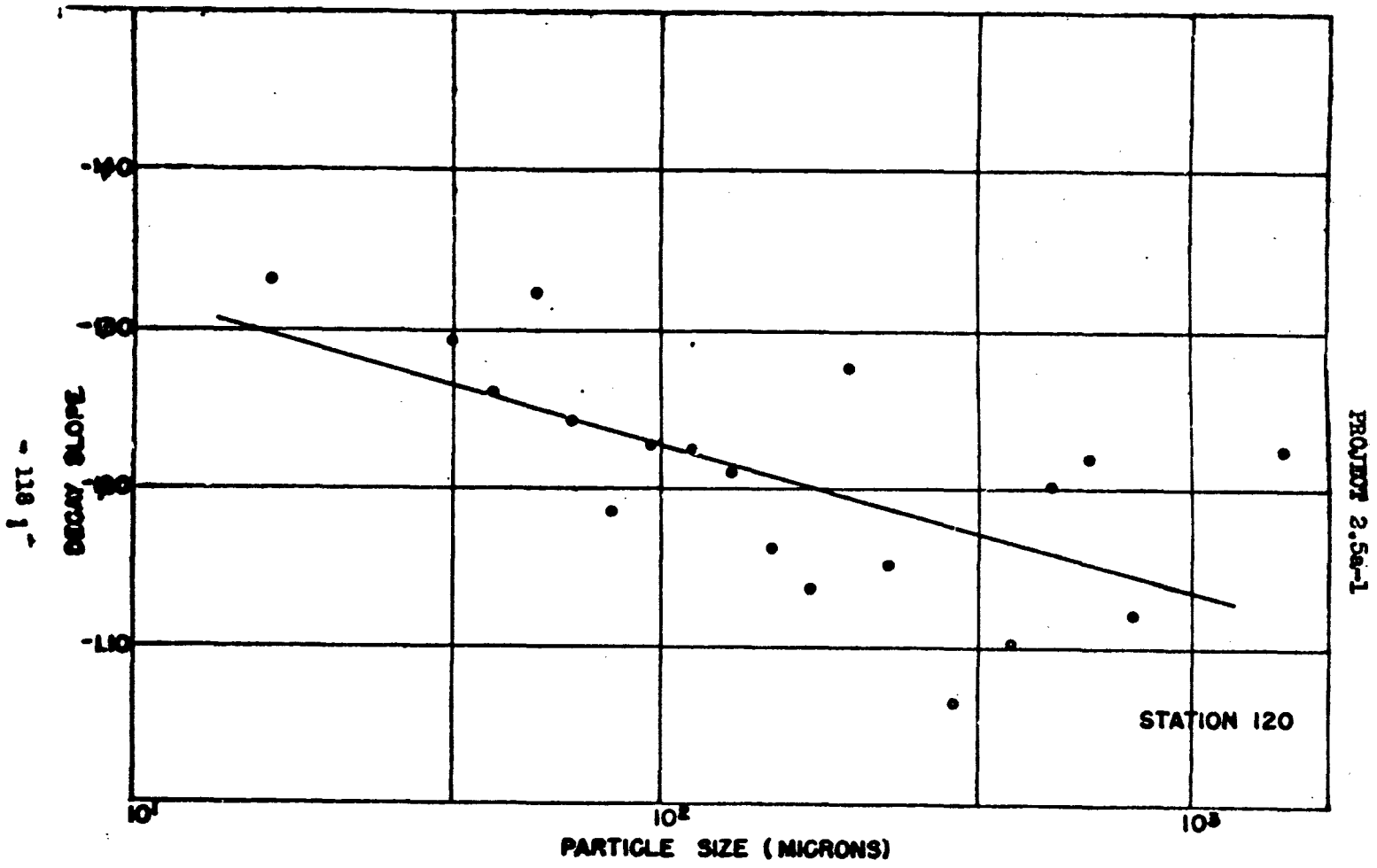

Fig. 4.36 Decay Slope vs Fall-out Particle Size, Station 120, Underground Shot

CHAPTER 5

DISCUSSION

5.1 CONCENTRATION OF ACTIVITY IN THE AEROSOL

Before proceeding to a discussion of some of the details of the activity concentration data, it is well to compare the data obtained by the four types of instruments which were employed. Such a comparison is made in Table 5.1, in which the ratios of the concentrations obtained from the particle separator, cascade impactor, and continuous air monitor, to those obtained from the filter sampler have been computed. The table illustrates, for one thing, the extremely large variations that may be expected in measurements of this sort made with existing sampling equipment. It is apparent that the data obtained by the particle separator varied from one tenth to ten times that of the filter sampler. There is apparent disagreement between the cascade impactor and the filter sampler, the former being smaller than the latter by a factor of the order of a several hundred. The cause of this disagreement is thought to be due to the fact that the cascade impactor, in obtaining a relatively small sample, is more susceptible to the loss of large particles, because collection of the particles is made on a glass slide, rather than on filter paper. Comparison between the continuous air monitor and the filter sampler suffers from the lack of data from the former, together with a contradiction on two of the four records obtained, that is, apparently the cloud did not reach the station until after the 115 min filter sampler sampling period was over. One of the remaining two records indicated the continuous air monitor data was ten times, the other one tenth as large than the filter sampler data. Probably the only conclusion that can be reached from this comparison is that the filter sampler concentration data is in systematic disagreement with the cascade impactor data, but is not in systematic disagreement with the particle separator or continuous air monitor data, although agreement in any particular case may be no better than plus or minus one order of magnitude.

It is possible that the comparison of the particle separator-filter sampler data may shed some light upon the question of the effect of non-isokinetic sampling upon the concentration data. It will be remembered that the particle separators were oriented with the axis of their sampling port in the vertical direction, while the filter samplers were oriented in the horizontal direction. Under these conditions one would expect that the particle separator, in collecting the largest particles

PROJECT 2.5a-1

TABLE 5.1

Comparison of Concentration of Activity Data

Station	Particle Separator[1] / Filter Sampler[1]	Cascade Impactor[2] / Filter Sampler[1]	Continuous Air Monitor[3] / Filter Sampler[1]
		Surface Shot	
8	3.8		
14	6.8		
15	9.2×10^{-1}		
21	2.5		
23	1.0	1.1×10^{-1}	
24	9.7×10^{-1}		
25		9.5×10^{-3}	
26		2.1×10^{-2}	
28	4.7×10^{2}		
29	1.2×10^{-1}		1.1×10^{-1}
30		3.2×10^{-2}	
35		3.6×10^{-2}	
38			9.6
40		2.6×10^{-2}	
		Underground Shot	
108	5.7×10^{-1}		
109	4.0		
114	3.5×10^{1}	2.1×10^{-2}	
115	1.5	1.6×10^{-2}	
119		1.2×10^{-1}	
120	2.6×10^{1}		
121	3.4		
123	1.0		
124	3.1	2.8×10^{-5}	
125		2.3×10^{-4}	
128	1.0×10^{1}		
129	1.1×10^{-1}		
130	1.1×10^{1}		
132		2.2×10^{-4}	
140		1.4×10^{-3}	

1 Average concentration over 115 minute sampling period.
2 Station numbers less than 25 and 125, concentration over 1 minute sampling period; greater than 25 and 125, over 115 minute sampling period.
3 Average concentration over 115 minutes computed from concentration vs. time curve.

would cause a systematic decrease in the particle separator-filter sampler concentration ratio with distance from ground zero. However, no such trend can be detected, and it is thought, therefore, that the effect due to non-isokinetic sampling, at least in the case of concentration data, may be masked by the spread already present in the data.

The question of the accuracy of the cloud model described in paragraph 4.1.1 is open to some conjecture. Certainly the records of the continuous air monitors indicate the cloud arrived later and stayed much longer at the most distant stations than is indicated by the cloud model. At the very close stations, the age of the cloud becomes extremely important because of the activity decay correction. At the stations of medium distance therefore, the cloud model can be expected to give the best results. The concentration of activity in the cloud proper, bases on the cloud model, has been plotted in Fig. 5.1 as a function of distance from ground zero. The data indicate the underground shot produced an aerosol 10 to 100 times as active as the surface shot.

5.2 PARTICLE SIZE DISTRIBUTION

As was indicated in Chapter 4, essentially only one instrument was employed to obtain the particle size distribution of the aerosol, the cascade impactor, and thus there can be no inter-instrument comparison of results. A discussion of the particle size distribution of the cloud, therefore becomes a discussion of the cascade impactor data. The most important fact to be emphasized is that sampling was non-isokinetic in the sense that the intake velocity was considerably less than the wind velocity, but that the intake throat was pointed toward ground zero, and therefore, generally speaking into the wind. Under these conditions the intake aerodynamics favor the large particles. However, as was indicated in paragraph 5.1, the impactor, though undoubtedly removing these particles from the airstream, must have shattered them, or else subsequently lost them, since no particles larger than about 40 microns were observed in the examination of the slides.

However, the tendency toward smaller particle sizes in the aerosol with increasing distance from ground zero was definitely observed in both shots. Figs. 5.2 and 5.3 illustrate this situation. It is apparent that the underground shot initially possessed a distribution containing larger particles than the surface shot, but that these particles rapidly fell out, leaving at distances of 20,000 feet a distribution containing smaller particles than the surface shot. This result may be explained by the fact that the underground shot cloud was

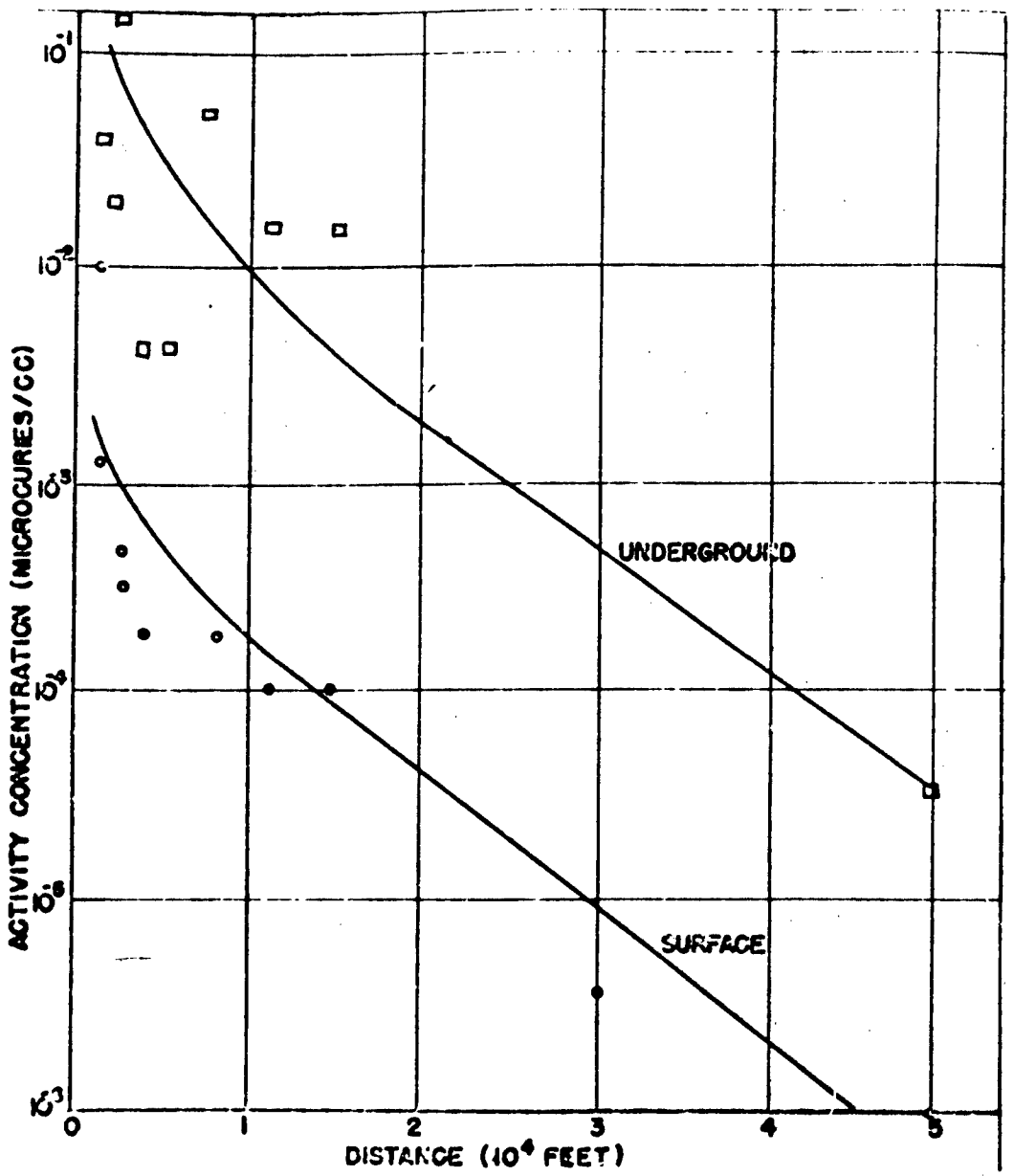

Figure 5.1 Concentration of Activity in the Cloud as a Function of Distance on the Downwind Leg. Filter Sampler Data. Activity was corrected to time at which cloud passed each station.

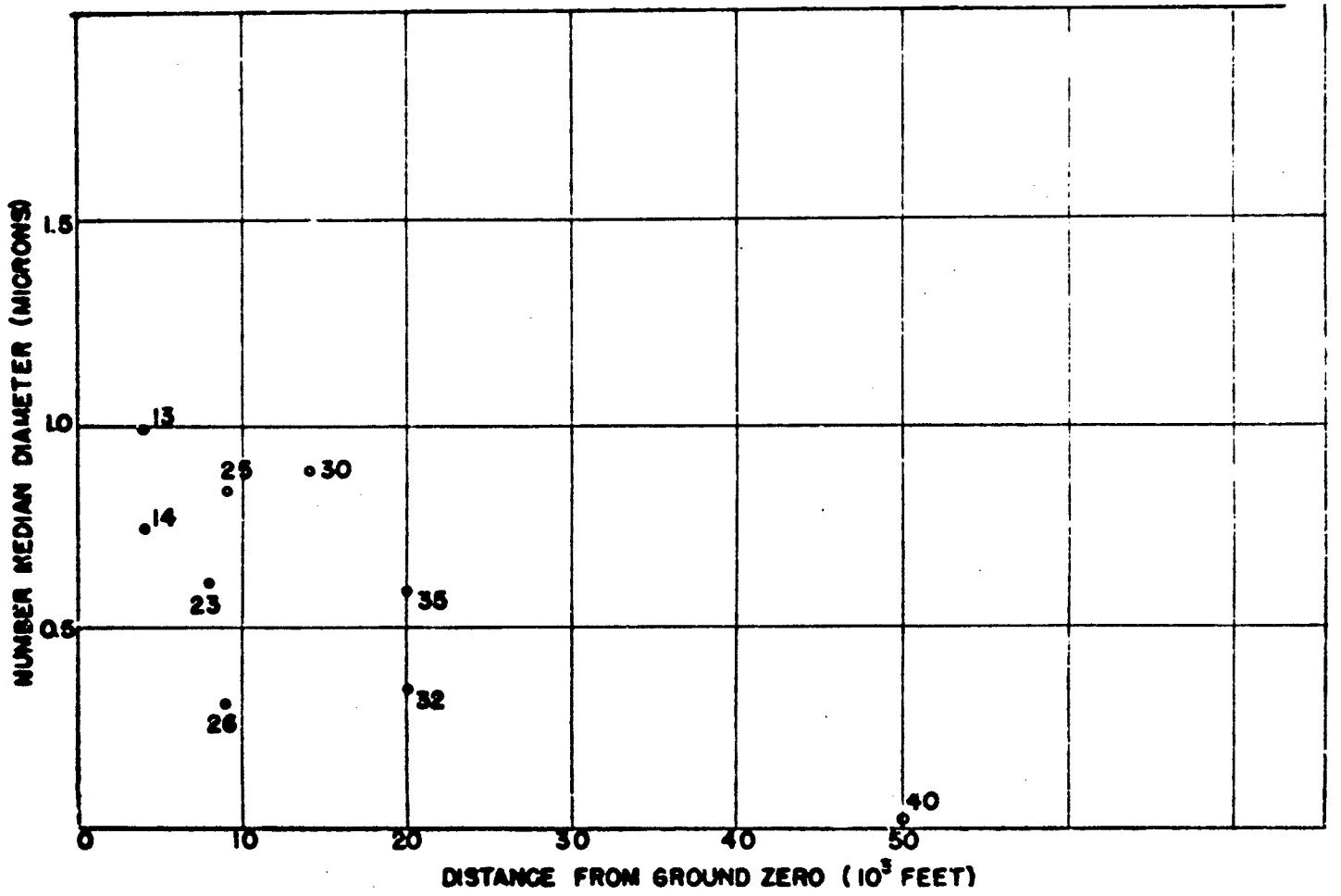

PROJECT 2.5a-1

Figure 5.2 Surface Shot Number Median Diameter of the Particles in the Aerosol as a Function of Distance from Ground Zero. Cascade Impactor Data.

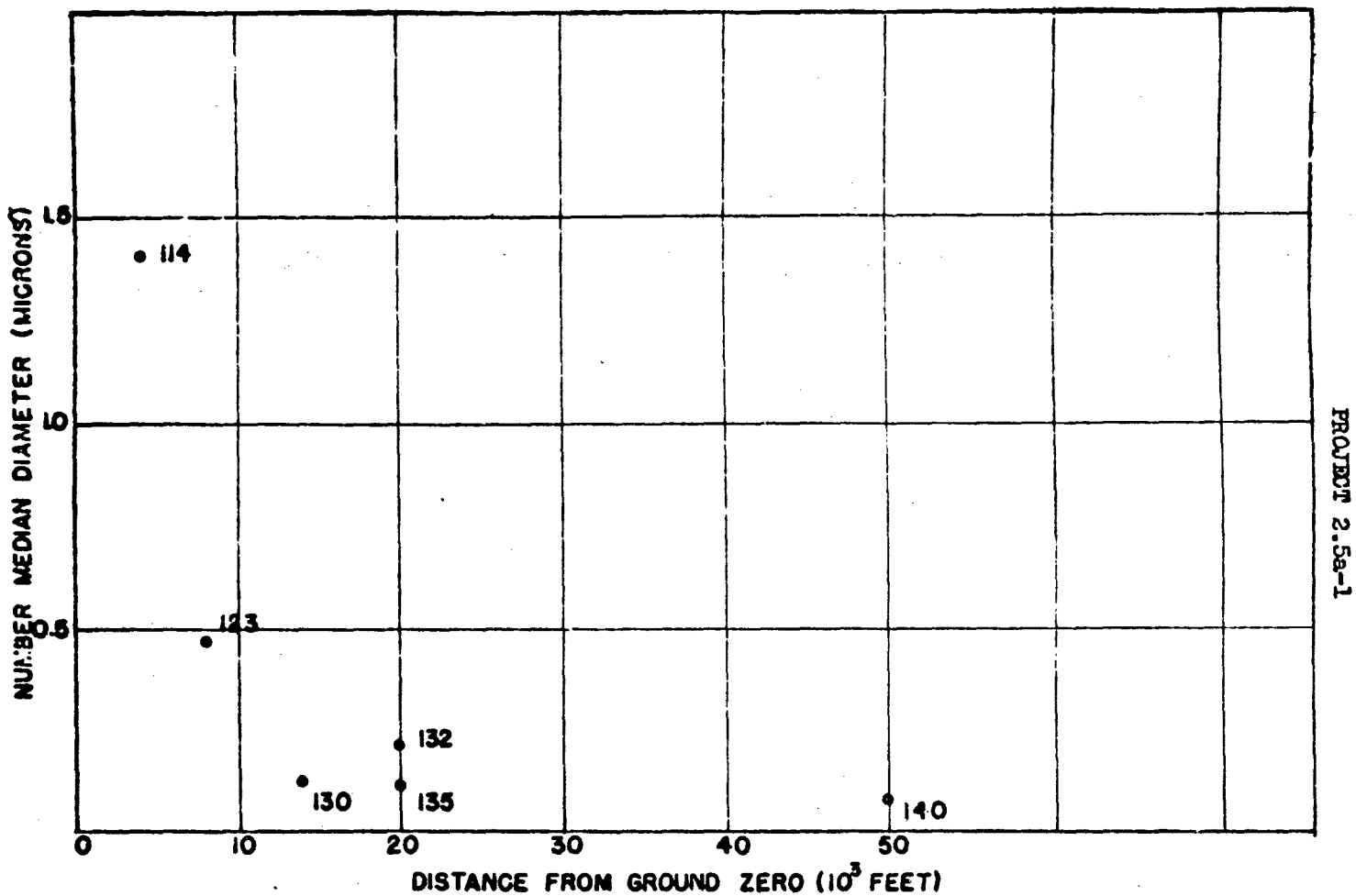

PROJECT 2.5a-1

Figure 5.3 Underground Shot Number Median Diameter of the Particles in the Aerosol as a Function of Distance from Ground Zero. Cascade Impactor Data.

lower than the surface shot cloud, giving the large particles less time in which to be carried by the wind out to the more distant stations. By the time both clouds reached 50,000 ft. the NMD of their distributions had reached a value of less than 0.1 micron.

The material on the fall-out tray was collected under favorable conditions in the sense that no appreciable wind sprang up between the time of the shot and the recovery of the trays, conditions under which very little material could have been removed or added as determined experimentally. The analysis of the material was carried out according to standard procedure and apparently no difficulties were encountered. Nonetheless the resulting distributions (see Figs. 4.12 through 4.15) indicated the fall-out had a very small NMD, less than one micron, a distinct anomaly inasmuch as the aerosol NMD apparently was about this size. In addition, the lines representing the size, area, and mass, distributions did not give a straight line trend. For these reasons, no attempt was made to fit straight lines to the data, with the result that convenient parameters describing the distribution were lacking, making a comparison of distributions difficult. It can be noted, however, that station 103, which is shown in the photographs as being in the base surge from the underground shot, had a noticeably larger percentage of particles less than 10 microns than the other four stations analyzed, giving weight to the idea that the base surge was composed of small particles.

5.3 RADIOACTIVITY AS A FUNCTION OF PARTICLE SIZE

It was hoped that the cascade impactor would size grade particles sufficiently so that activity measurements made on the five slides would give an indication of the activity of the particles in the aerosol as a function of particle size. However, these data, which are contained in Tables 4.10 and 4.11, present such large scatter as to make such a correlation impossible. An example of this is easily seen by consideration of the percentage of activity on the first slide. One would expect that the first slides on the nearest impactors would contain a large percentage of the total activity of the impactor, while the first slides on the farther impactors would contain less, since there would be fewer of these very highly active particles present in the aerosol at the farther stations. Even this effect, which should be very pronounced, is not evident. A partially satisfactory explanation of this can be made by the fact that the cascade impactor, in its collection of particles, size grades them only by virtue of widely overlapping efficiency curves, and that a wide spectrum of particle sizes may be found on any one slide, although the NMD of the distribution varies from slide to slide.

This, of course, does not affect the particle size analysis by virtue of the way in which it is carried out, however, it might frustrate any work dependent upon size grading.

It is unfortunate that a larger number of conifuges did not give satisfactory data. Although all conifuge cones were radioautographed, only a few showed any darkening at all, and only one of these showed a smooth distribution of film density. The others had only splotches of activity, which probably indicated the presence of turbulence in the cone volume. The fact that most conifuge cones were not sufficiently active to produce radioautographs can be attributed to the small flow rate of the instrument.

The activity as a function of particle size data obtained from the fall-out trays appears to be satisfactory, except that a self-absorption correction, originally considered to be almost negligible, apparently is necessary for the large particle sizes. This question is discussed in more detail in paragraph 5.5.2.

It should be pointed out that the specific activity data from the fall-out, which indicates the relative activity of each particle size range, can be applied to the mass distribution of the aerosol as determined from the cascade impactor to yield the distribution of activity as a function of particle size of the aerosol. The assumption made is that, in any given particle size range at any given station, the specific activity of the aerosol is the same as that of the fall-out. If this is not the case, the implication is that there must be some selection on the basis of activity in determining which particle of a given size range will remain in the aerosol or will fall out.

5.4 PERCENTAGE OF ACTIVE PARTICLES

If the percentage of active particle data (paragraph 4.4) of the cascade impactor and the fall-out tray for the underground shot are combined, it appears that the percentage of active particles is a monotonic function of particle size over the range of particle sizes covered by the two types of data, i.e., from 10^{-1} to 10^{3} microns. In fact it appears that a straight line, with a slope of one, representing a linear function, fits the data well.

Since both the cascade impactor data and the fall-out tray depended upon a radioautographic method of differentiating the active from the inactive particles, it was thought that the exposure time of the radioautograph would affect the results. This was not borne out by results of the cascade impactor, since a number of radioautographs of different exposure times showed no apparent change in the percentage of active particles.

5.5 STUDY OF FRACTIONATION

5.5.1 Radiochemistry

The data concerning the nuclide activity per unit mass of active material as a function of particle size, which is contained in Table 4.15, provided a method of investigating the mechanism whereby particles acquire activity. The data for Sr^{89} and ZR^{95} have been plotted in Figs. 5.4 and 5.5. Referring to Fig. 5.4, it appears that a straight line with a slope of 1 may be fitted to the data, whereas this is not possible with the data in Fig. 5.5. Allowing for some over-simplification, it appears that the Sr^{89} activity is a function of particle surface, whereas that for Zr^{95} tends to be more of a volume function. Ba^{140} gives a plot similar to the Sr^{89} plot, while Ce^{144} is similar to Zr^{95}. Further study is being made of these data, particularly with respect to the question of whether the activity of Zr^{95} and Ce^{144} is concentrated in a shell rather than a volume. Examination of the decay chains of these four nuclides provides a plausible reason why there should be a difference in the mechanism for acquiring radioactivity. The decay chains are as follows[4]:

$$Kr^{89} \xrightarrow{2.6m} Rb^{89} \xrightarrow{15.4m} Sr^{89}$$

$$Kr^{95} \xrightarrow{short} Rb^{95} \xrightarrow{short} Sr^{95} \xrightarrow{short} Y^{95} \xrightarrow{10.5m} Zr^{95}$$

$$Xe \xrightarrow{16s} Cs \xrightarrow{66s} Ba^{140}$$

$$Xe^{144} \xrightarrow{1s} Cs^{144} \xrightarrow{short} Ba^{144} \xrightarrow{short} La^{144} \xrightarrow{short} Ce^{144}$$

It may be seen that Ba^{140} and Sr^{89} both have gaseous precursors that have half-lives long in comparison with the lifetime of the fireball. Since gases such as krypton and xenon are not significantly subject to adsorption above liquid air temperatures, it is logical to suppose that while the Zr^{95} and Ce^{144} chains passed the rare gas stage early enough to be adsorbed during the particle growth process, no appreciable amount of Kr^{89} and Xe^{140} decayed before the particles had ceased to grow. Hence the Sr^{89} and Ba^{140} activities were confined to the outermost surfaces of the particles.

---

4 C. D. Coryell & N. Sugarman, op cit, pp. 1996-2001.

5.5.2 Activity of the Radioactive Particles

In order to investigate the mechanism whereby particles become radioactive, the data described in paragraph 4.5.2 activity of the radioactive particles as a function of their size, surface area, and mass were calculated. (The latter, it will be noted would be the sum of all the nuclide activities of the kind discussed in the paragraph immediately above if a radiochemical analysis could be performed on all the nuclide species.)

One of the questions that arose in the study of the data was the effect of self absorption and self scattering upon the measured activity of the different particle size fractions. The former is susceptible to quantitative treatment if the range curve for the activity is known, while the latter is as yet not well understood. The complexity of the combination can perhaps best be seen by examining the data of Nervik and Stevenson[5], who have plotted a self-scattering and self-absorption correction factor versus sample thickness, with beta energy as a parameter, for NaCl and $Pb(NO_3)_2$.

A simple calculation can be made to investigate the magnitude of the self-absorption. Assuming:

(1) The attenuation of beta particles is described by the equation

$$e^{-\frac{0.693}{T_{\frac{1}{2}}} w} \qquad (5.1)$$

where w is the path length in milligrams/cm^2, and $T_{\frac{1}{2}}$ is the half thickness of the particle for the fission product radiation. The latter was taken to be 20 mg/cm^2 in accordance with the data of paragraph 4.5.4.

---

[5] W. E. Nervik and P. C. Stevenson, "Self-Scattering and Self-Absorption of Betas by Moderately Thick Samples". Nucleonics, I, (1952), 19.

pp. 128-129 Deleted

(2) The particles are cubical, so that the mean path length travelled by a beta in escaping from the particle is

$$\overline{l} = \frac{s}{2} \qquad (5.2)$$

where s is the side of the cube.

(3) The density of the particles is 2.7 grams/cm^3, making the thickness factor of the particle material equal to 2.7×10^{-1} mg/cm^2/micron. The relative self-absorption of a 1 micron particle is:

$$e^{-\frac{0.693}{20} \times 0.5 \times 2.7 \times 10^{-1}} = e^{-.0048} \approx 1 \qquad (5.3)$$

while that for a 1000 micron particle is:

$$e^{-\frac{0.693}{20} \times 500 \times 2.7 \times 10^{-1}} = e^{-4.8} \approx \frac{1}{120} \qquad (5.4)$$

Thus the correction factor for self-absorption for a 1000 micron particle is 120 times that for a 1 micron particle, and therefore is of great importance. Previous calculations had led to the belief that this correction was negligible.

No data is available to estimate the effect of self-scattering, but it is probable that it is negligible in comparison to the correction for self-absorption.

It has been suggested that the necessity for making these corrections could be side-stepped by crushing the large particles before measuring their activity. This is presently being carried out on some of the fractions that are still sufficiently active.

5.5.3 Decay Slopes

A study of the variation of decay slope with particle size (paragraph 4.5.3) has yielded no information other than further proof of fractionation.

CHAPTER 6

SUMMARY

It was expected that the considerable quantities of dirt thrown up by the Jangle explosions would trap a relatively large proportion of the fission products of the bomb, creating highly radioactive aerosols containing relatively large particles.

The concentration of beta activity in the aerosols was found to be 10^{-3} and 10^{-1} microcuries per cubic centimeter for the surface and underground shots respectively. These are based on filter sampler data taken from the nearest stations (2000 ft. to 4000 ft.) on the downwind leg, as modified by an estimation of the arrival and departure time of the cloud.

The number median diameters of the particles in the aerosols were 1.0 and 1.5 microns for the surface and underground shots respectively, at stations 4000 ft. downwind, decreasing to less than 0.1 microns at 50,000 ft. for both shots. These figures were obtained from the cascade impactor. The particle size distribution of the fall-out was also determined at a number of stations of the underground shot.

No satisfactory data giving activity as a function of particle size in the aerosol were obtained due to unsatisfactory operation of the instruments designed to size grade aerosol particles during the sampling process. These data, however, were determined for the fall-out at a number of stations on the underground shot. The percentage of active particles in the surface shot aerosol was determined to be 0.01 per cent for particles approximately one micron in diameter. For the underground shot fall-out, this percentage was found to be 20 per cent for particles approximately 100 microns in diameter.

Data of the various consequences or manifestations of fractionation were made on size-graded particles of fall-out from the underground shot, and study of these data have made possible a number of interesting conjectures regarding the mechanism whereby particles become radioactive.

APPENDIX A

DEFINITION AND ABBREVIATION OF TERMS

BCAM	- Brookhaven Continuous Air Monitor
BNL	- Brookhaven National Laboratory
CRL	- Chemical and Radiological Laboratories
Decay Slope	- the exponent in the decay equations $A = ct^n$
Fall-out	- particulate matter once a part of the aerosol that has precipitated to the ground
Fractionation	- any variation in the fission product nuclide abundance, usually applied to the variation as a function of particle size
Isokinetic	- actually "equal motion", but is generally applied to particulate sampling that is carried out so as not to be selective in any way
MF	- molecular filter
NIH	- National Institutes of Health
NRDL	- Naval Radiological Defense Laboratory
RAS	- Radiological Air Sampler
TCAM	- Tracerlab Continuous Air Monitor

APPENDIX B

CALIBRATION OF THE BROOKHAVEN CONTINUOUS AIR MONITOR

The counting efficiency of this instrument may be obtained by passing a small rectangle of filter tape of width w and length s (s is equal to w for the Brookhaven air monitor), see Fig. B.1, inserted into the center line of an uncontaminated filter tape. This small section of filter tape bears a uniformly distributed known beta activity, G of the same species as for which the calibration is desired. As the tape passes under the counter in the x direction, a count rate is recorded which may be converted into a plot of observed counts per unit time versus distance. Such a plot will have the appearance of the graph shown in Fig. B.2, and should be symmetrical about the origin. The maximum count rate at $x = 0$, C_o is the count rate when the counter face is exactly covered uniformly contaminated filter tape Cu is the finite summation of the rates obtained when the center of the standardizing rectangle is at x position equal to 0, $\pm s$, $\pm 2s$, $\pm 3s$, etc. and is thus

$$C_u = c_o + \sum_{n=1}^{n=\infty} 2c_n \qquad (B.1)$$

Empirically it has been found that with counters positioned close to the tape that Eq. B.1 can be reduced to

$$C_u = c_o + 2c_1 + 2c_2 \qquad (B.2)$$

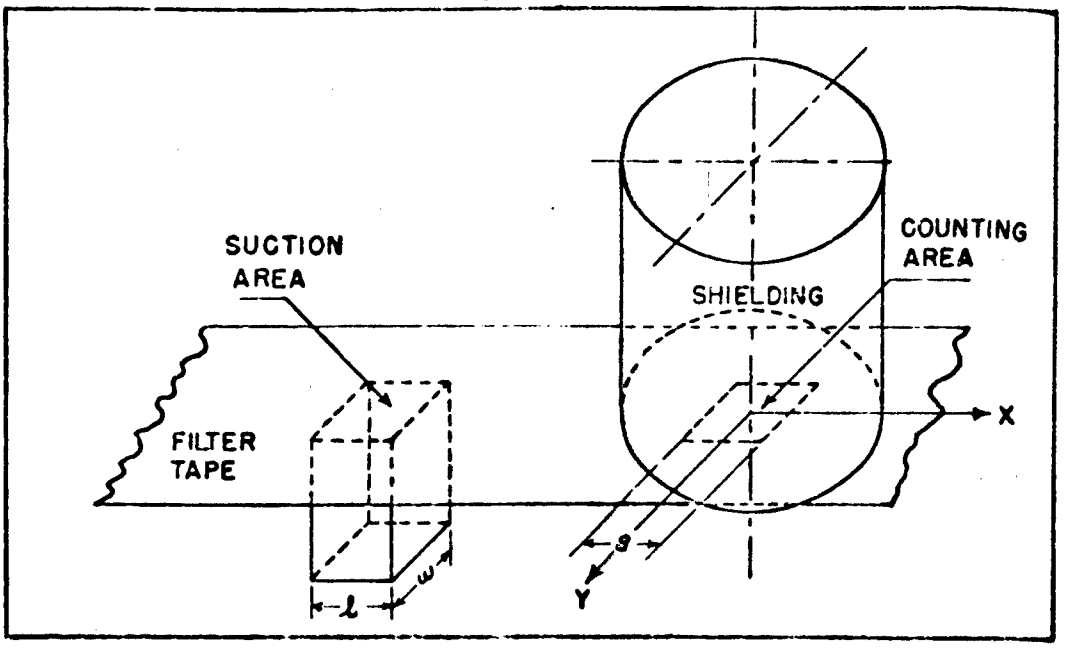

Fig. B.1 Schematic Drawing of the Brookhaven Continuous Air Monitor

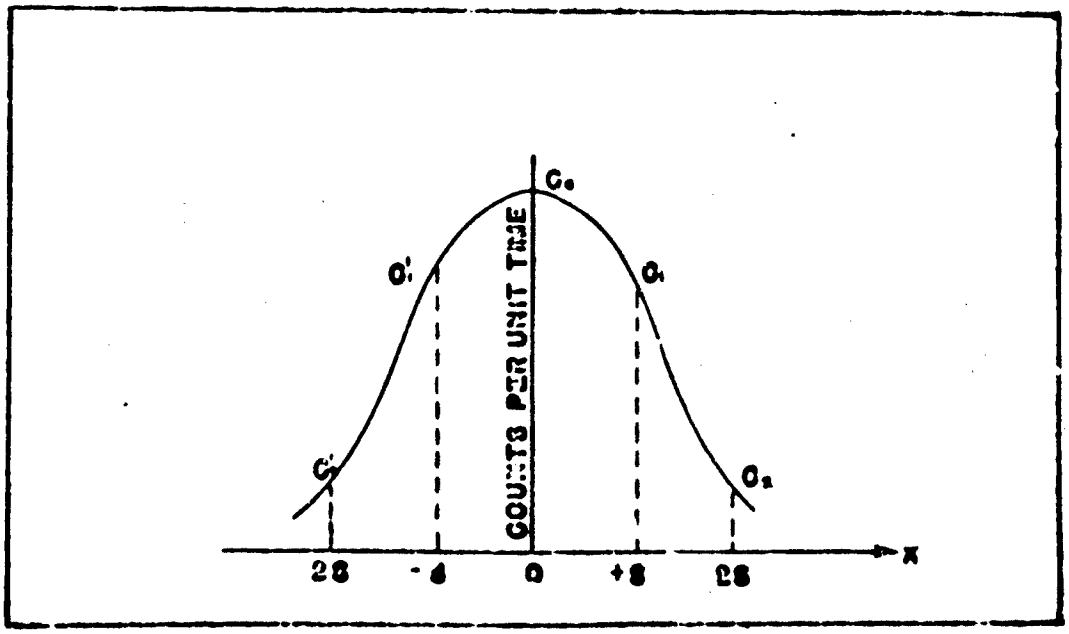

Fig. B.2 Count Rate as a Function of Displacement for the Brookhaven Continuous Air Monitor.

The fraction of the total counting rate contributed by the segment of width w and length S positioned directly in front of the tube is

$$\frac{c_o}{c_o + c_{o1} + c_{o2}} = \frac{c_o}{c_u} = f \qquad (B.3)$$

The efficiency E of the segment in this position may be defined as

$$c_o = C_u f = EG \qquad (B.4)$$

The activity per standard segment (width w and length s) is given by

$$G = aV \qquad (B.5)$$

where a = activity per unit volume of cloud; V = volume of air sampled through the standard segment. From Eq. B.4

$$C_u = E\,aV \qquad (B.6)$$

$$a = \frac{c_u f}{EV}$$

This equation limits a to the average value of the time interval during which the unit segment of paper was contaminated. For the sake of clarity the midpoint of this time interval can be taken as the time corresponding to the value a.

To obtain an unknown activity concentration a from the instrument count rate meter readings C_u, it was necessary to determine the instrument constants E, f, and V. E and f were determined by the following procedure: With the center of the window as a reference point, the standard activity paper was moved one and two inches on either side and the

counting rates observed. The sum of the counting rates in all such positions gives the counting rate of a uniformly contaminated filter paper of infinite length. Proceeding in this manner the results shown in Table B.1 were obtained.

TABLE B.1

Efficiency Data for Brookhaven Monitor

Distance From Center of Window	Counts Per	Incremental Efficiency (per cent)
0	501	23
∮ 1 inch	35.5	1.61
∮ 2 inch	2.35	0.11
- 1 inch	58.9	2.67
- 2 inch	2.0	0.09
	Total 599.75 ≈ 600	

These results are plotted in Fig.B.3. The activity of the one square inch standard corresponded to 2.2×10^3 disintegrations per second. Thus

$$f = \frac{501}{600} = .83$$

$$E = \frac{5.01 \times 10^2}{2.2 \times 10^3} = .23$$

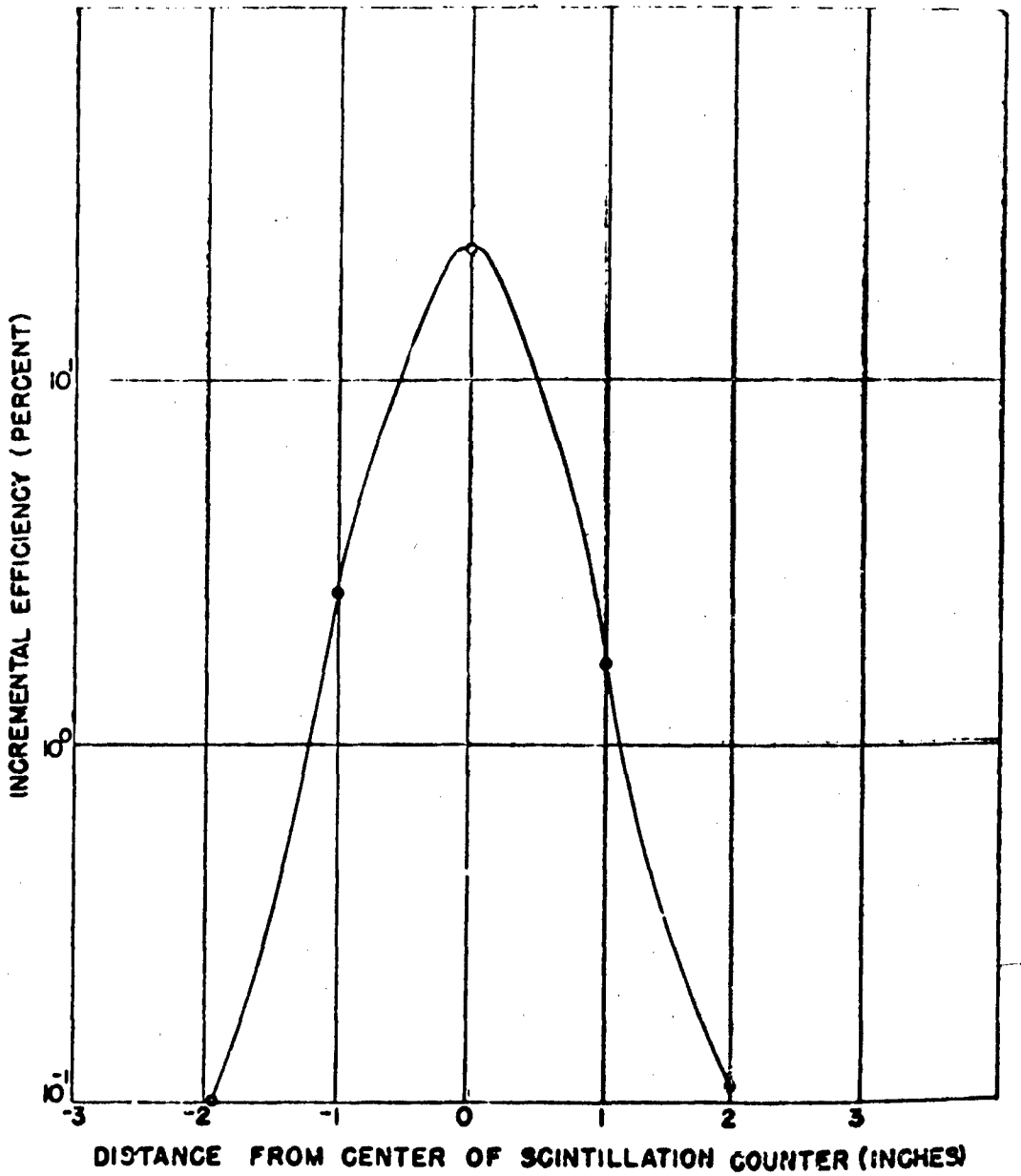

Fig. B.3 Incremental Efficiency as a Function of Distance for the Brookhaven Continuous Air Monitor

Since the sampling port measured 1 inch wide by 1.75 inches long, the filter tape transport velocity was 4 inches/hour and the flow rate through the sampling port was 3.5 cubic feet per minute, the value of V was found to be:

$$V = 1.6 \times 10^{6} \text{ cm}^3$$

Therefore, the counts per minute on the instrument count rate meter may be converted to microcuries per cubic centimeter by the equation:

$$\frac{(\mu c)}{(cm^3)} = 1.1 \times 10^{-12} \text{ (c/m)} \qquad \text{(B.8)}$$

APPENDIX C

CALIBRATION OF THE TRACERLAB CONTINUOUS AIR MONITOR

Interesting two dimensional counting geometry problems occur if a continuous air monitor is constructed with both circular suction and counting areas (of radii R and r respectively) as is the case for the Tracerlab continuous air monitor. (See Fig. C.1).

For simplicity in the following derivations, the steady-state conditions of an aerosol of constant beta activity per unit volume, a flowing at a constant volumetric flow rate, V depositing activity at a uniform rate, q (equal to $aV/\pi R^2$) per unit area on a filter tape moving at a constant velocity, u has been assumed. It is also convenient to consider first a previously contaminated filter tape being rerun through the monitor with the coordinate axes x,y and x', y' as shown in Fig. C.1.

It may be noted that the activity concentration, Z deposited upon the filter tape is proportional to the cord length of the suction circle in the x' direction and is given by the relation,

$$Z = \frac{2q}{u}\sqrt{R^2 - y^2} \qquad (C.1)$$

with the restriction that

$$-R \leq y \leq R$$

and Z can thus be represented graphically as the elliptic sheet, infinite in the x direction shown in Fig. C.2.

As the contaminated tape with its elliptical distribution of activity passes under the counter window, the counting efficiency of each differential area is a function of x and y (or O and in polar coordinates). This function can be determined experimentally by placing a small, known, uniformly contaminated filter paper standard in the filter tape and passing it under the counter in the x direction as was done to obtain the data shown in Fig. C.3. Inasmuch as the efficiency of the G-M counter should be symmetrical about its central axis, the entire function can be represented by a solid of revolution, the

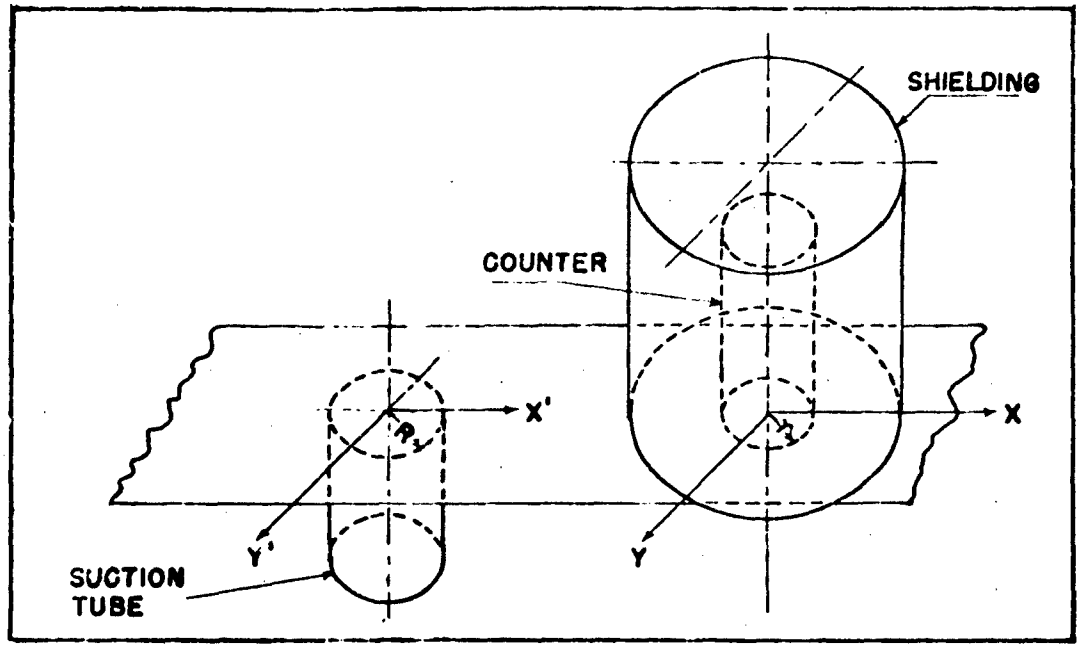

Fig. C.1 Schematic Drawing of the Tracerlab Continuous Air Monitor

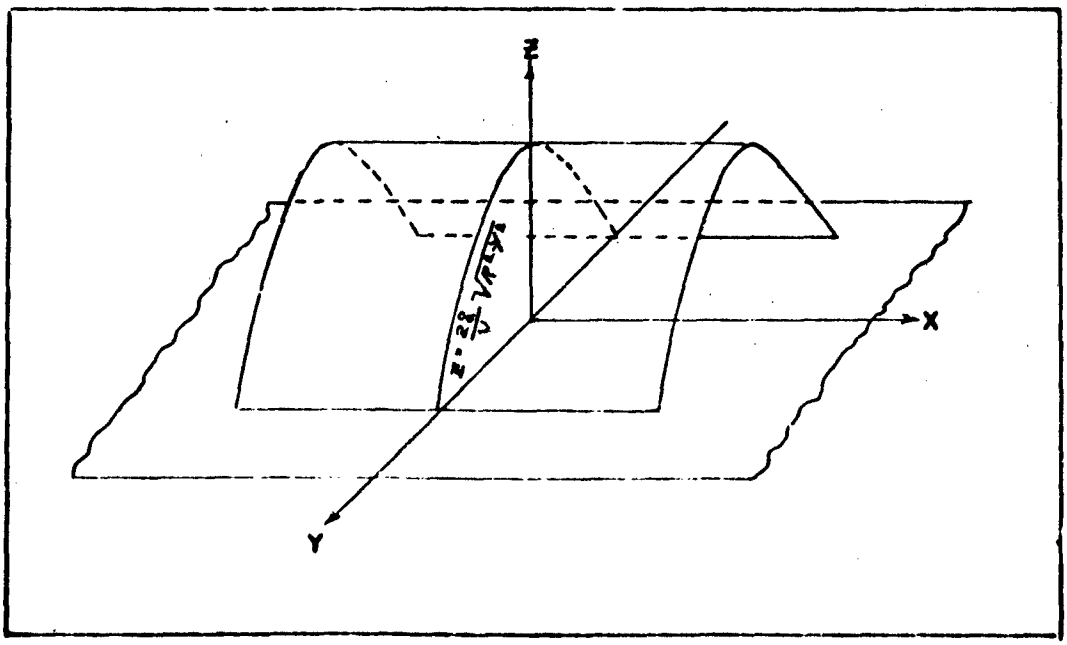

Fig. C.2 Activity Concentration as a Function of Tape Position for the Tracerlab Continuous Air Monitor

PROJECT 2.5a-1

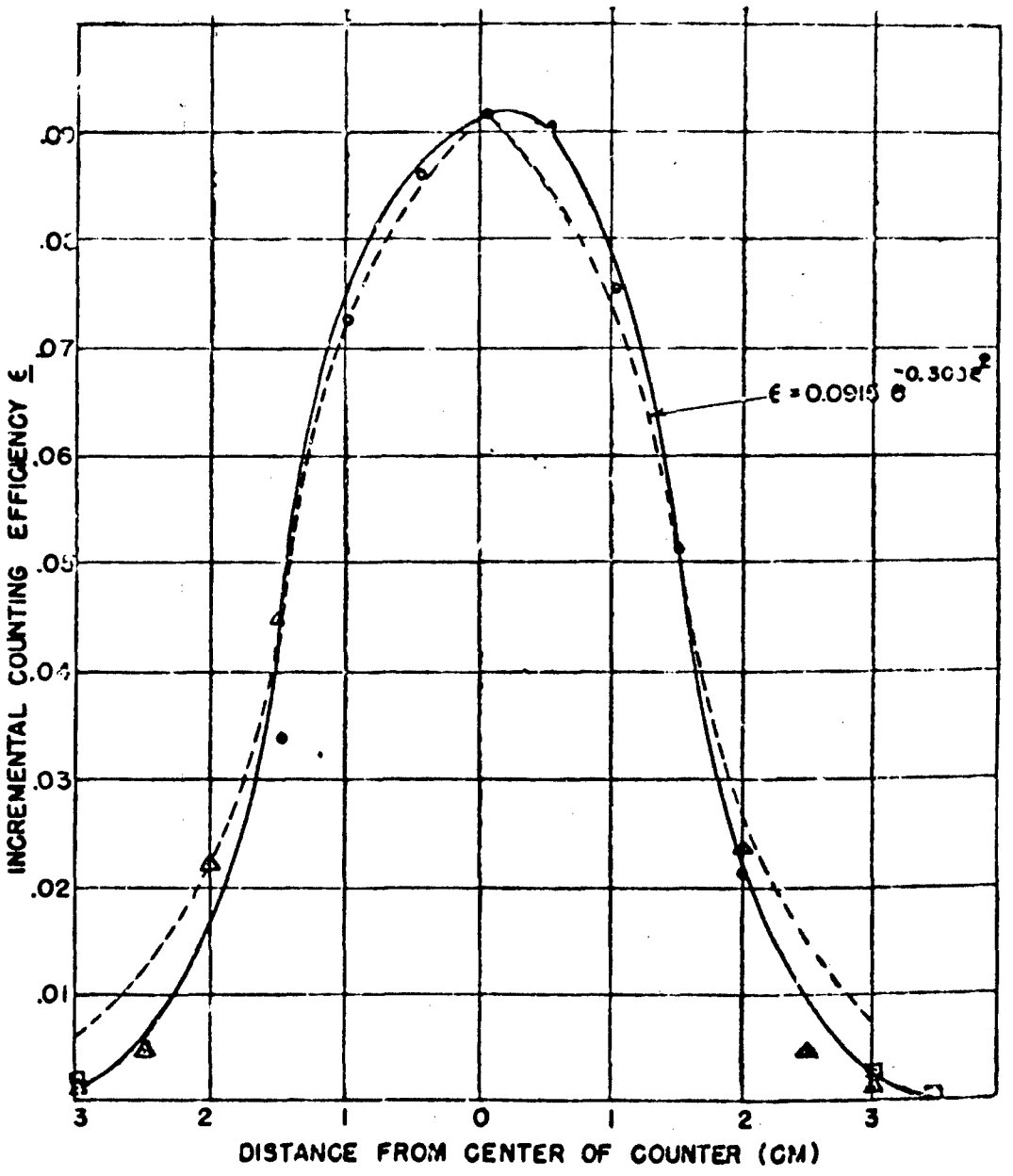

Fig. C.8 Variation of Counting Efficiency with Distance for the Tracerlab Air Monitor.

first quadrant of which is shown in Fig. C.4.

The differential count rate, z summed up by the G-M tube of the air monitor is the product of the activity concentration and the counting efficiency for each element of area of the x,y plane of the filter tape. Thus

$$z = \epsilon Z \qquad (C.2)$$

and can be represented by the solid sketched in the first quadrant of Fig. C.5.

The count rate, A finally recorded on the air monitor recorder is the volume between the surface escribed by the function z and the x,y plane in Figure C.5 and is approximately expressed by the definite double integral

$$A = 4 \int_0^R \int_0^{\sqrt{R^2 - y^2}} z \cdot dy \cdot dx \qquad (C.3)$$

or in the more convenient cylindrical coordinates by

$$A = 4 \int_0^R \int_0^{\frac{\pi}{2}} z \cdot \rho \cdot d\theta \cdot d\rho \qquad (C.4)$$

It may be noted that the upper limit of integration, R, for ρ introduces a small error due to the neglected volumes in the x direction

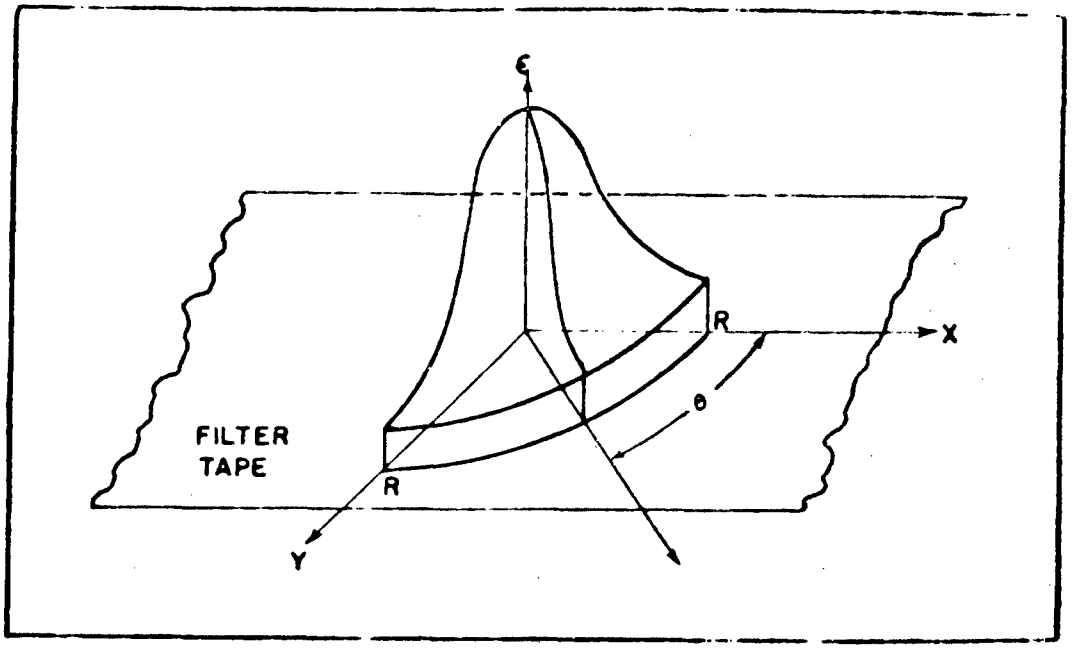

Fig. C.4 Differential Counting Efficiency as a Function of Tape Position for the Tracerlab Continuous Air Monitor.

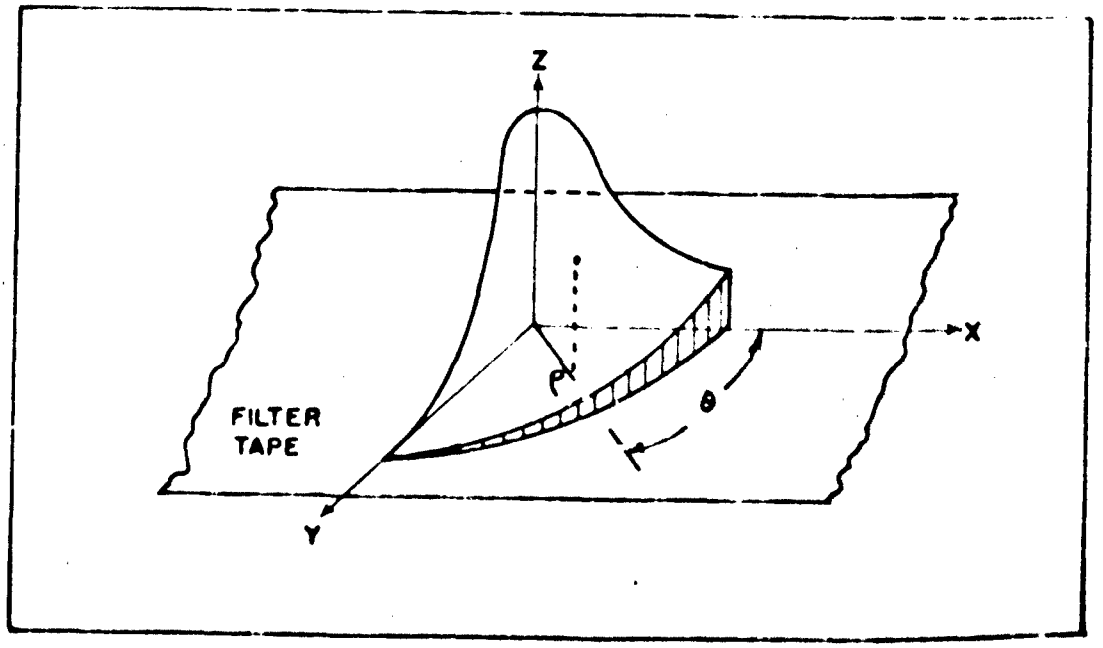

Fig. C.5 Differential Count Rate as a Function of Tape Position.

which should be trivial in the case of the well shielded Tracerlab air monitor.

The function

$$\epsilon = \alpha e^{-\beta\rho^2} \qquad (C.5)$$

may be arbitrarily selected to represent the solid of Fig. C.4. Substitution of this and Eq. C.1 into Eq. C.4 after changing to cylindrical coordinates by the substitution

$$y = \rho \sin\theta$$

results in the relation (C.6)

$$A = 4 \int_0^R \int_0^{\frac{\pi}{2}} e^{-\beta\rho^2} \cdot \rho \cdot \frac{2qR}{u} \sqrt{(1 - k^2 \sin^2\theta)} \, d\theta \, d\rho$$

in which the function, $1-k \sin\theta$ can be recognised as the elliptic integral of the second kind, $E(k,\theta)$. As the upper limit of the first integral is $\pi/2$, the complete elliptic integral, $E(k)$ can be obtained from tables 1 for various values of k where k is equal to ρ/R.
Equation C.6 thus becomes

$$A = \frac{8\alpha qR}{u} \int_0^R \rho \, e^{-\beta\rho^2} \cdot E(k) \cdot d\rho \qquad (C.7)$$

1 R. S. Burington, Handbook of Mathematical Tables (2nd ed; Sandusky, Ohio: Handbook Publishers, 1945) p.263.

and can be readily evaluated by graphical integration of a plot of the term within the integral sign versus ρ noting that k varies from 0 to 1 in the interval ρ = 0 to R. In terms of air concentration, Eq. C.7 becomes

$$\left(\frac{uc}{cm^3}\right)_{Replay} = \left[\frac{(1.77 \times 10^{-7})}{\alpha V} \frac{(u)(R)}{\int_0^R \rho e^{-\mu^2 r^2} E(k)\, d\rho}\right] A \qquad (C.8)$$

Thus the beta activity concentration of the sampled aerosol is a simple multiple of the recorded counting rate when the filter tape is played back through the Tracerlab air monitor.

A somewhat more complicated problem occurs during the build-up of activity upon the filter tape. Thus in Fig. C.1 the coordinate axes x,y and x',y' coincide. The deposition of activity upon the tape may be represented by the shape in Fig. C.6. Beyond ρ equal to R in the x direction, the surface becomes identical to the elliptic sheet of Fig. C.2 but within the region

$$0 \leq \rho \leq R$$

the activity concentration may be expressed by

$$Z = \frac{(q)}{u} \frac{(R \mathrel{/} x)}{R} \sqrt{R^2 - y^2} \qquad (C.9)$$

which may be transformed to cylindrical coordinates by the substitutions

$$x = \rho \cos \theta \text{ and } y = \rho \sin \theta$$

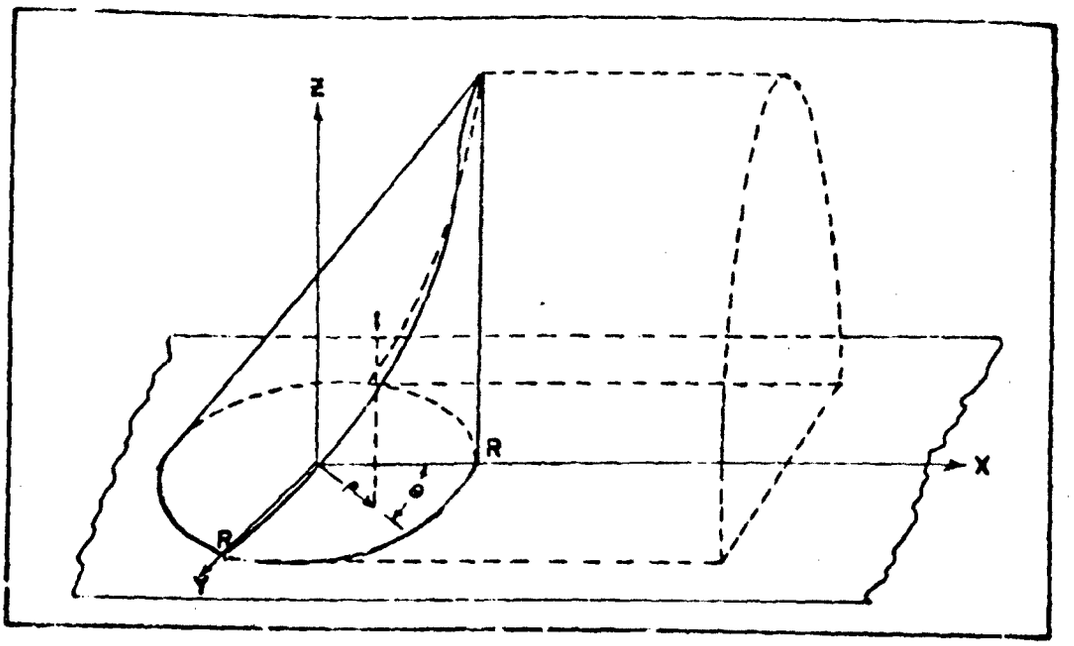

Fig. C.6 Activity Concentration During Deposition as a Function of Tape Position for the Trecerlab Continuous Air Monitor.

and Eq. C.9 becomes

$$z = \frac{(qR)}{u} \left(1 \pm k \cos\theta\right) \sqrt{1 - k^2 \sin^2\theta} \qquad (C.10)$$

Substitution of Eq. C.10, C.2 into Eq. C.4 for the first and second quadrants results in

$$A = 2 \int_0^R \int_0^{\pi} \alpha_0 - \beta\rho^2 \cdot \rho \cdot \frac{(qR)}{u} \sqrt{(1 \pm k \cos\theta)\ 1 - k^2 \sin^2\theta}\ \cdot d\theta\, d\rho \qquad (C.11)$$

or

$$A = \frac{2\sigma R}{u} \int_0^R \rho e^{-\beta\rho^2} \left[\int_0^{\pi} E(k,\theta)\, d\theta + k \int_0^{\pi} \sqrt{1 - k^2 \sin^2\theta} \cdot \cos\theta \right] . d\rho \qquad (C.12)$$

As it can be easily seen that

$$\int_0^{\pi} 1 - k^2 \sin^2\theta \cdot \cos\theta = 0 \qquad (C.13)$$

and also since

$$\int_0^{\pi} E(k,\theta)\, d\theta = 2 \int_0^{\pi/2} E(k,\theta) \cdot d\theta \qquad (C.14)$$

Equation C.14 may be simplified to

$$A = \frac{4\sigma R}{u} \int_0^R e^{-\beta\rho^2} \cdot E(k) \cdot d\rho \qquad (C.15)$$

which gives the counting rate for the moving tape. It may be noted that this is half of Eq. C7 so that the graphical integration need be performed only once for both cases. By use of Eq. C.7 and C.15, the initial and several replay results may be combined to investigate the radioactive de-

cay characteristics of the aerosol sampled by the Tracerlab air monitor.

An experimental determination of the value of the constants in these equations was made by means of the following procedure: A standard activity sample was prepared by placing an aliquot of a fission product mixture on a small (5 x 5 mm) square of filter tape from the Tracerlab continuous air monitor. This mixture was selected because of its beta range curve was considered to approximate that of the fission products resulting from the surface and underground detonations. The standard square was calibrated for its absolute beta activity while on a 4 mg/cm cellophane additional backscatterer in order to duplicate the conditions under which the tape itself is counted. This was done by raising the G-M counter in its shield to a higher position and mounting the square and reference activity standards on cards positioned on the lower bracket. Range curves for the reference standards as well as the calibrating square were determined on another counter with a shorter air path and thinner G-M tube window. These data were combined after appropriate corrections for air path, aluminum absorber of the air monitor, and the tube window so that the absolute beta activity of the filter paper square was determined by the average of two Tracerlab simulated P^{32} and two I^{131} reference standards which were stated to be accurate to ten per cent.

The standardized square was placed in a 5 x 5 mm square hole (backed with a similar 4 mg/cm^2 backscatterer) in a movable strip of air monitor filter paper in such a manner that the center of the standard square approximately coincided with the central axis of the G-M counter. Activity measurements for this square were made by moving it along the center line of the path followed by the tape, stopping at half centimeter intervals beginning 3 cm before, and 5 cm after departure of the center point of the standard from the central axis of the differential counting efficiency are given in Table C.3 and are plotted in Fig. C.5. The slight asymmetry of the curve is apparently due to a one millimeter error in positioning the calibrating standard. For purposes of comparison, the Gaussian curve used to approximate this function has been sketched in as a dotted line.

The function

$$\epsilon = \alpha e^{-\beta\rho^2} \qquad (C.16)$$

was selected to represent the two dimensional efficiency of the Tracerlab air monitor G-M tube (See Fig. C.4). By use of the smooth curve of Fig. C.3 the constants and of Eq. C.5 were found to be 0.0915 and 0.308 respectively for Unit No. 1. The integral of Eq. C.7 was then evaluated by tabulation of the values of the function

$$\rho e^{-\beta\rho^2} \cdot R(k) \qquad (C.17)$$

as a function of ρ and k as shown in Table C.2 and plotted in Fig. C.7. This curve was graphically integrated by the method of Moore[2] between the limits zero and R with the result that

$$\int_0^R e^{-\beta\rho^2} \cdot E(k) \cdot d\rho = 2.14 \qquad (C.18)$$

Substitution of this value into Eq. C.8 and rearranging resulted in the relations

$$\frac{(uc)}{cm^3}_{\text{Initial}} = (2.2 \times 10^{-11})(A) \qquad (C.19)$$

and

$$\frac{(uc)}{cm^3}_{\text{Replay}} = (1.1 \times 10^{-11})(A) \qquad (C.20)$$

which gave the air beta activity concentration from the observed initial and replay counting rates from the Tracerlab continuous air monitor.

In order to confirm the validity of the equations derived above as well as the accuracy of the emperical constants α and β, the calculated overall counting efficiency, ϵ_{ov} of a large circular (2.25 in. in diameter) filter standard was compared with the experimentally determined efficiency of a comparable standard. The overall counting efficiency can be obtained by integration of the expression

$$\epsilon_{ov} = \frac{4}{\pi R^2} \int_0^R \int_0^{\pi/2} e^{-\beta\rho^2} \cdot \rho \cdot d\theta \cdot d\rho \qquad (C.21)$$

[2] A. D. Moore, Proceedings of the Society for the Advancement of Engineering Education, California Meeting, 48, 452, (1940).

PROJECT 2.5a-1

TABLE C.1

Tracerlab Air Monitor Efficiency as a Function of Distance, x

Distance From Center of Counter cm	Scale of Instrument	Counts Per Minute	Differential Counting[a] Efficiency
0	100	37,500	0.0915
0.5	100	37,000	0.0903
1.0	100	31,000	0.0757
1.5	100	21,150	0.0516
2.0	100	9,040	0.0221
2.0	20	9,800	0.0239
2.5	20	1,970	0.0048
3.0	20	600	0.00146
3.0	2	750	0.00183
3.5	2	350	0.00085
- 0.5	100	35,400	0.0863
- 1.0	100	29,800	0.0751
- 1.5	100	13,500	0.0329
- 1.5	20	18,300	0.0446
- 2.0	20	9,300	0.0227
- 2.5	20	2,170	0.0053
- 3.0	20	700	0.0017
- 3.0	2	760	0.0019

(a) The absolute beta activity of the 6 mm square standard was approximately 4.13×10^6 d/min after correction for absorbers, tube window and air.

TABLE C. 2

Tabulation of the Function $\rho e^{-\beta\rho^2} \cdot E(k)$

ρ	ρ^2	$\kappa = \frac{\rho}{R}$	$\sin^{-1}\kappa$	$E(K)$ [a]	$e^{-\beta\rho^2}$	$\rho e^{-\beta\rho^2}$	$\rho e^{-\beta\rho^2} \cdot E(k)$
0	0	0	0	1.57	1	0	0
0.5	0.25	0.174	10	1.559	0.926	0.463	0.724
1.0	1.0	0.348	20.5	1.52	0.736	0.735	1.12
1.2	1.44	0.417	24.5	1.50	0.642	0.771	1.16
1.44	2.07	0.5	30	1.468	0.530	0.761	1.12
1.5	2.25	0.521	31.4	1.457	0.500	0.750	1.091
1.6	2.56	0.556	33.8	1.44	0.456	0.728	1.05
1.7	2.89	0.59	36.1	1.425	0.411	0.698	0.996
2.0	4.0	0.695	44	1.36	0.293	0.586	0.797
2.2	4.84	0.764	49.8	1.306	0.225	0.495	0.646
2.4	5.76	0.834	56.5	1.23	0.170	0.408	0.502
2.6	5.76	0.834	56.5	1.23	0.170	0.408	0.502
2.88	8.3	1.0	90	1.0	0.078	0.224	0.224

(a) R. S. Burington, Handbook of Mathematical Tables (2nd edition; Sandusky, Ohio: Handbook Publishers, 1946) p. 263.

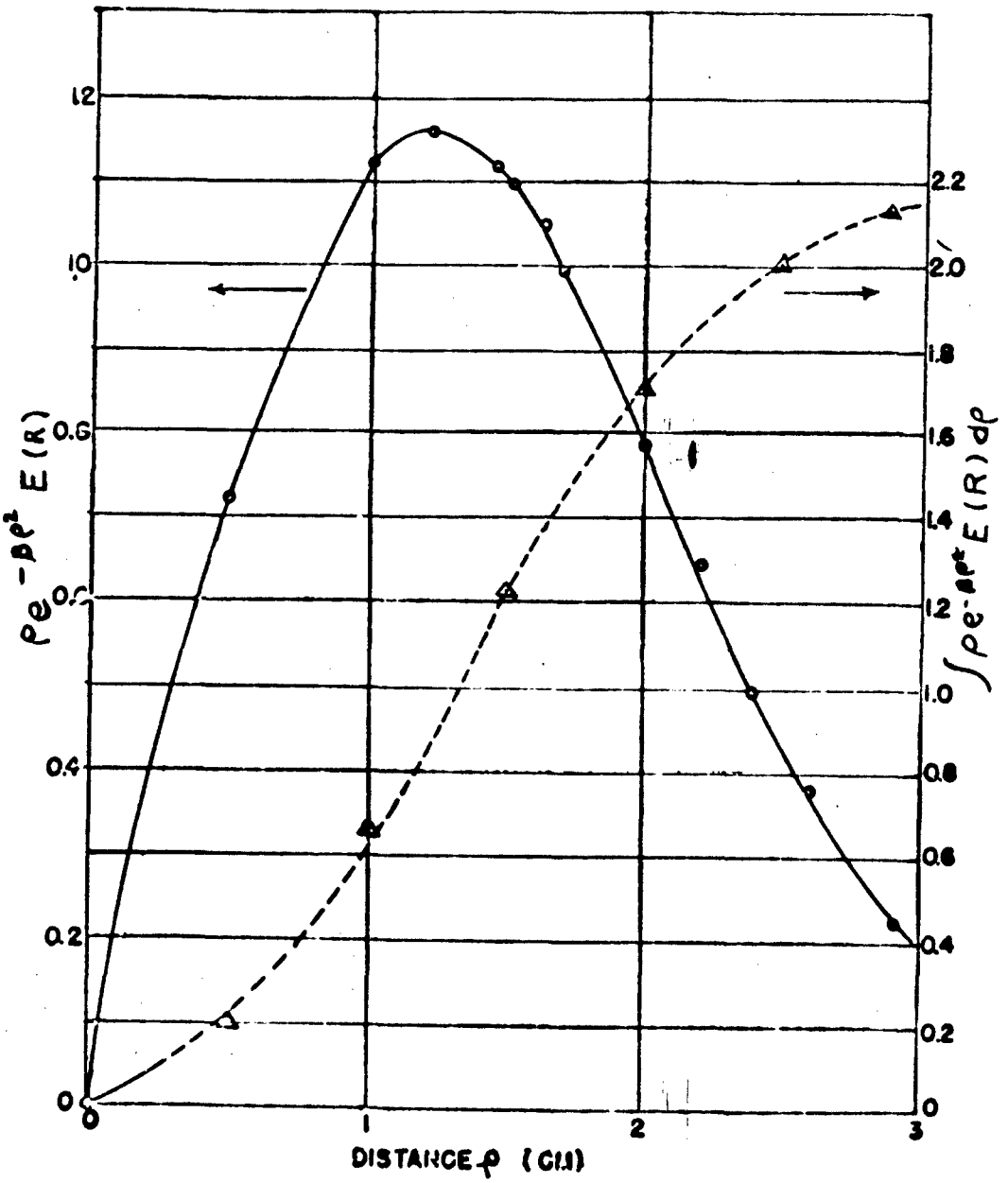

Fig. C.7 Plot of the Function of Table C.2 Versus ρ and Its Intergral Curve.

which may be derived by applying the same reasoning as used in Appendix B. Integration of Eq. C.21 results in

$$\epsilon_{ov} = \frac{\alpha}{\beta R^2} \left(1 - e^{-\beta R^2}\right) \qquad (C.22)$$

Substitution of the numerical values for α, β, and R into this equation results in

$$\epsilon_{ov} = 0.033$$

for the calculated counting efficiency of a uniformly contaminated standard 2.25 in. in diameter. For comparison, standard activity papers were prepared by spraying circular discs 2.25 in. in diameter with radioactive dust and calibrating them with a G-M counter of known geometry. The calibrated discs were placed under the G-M tube of the air monitor and the activity observed with the following results:

TABLE C.3

Efficiency Data for Tracerlab Air Monitor for Circular Uniformly Contaminated Area(a)

Standard	Activity d/min. Corrected for Window, Air and Absorber	Observed c/min	Efficiency
1	1.38×10^5	3.98×10^3	0.029
2	1.36×10^6	2.98×10^4	0.022
3	4.3×10^5	9.82×10^3	0.023
			Aver. = 0.025

(a) Data for Unit No. 1. Average value for units four and five were 0.024 and 0.032 respectively.

The agreement between the values presented in Table C.3 and the calculated value is considered to be sufficiently close to confirm the validity of the derived expressions and the constants employed, especially in view of the fact that completely uniform distribution of the radioactive dust over the filter paper discs was difficult to attain by the method employed. Due to the greater experimental simplicity, more direct approach, and the greater care exercised in its preparation and calibration, the small 5 x 5 mm square standard was used as the basis for the activity concentrations reported in paragraph 4.12.

APPENDIX D

EVALUATION OF INSTRUMENTS

D.1 INTRODUCTION

The evaluation of the hazard to personnel from an AED cloud can be made from studies of data on activity and particle size of the generated aerosol. Such a study requires four types of information. These are:

(a) Properties of the cloud expressed as activity and mass per unit volume and time.

(b) Properties of fall-out expressed as activity and mass per unit time.

(c) Particle size distributions of (a) and (b) expressed as a function of time.

(d) Radiochemistry of (a) and (b) above.

Since the collection of these data is a field operation, laboratory accuracies should not be expected; even though laboratory equipment be employed.

A brief description has been prepared of each item of sampling equipment used for Operation JANGLE. It is intended to discuss the advantages and disadvantages associated with each instrument insofar as its ability to collect samples for the above data; this information should aid (1) the design of improved sampling instruments, and (2) the selection of instruments for use in future tests.

D.2 CONTINUOUS AIR MONITOR

In this instrument the aerosol is drawn through a moving strip of filter material which removes particulate matter. The activity of the collected particles is then measured by conventional alpha and beta counters as the strip is moved through the counting chambers.

Operation JANGLE employed two continuous air monitors - Brookhaven and Tracerlab. The Tracerlab instrument is a refinement of the Brookhaven model in that it is more compact. The Tracerlab measures activity at the same time as sampling. However, this may or may not be an advantage, since contamination of counting equipment is possible. The Brookhaven continuous air monitor measures activity shortly after collection.

The continuous air monitor furnishes a complete record of (1) alpha, and (2) beta plus gamma radiation for any desired period of time. This valuable record is not produced without great difficulty since the continuous air monitors are bulky, delicate, and complex from the viewpoint of field operation. They require a good AC power supply and must be protected from all so-called bad weather conditions. The instrument weighs about 500 pounds.

D.3 FILTER SAMPLER

The filter sampler is another cloud or aerosol sampling instrument which collects particulate matter on filter paper. The collection is made by pulling air through the paper at from 1 to 6 cfm. The paper is then removed and its activity determined by proper alpha and/or beta plus gamma counters.

The filter sampler may operate from battery or AC power generator and is rugged, light weight (about 20 pounds), and simple to operate. Data on AED cloud activity collected with this instrument is difficult to interpret for two principal reasons: (1) The variation of activity with time cannot be obtained except by auxiliary apparatus, (2) the predetermined flow rate is subject to errors due to clogging of the collection paper. The exact clogging effect is difficult to determine except by visual operation of the instrument which is impossible in field operation.

D.4 INTERMITTENT AIR SAMPLER

The intermittent air sampler collects the cloud and/or fall-out particulate matter on each of twelve (12) filters so arranged that each filter is employed for a preset time of operation. The collected aerosol particles may be counted for alpha and beta plus gamma activities.

The resulting record will furnish data concerning the variation of activity with each time interval employed. Clogging effects will not be encountered for most cases, since the sampling time intervals may be kept short (say 10 minutes).

This instrument is light weight and is operated from batteries. The unit complete with batteries weighs about 25 pounds. Although the unit is compact, it is not rugged and requires shielding from rain and dust. The arrangement of the filters is such that they are unprotected from fall-out.

D.5 PARTICLE SEPARATOR

The particles separator is designed to fractionate particles from the ABD cloud. The fracionation is to be done at the time of sampling and is accomplished by a series of wire screen cloths with openings of 37, 44, 53, 61, 73, 88, 106, 125, 148, 177, and 210 microns. A molecular back up filter is employed for collection of particles less than 37 microns.

In theory, each screen is counted and the relationship between particle size and activity determined. It has been shown that small particles tend to stick to screen wires instead of being captured on their proper sized screen.

The separator is a small piece of equipment, but requires auxiliary vacuum and power supply. The separator weighs about 1 pound without vacuum pump.

D.6 CONIFUGE

The conifuge samples cloud aerosol for particle size analysis in range of 0.3 to 10 microns at the rate of about 170 cc per minute as air is drawn between two conical surfaces (rotating at 5000 rpm) which are separated approximately one-eighth inch apart. The particulate matter is centrifuged out with respect to mass. A section of the outside plastic conical surface is cut out and examined microscopically for particle size. Electron microscope screens are located on the plastic.

The conifuge is quite rugged but produces excessive vibration of auxiliary equipment. It requires a power supply which may be either generator or batteries. The instrument without power supply weighs about 30 pounds and is well protected from elements (weather) except for dust protection.

Particle size analysis of conifuge samples obtained in the field has not been entirely successful even though the theory is good. Since the surface area for collection of particles is large, the instrument is capable of long periods (1-2 hrs.) of operation for most field sampling duties.

There is no method for obtaining particle size vs. time of collection data.

Isokinetic sampling is not obtained.

D.7 CASCADE IMPACTOR

The cascade impactor is a cloud or aerosol sampling instrument; operated to obtain a sample for particle size analysis in range of 0.1 to 20 microns. Air at the rate of 12.5 liters per minute is drawn through a series of five jets with decreasing orifice diameter. The air stream from each jet impinges upon a glass plate which collects the particulate matter. The first plate, which is opposite the coarse stream, collects the largest particles while the last plate collects the smallest particles. The instrument weighs about 30 pounds including the vacuum pump, but not including AC or DC power supply.

The volume of sample is large but can be maintained for but a minute for most field sampling jobs, since the collecting area is small. It is difficult to predetermine exact sampling times desired and remote control or alarm control is complex.

The instrument is fairly rugged, and is well protected from elements although dust protection is not adequate.

When proper sampling time is used, an ideal sample is obtained and fractionation allows some approximation to be made of the relationship between particle size and activity.

D.8 THERMAL PRECIPITATOR

The thermal precipitator is an aerosol sampling instrument whereby particles are precipitated on a cold surface through their reaction from a hot filament. Particles from 0.02 to 10 microns are resolved as aerosol is sampled at the rate of approximately 7 cc/min.

The thermal precipitator has been used in the field and isokinetic sampling attempted. The instrument is bulky (weight 40 pounds) delicate, complex, and requires a large DC power supply. However, a good sample for particle size analysis can be obtained.

Except for dust, adequate weather protection is provided but no attempt has been made to provide particle size vs. time data.

D.9 ELECTROSTATIC PRECIPITATOR

The electrostatic precipitator is an instrument which may be used to collect particles for particle size and/or activity measurements. Air is drawn through a metal cylinder between which and an inside electrode, there has been applied an electrical potential of several thousand volts. The sampling rate can be varied according to the design of the power supply.

The precipitator operates at high collection efficiency, has no clogging effects, and can be readily adapted for counting. However, no technique is available for obtaining activity vs. time data with the instrument.

Particle size analysis could be made of the collected sample, although no exact techniques are known. There is no fractionation of particles nor any particle size vs. time techniques.

In general, the precipitator requires specialized auxiliary electronic equipment (power supply) and a good AC source. There is no information on its behavior under conditions of high humidity. The use of high voltages makes it a dangerous piece of equipment especially so in wet climates.

The precipitator complete with high voltage power supply and vacuum equipment weighs about 40 pounds.

D.10 DIFFERENTIAL FALL-OUT COLLECTOR

The differential fall-out collector is an improvement of the fall-out tray in that fall-out variation with time may be determined. The use of slides for particle size analysis makes this a desirable instrument. The collector is operated by a mechanical clock which rotates a disc beneath a slotted cover in such manner as to collect fall-out on the disc.

The instrument is light weight (5 pounds), fairly rugged, and complete except for minor design changes. There appears to be an improper seal on the cover which allows dust leakage. No information is available on the protection afforded against a wet, humid atmosphere.

D.11 CONCLUSIONS AND RECOMMENDATIONS

None of the sampling equipment discussed here is entirely satisfactory. Although some instruments approach the desired type, there is a need for sampling equipment to furnish the data listed in the introduction. In order to obtain such improved experimental results with greater efficiency and therefore economy, the following considerations should be incorporated into redesign of sampling equipment.

(1) Permit alpha and/or beta plus gamma activity measurements of cloud and fall-out samples.

(2) Approach 100 per cent sample collection efficiency.

(3) Simple and accurate flow calibration.

(4) Well adapted for high counting geometry with a minimum of manipulation.

(5) Keep field installation effort at minimum.

(6) Operation in wet, humid as well as hot, dry, or cold climates not affected by dust.

(7) Suitable for operation from stationary ground position as well as moving vehicle or aircraft.

(8) Prepared for remote control of starting and stopping mechanisms.

(9) Power requirements suitable for AC or DC circuits to be operated by battery or generator.

(10) Keep sample pick-up time short to allow rapid recovery of samples from highly radioactive fields.

(11) Allow quick removal of equipment from field, vehicle or aircraft.

(12) Permit replacement of sampling equipment as a unit-furnish with plug-in receptacles for electrical as well as air and vacuum connections.

(13) Reduce the need of tools in assembly, sample pick-up, and roll-up operations.

(14) Allow shipment via truck, express, or aircraft with a minimum of packing.

(15) Allow decontamination by washing with hot water and/or steam.

APPENDIX E

INTERIM REPORT, ARMY CHEMICAL CORPS, CONTRACT NO. DA-18-108-CML-2532

with Tracerlab, Inc., R.D. Epple, Project Director[1]

E.1 PREFACE

This Interim Report contains the experimental results of the work on JANGLE, together with the interpretations that can be made at this time. Each of the three parts of the report are independent units, and have therefore been assembled with this in mind. Each section consists of a short introduction that indicates the purpose of the work. This is followed by the experimental results and a discussion of the significance of the results.

It is anticipated that the final report will add to this report sufficient information to permit a thorough evaluation of the results. It will include considerable detailed information about the experimental procedures developed in this laboratory.

E.2 ACKNOWLEDGMENT

This report has been written by the following members of the Tracerlab staff:

Charles Sherman	Counting Program and Decay Curves
James Shearer	Particle Size Distribution
Robert Epple	Radiochemistry

1. This report is reproduced here in its entirety, and is edited only with respect to format.

E.3 COUNTING PROGRAM

The object of the counting program was to measure the radioactivity contained on filter papers which sampled the cloud under certain known conditions of operation, and to determine the radioactivity as a function of time after time-zero. These two aspects of the program are necessary for the evaluation of the radiation hazard to personnel in the vicinity of an atomic explosion. Solution of the radiation hazard problem also requires knowledge of the distribution of sizes of the radioactive particles; this part of the problem is treated on Section E.4.

E.3.1 Filter Sampler Activity

Table E.1 and Table E.2 give the beta activity of each filter paper received. These activities were measured with a "wrap around" counter set up which used a Tracerlab TGC-5A tube. Each paper was wrapped around a cylindrical lead jig of such diameter that it just fit over the tube. The lead jig had an opening of 43^2cm which faced the thin-walled (30 mg/cm^2) portion of the tube. Thus the remaining part of the paper was shielded from the tube by the 1/8 inch thick wall of the lead jig, and the activity of 43 cm^2 from the central part of each paper was measured. Each paper was left in its plastic bag for counting to avoid contaminating the apparatus. The effective absorber thickness along radii of this cylindrical arrangement is then approximately 20 mg/cm^2 of plastic plus 30 mg/cm^2 of glass. A smaller area was measured for some of the most active papers.

In Tables E.1 and E.2 the time of each measurement is given in hours after time-zero in the second column. The activity of each paper (cpm) corrected for background is given in the third column. For purpose of comparison it is necessary to correct each activity measurement to some standard time after time-zero. 600 hours after time-zero has been used, and each activity measurement corrected to this time by use of the measured decay curves (see Figures E.1-E.5). Each corrected activity measurement has been multiplied by the appropriate area factor (100/43) (is the factor in most cases) giving the total beta activity of each paper at 600 hours; these results appear in the fourth column. This latter result was not calculated for those cases where the activity was extremely small. Blank spaces in the third column indicate that the observed counting rate was lower than the background rate.

Although the counting set-up described above has not been thoroughly calibrated, it is known that the disintegration rate is related to the counting rate by the following approximate equation:

$$\text{dpm} \approx 18\ (\text{cpm}).$$

PROJECT 2.5a-1

TABLE E.1

Filter Sampler Counting Data, Surface Shot

Sample	Time of Count After T_o Hours	CPM	CPM For Whole Area at 600 Hours
S-1X-1 *	215	5013	3430
2 *	215	2.2	
3 *	215	2.9	
S-4X-1	not received	-	
2	602	2.5	
3	603	2.5	
S-7X-1	268	297	266
2	268	-	
3	268	2.8	
S-8X-1	266	225	202
2	266	0.9	
3	266	-	
S-9X-1	not received		
2	604	0.6	
3	605	5.7	
S-10X-1	194	71.3	43
2	194	-	
3	194	-	
S-15X-1	191	147.3	91
2	191	-	
3	191	0.5	
S-16X-1	196	155.6	95
2	196	-	
3	196	-	
S-21X-1	240	446.0	347
2	240	-	
3	240	0.6	

*These numbers refer in each case to the first, second and third filter papers collected at each station.

PROJECT 2.5a-1

TABLE E.1 (Cont'd)

Sample	Time of Count After T_o Hours	CPM	CPM For Whole Area at 600 Hours
S-22X-1	216	527	362
2	216	0.2	
3	216	0.8	
S-23X-1	265	1284	1150
2	265	0.9	
3	265	3.7	
S-24X-1	240	532	415
2	240	-	
3	240	-	
S-27X-1	218	1918	1310
2	218	0.2	
3	218	9.4	
S-29X-1	287	2022	2050
2	287	-	
3	288	4.1	
S-31X-1	244	-	
2	245	-	
3	263	0.8	

TABLE E.2

Filter Sampler Counting Data, Underground Shot

Sample	Time of Count After T_o Hours	CPM	CPM For Whole Area at 600 Hours
U-101X-1			
2	not received		
3			
U-104X-1	190	41.7	38
2	190	2.2	
3	190	5.9	5.1

PROJECT 2.5a-1

TABLE E.2 (Cont'd)

Sample	Time of Count After To Hours	CPM	CPM For Whole Area at 600 Hours
U-107X-1	1940	3540	33,100
2	144	40.4	29
3	144	34.9	25
U-108X-1	1940	3070	342,000
2	384	139	216
3	384	132	205
U-109X-1	1940	2343	21,900
2	169	34.7	27
3	169	43.7	34
U-110X-1	192	30.3	26
2	192	10.3	8.9
3	192	5.2	4.4
U-115X-1	165	6360	4940
2	165	10.4	8.2
3	165	17.1	13
U-116X-1			
2	not received		
3			
U-121X-1	1940	3474	32,400
2	168	62.3	49
3	168	95	74
U-122X-1	121	6.9	4.0
2	121	2.5	
3	121	-	
U-123X-1	1940	8635	842,000
2	433	389	650
3	433	1206	2010

PROJECT 2.5a-1

TABLE E.2 (Cont'd)

Sample	Time of Count After T Hours	CPM	CPM For Whole Area at 600 Hours
U-124X-1	1940	3205	29,800
2	193	50.1	43
3	193	174	150
U-127X-1	1940	4940	551,000
2	360	625	910
3	360	1970	2870
U-129X-1	1940	6640	622,000
2	167	782	608
3	167	1280	995

Since our counting arrangement has a much higher efficiency for beta rays than gamma rays the activities listed in Tables E.1 and E.2 are essentially the beta activities; it is estimated that 1/2-1% of this is due to gamma activity.

In order to measure the alpha activity of these papers it is necessary to obtain a very thin sample (not more than 2-3 mg/cm^2). This has been done by dissolving a small portion of one of the most active papers from each shot, and evaporating the resulting solution on a platinum planchet until the maximum allowable thickness has been obtained. The beta and alpha activities of these samples will be measured and the alpha activity of each of the other papers estimated by using this beta: alpha ratio and the measured beta activities. Nuclear track plates will be used to measure the alpha activity since this has proven to be one of the most reliable methods of measuring alpha activity. This work is in progress although results are not available yet.

It can be seen from Tables E.1 and E.2 that the majority of the activity is present on the first paper in the series of three papers. In the cases of U-107X and U-110X, however, the activity of the last paper in the series (#3) is about 15% of the activity of the first paper (#1). It should be noted that these two sets of papers came from adjacent stations on one side of the station layout. The three papers from each of these two sets were radioautographed for 17 days beginning February 4, 1952, in an attempt to investigate further the nature of the radioactive particles which they contained. Although the activity of these papers was not great enough to permit any definite statements to be made from this type of in-

vestigation, it was found that the number of spots on the radiographs of the last papers in each series was less than 15% of the number of spots on the radiographs of the first papers. This is consistent with the hypothesis that the particles on the last papers of the series are smaller than the particles on the first papers.

E.3.2 Filter Sampler Activity Decay

Beta decay curves for the designated papers were obtained with the counting arrangement described previously and appear in Figures E.1 through E.7. Decay measurements were taken on the first paper in the series of three since this one had the majority of the activity. Paper U-122X was received and counted, but did not contain enough activity for decay measurements. In Figures E.1-E.7 counts per minute is given on dotted curve drawn through each set of experimental points represents a decay which is inversely proportional to the time; it is fitted to the data at 600 hours. This type of decay agrees with the Hunter and Ballou results for fission product decay for times between about 100 and 900 hours, and is seen to agree approximately with the data here. For times greater than about 900 hours, the data is seen to decay slightly faster than the dotted curve which is also in agreement with the Hunter and Ballou results. The data is given here up to about 1200 hours (50 days) after time-zero; further data is being taken and will be given in a future report.

E.3.3 Discussion

The data of Tables E.1 and E.2 when combined with the diagrams of the station layout show the spatial distribution of the activity with respect to ground-zero. It is seen that the majority of the activity covers only two arms of the four-armed station layout system, and that in some cases, more activity was collected on the distant papers than on the near ones. Figures E.1-E.7 give the activity as a function of time after time-zero. As we have seen, this data agrees well with the Hunter and Ballou results for fission product decay for the range of times under consideration. It would be desirable for the purposes of evaluating radiation hazards to know the shape of the decay curve for a wider range of time than has been possible here. The data is being extended to longer times in those cases where the activity is sufficient. Although measurements were begun as soon as the papers were received in this laboratory, the earliest data is between 100 and 200 hours after time-zero. Since we have good agreement with the Hunter and Ballou results for the range of time over which the measurements were made, it is reasonable to assume that our best approximation for earlier times is also the Hunter and Ballou results. One qualification must be made; when induced activities are present in appreciable amounts, the decay curve will differ from that of Hunter and Ballou results. Evidence of such activity is seen in some of the figures where the experimental curve differs from the dotted curve at early times.

We have presented data in this section which when combined with other known data (such as amount of air sampled per filter paper, position with respect to ground-zero, prevailing atmospheric and wind conditions, etc.) can be used to evaluate the radiation hazard to personnel in the vicinity of an atomic explosion at various times after the explosion.

E.4 PARTICLE SIZE DISTRIBUTIONS

E.4.1 Radioactive Particles

These particles were found by first dispersing the filter paper fibers with a needle in a layer of collodion on a glass slide, and then radioautographing the slide. The developed film was realigned with the slide and a search made under each "spot". If the field of view was too crowded, that area of collodion was redispersed and radioautographed again. Most of the particles were found to be spherical, but we found more irregular shapes on JANGLE than on previous tests. When a particle has been found, its diameter is measured, and its approximate color and shape are noted. The diameters of all the particles found are then classed into groups such that all particles of group i have diameters D such that:

$$D_i - \frac{\Delta D}{2} < D \leq D_i + \frac{\Delta D}{2} \qquad (E.1)$$

where the group width ΔD is 0.5 microns.

If N_i is the number of particles in the ith group, then the total number N is simply:

$$N = \sum^{i} N_i \cong \int_{0}^{\infty} \frac{dN}{dD}\, dD \qquad (E.2)$$

where we have made the assumption that the size distribution will approach a smooth curve as N becomes large.

The results for N_i vs D_i are shown in E.8 for the surface shot, Stations 29, and 30, and Fig. E.9 for the underground shot Stations 129 and 130.

There are several sources of error in our measurement. First, the radioautograph will not give a visible spot when the particle is weakly radioactive. This means that as the particle diameter becomes smaller, the efficiency of recovery decreases. Second, the difficulty of seeing a particle increases as the diameter decreases, further lowering the efficiency of recovery. Furthermore, it is not possible to correct for these effects in a quantitative way, since all the factors involved are not completely under our control. It is our feeling, based on past experience, that we can always recover particles of diameter $D > 4$ microns with 100% efficiency. In some special cases this limit can be decreased.

PROJECT 2.5a-1

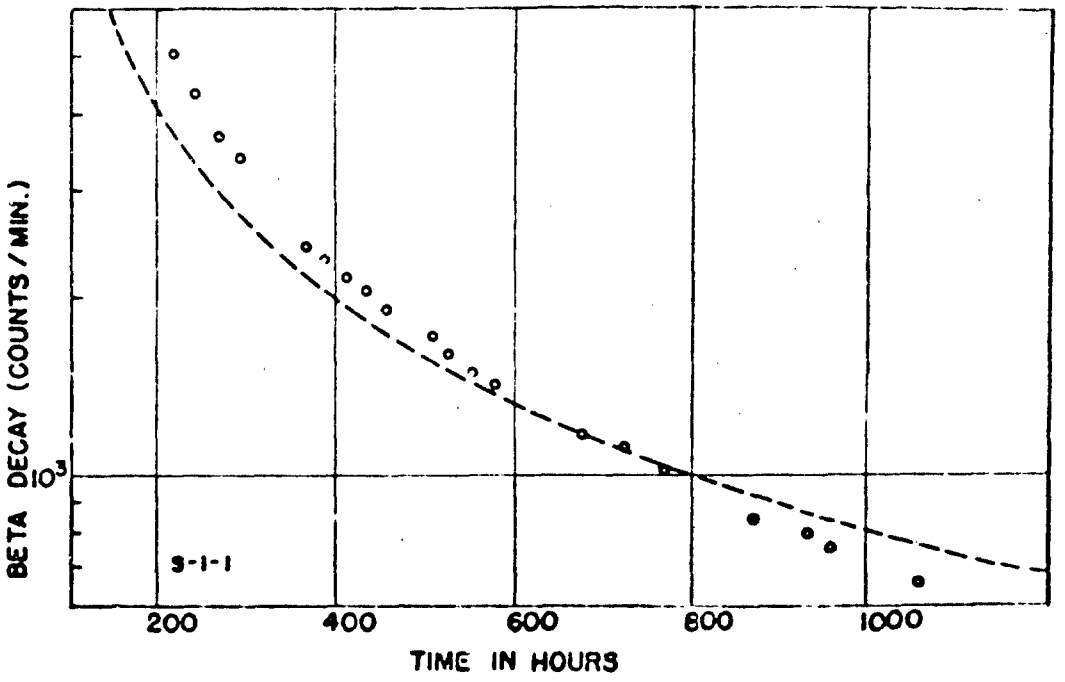

Fig. E.1 Beta Decay Curve, First Filter Paper of Filter Sampler at Station 1, Surface Shot.

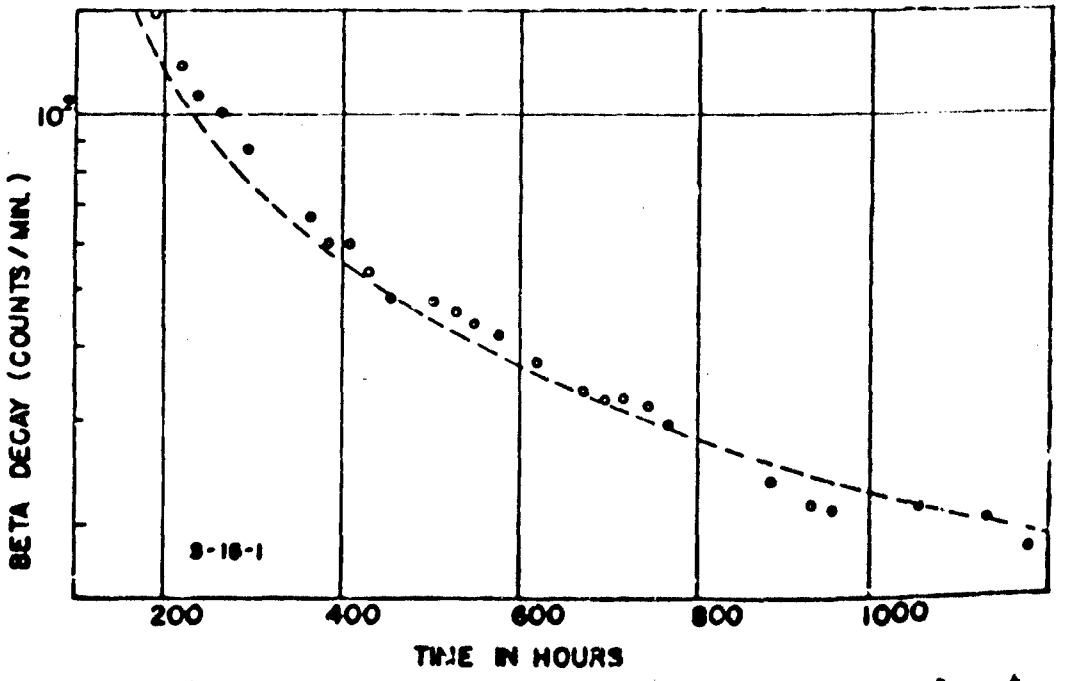

Fig. E.2 Beta Decay Curve, First Filter Paper of Filter Sampler at Station 16, Surface Shot.

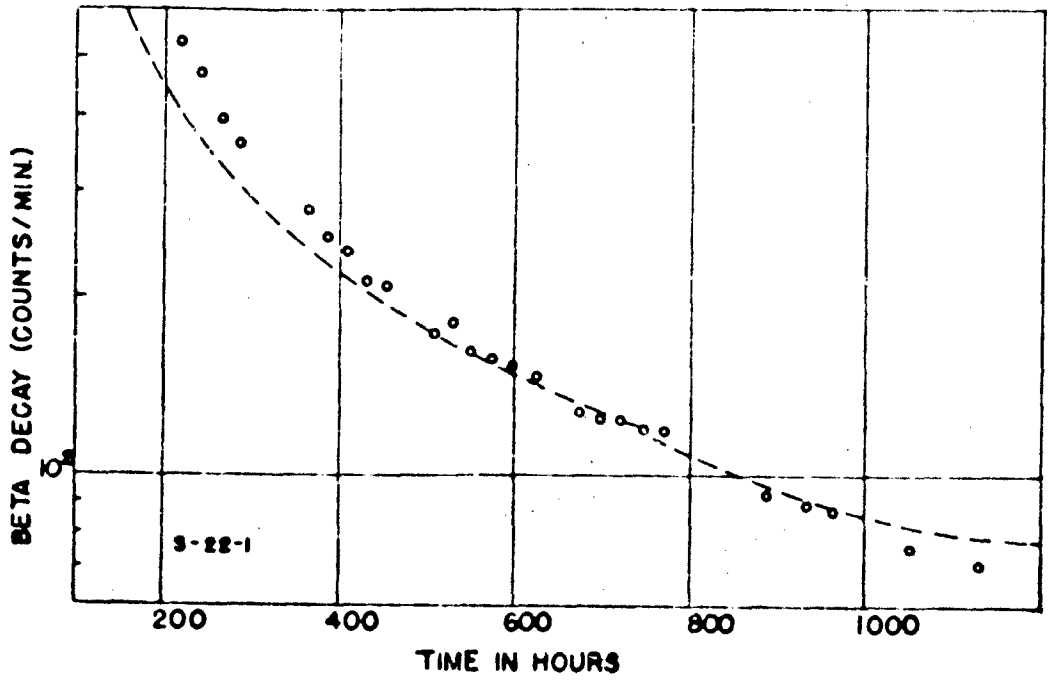

Fig. E.3 Beta Decay Curve, First Filter Paper of Filter Sampler at Station 16, Surface Shot.

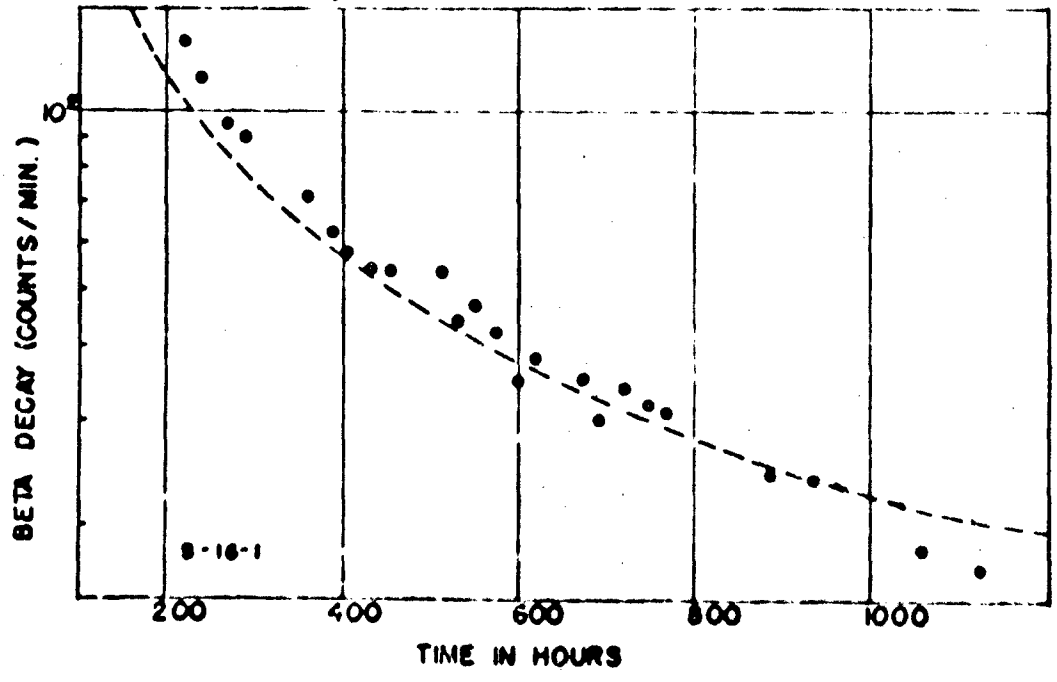

Fig. E.4 Beta Decay Curve, First Filter Paper of Filter Sampler at Station 22, Surface Shot.

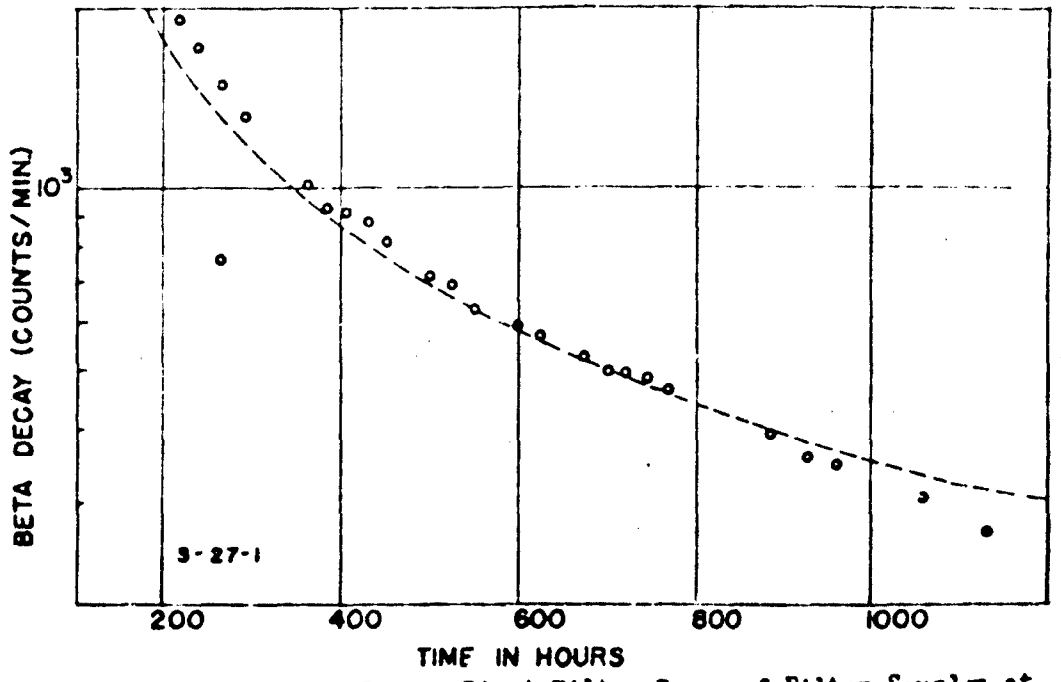

Fig. E.5 Beta Decay Curve, First Filter Paper of Filter Sampler at Station 27, Surface Shot.

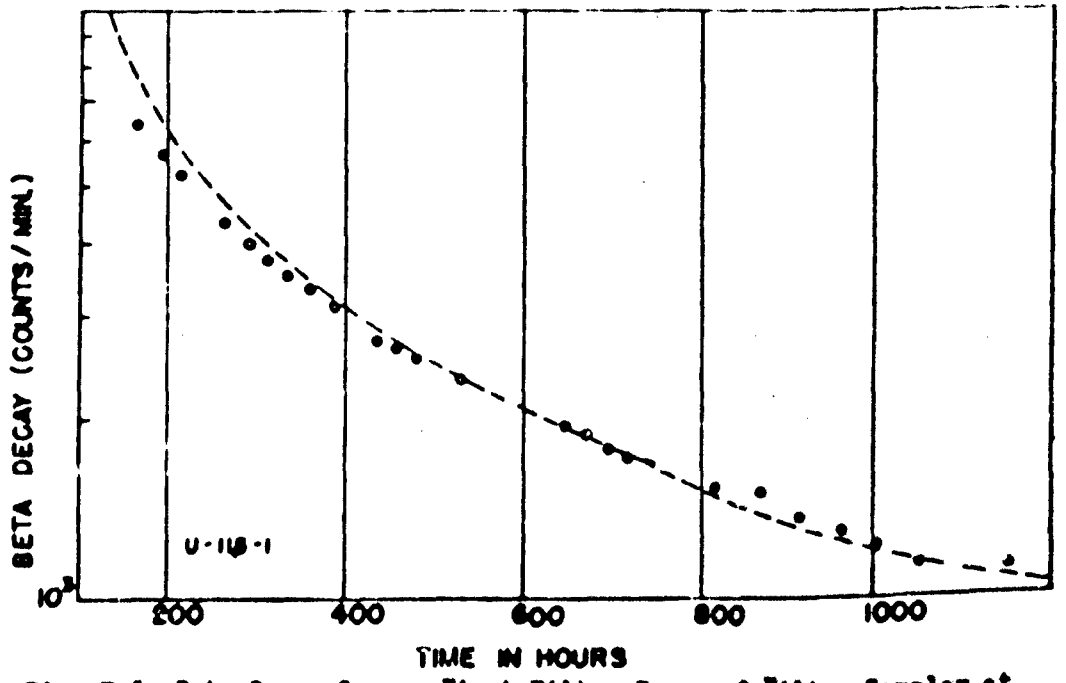

Fig. E.6 Beta Decay Curve, First Filter Paper of Filter Sampler at Station 118, Underground Shot.

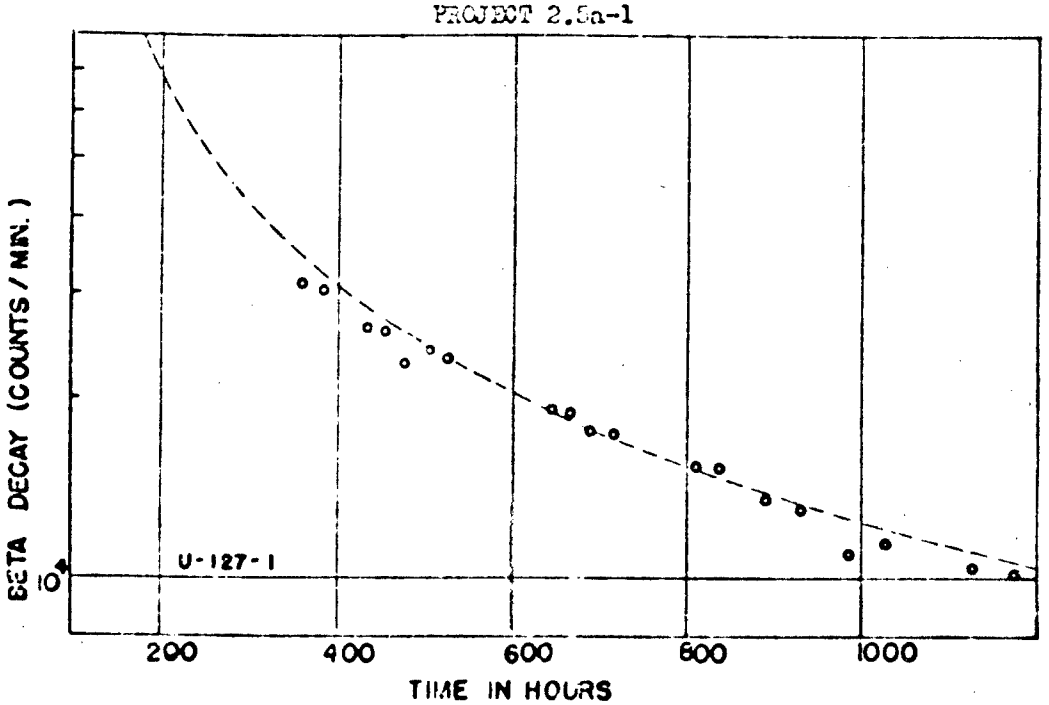

Fig. E.7 Beta Decay Curve, First Filter Paper of Filter Sampler at Station 127, Underground Shot.

It should also be mentioned that the upper limit of the size distribution curve is determined by the total number of particles which are measured. If 10,000 particles were measured instead of 1000, one could extend the distribution curve to slightly larger diameters.

We now define the size distribution function P:

$$P \equiv \frac{1}{N}\frac{dN}{dD} \qquad (E.3)$$

P is the probability of finding one particle of the population of N particles whose diameter is greater than D and less than D + dD. Since we believe that the efficiency of recovery for particles larger than 4 microns is roughly constant, the slope (dP/dD) of our size distribution curve will be equal to the slope of the true size distribution within experimental errors. It will be convenient to define two new parameters:

$$\frac{1}{b} \equiv \frac{1}{P}\frac{dP}{dD} \qquad (E.4)$$

$$n \equiv \frac{dP/P}{dD/D} = \frac{D}{b} \qquad (E.5)$$

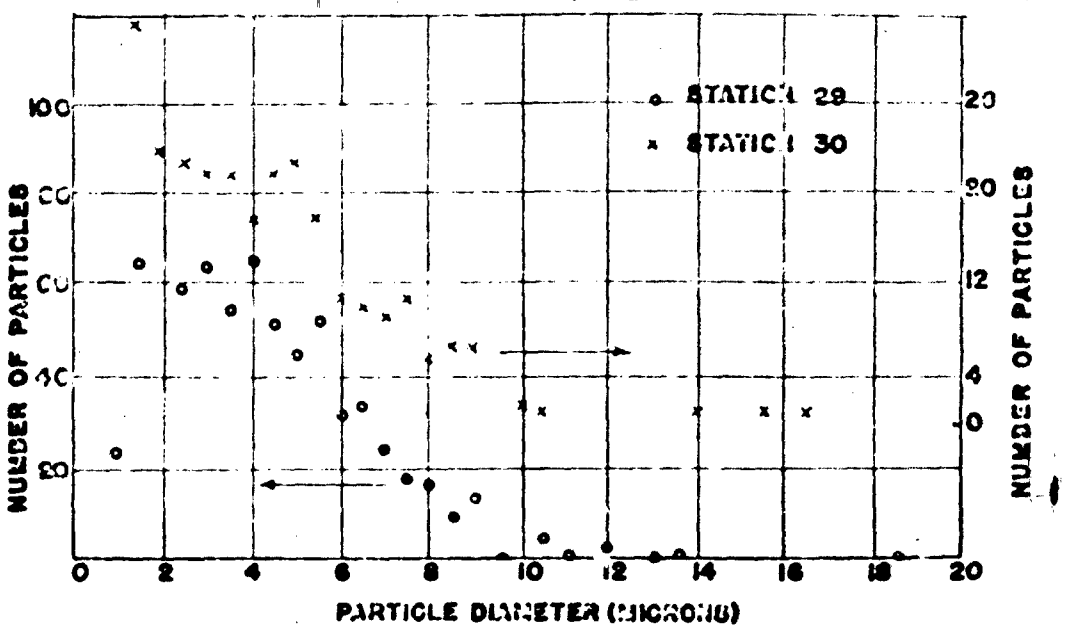

Fig. E.8 Particle Size Distribution of Radioactive Particles on First Filter Paper of Filter Samplers at Stations 29 and 30, Surface shot.

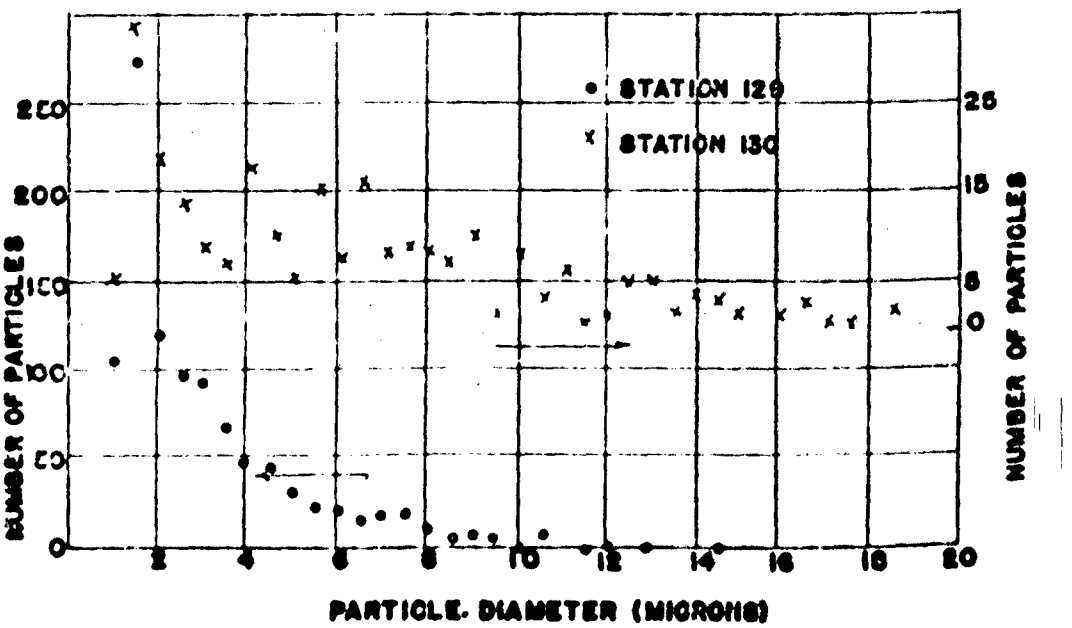

Fig. E.9 Particle Size Distribution of Radioactive Particles on First Filter Paper of Filter Samplers at Stations 129 and 130, Underground Shot.

PROJECT 2.5a-1

TABLE E.3

RADIOACTIVE PARTICLE SIZE DISTRIBUTION PARAMETERS

Filter Paper	b (microns)	n	Range of Sizes of Most Particles Found (in microns)
S-29M	2.5	2.8	3-11
S-30M	3.8	1.6	3-9
U-129M	2.4	1.4	2-6
U-150M	7.0	1.0	2-12
AFOAT Surface	3	2	3-9
" Underground	6	1.3	4-12

In general, the parameters b and n are functions of the diameter D; two special cases are of interest, however:

$$(P)_{b\ const} = (const)\ e^{-D/b} \qquad (E.6)$$

$$(P)_{n\ const} = (const)\ D^{-n} \qquad (E.7)$$

To determine b and n from the experiment, we notice that $\frac{1}{b}$ is given by the negative of the slope of a plot of log P vs D, and (-n) is the slope of the plot of log P vs log D. Drawing the best straight lines through the experimental points gives us our best estimates of n and b in the size range studied.

The experimental values of b and n are reported in Table E.3 where results obtained for two AFOAT Papers are also shown for comparison.

2.4.2 "Cross" Particles

At the suggestion of Col. Robbins the particle group attempted to find the size distribution of all particles collected on filters U-129X1 and U-107X1, not just the radioactive particles. Active portions of these filter papers were dispersed on glass slides and all particles observed under the microscope were measured for "diameter". In this case the definition of "diameter" is the longest observable dimension. For comparison purposes we also prepared "blanks". "Filter paper blanks" were simply smears of the collodion which was used for dispersal purposes.

The result of this work was that all three types of samples contained the same number of particles per unit area, and, as one would expect from this result, all three had the same size and color distribution. Our conclusion, then, is that we measured mostly laboratory dust, and that the standards of cleanliness necessary for this work are much higher than for radioactive particle work.

This work was repeated on AFCAT filter number U-13-B, which was 10 times as radioactive per unit area as ACC filter U-129X1. The result was again found to be negative.

In view of these disappointing results, the only result that can be quoted is an upper limit to the number of inactive particles present per radioactive particle. From the work done on AFCAT filter U-13-B, one can say that there are fewer than 10^4 nonradioactive particles per radioactive particle, where nonradioactive particles are defined as being optically detectable (1), and where radioactive particles are defined as being optically detectable and as having sufficient activity to produce a spot on photographic film. The work on the ACC filters would give higher upper limits, due to the fact that less debris was collected on them.

E.5 RADIOCHEMISTRY

E.5.1 Introduction

The original purpose of this part of the program was to establish the shape of the fission yield curve by radiochemical analyses for those elements occurring at several points of inflection of the curve. The elements chosen were Mo^{99}, Ba^{140}, Sr^{89}, Ag^{111}, Cd^{115}, and $Cs^{136-137}$. It was originally considered that an upward displacement of the curve in the neighborhood of Cd was indicative of the release of large numbers of neutrons, while horizontal displacements of the slopes of the curve (such as that including Ag) could be used to identify the fissionable material. Although there is no reason to use chemical analysis to answer this latter question about our own bombs, it has always been recognized that the successful application of these tests to debris from foreign bombs would require that these tests be applied to bombs of known fissionable content.

A gradually increasing uncertainty has arisen because of the fractionation of activity associated with debris from explosions of atomic weapons.

An examination of the results presented in the tables that follow will show that fractionation in JANGLE occurred to such an extent that it is impossible to associate a counting ratio with a particular shot unless the origin of the sample is known. In addition to the samples supplied from stations set up as part of this contract, other samples from Air Force collections and an independent source have been analyzed and are reported in these results.

E.5.2 Experimental Details

The results that are incorporated here are counting rates of standard weighing forms of the elements involved, corrected for decay by extrapolation backward to the known time-zero for each shot. Although the decay curves are not included in this interim report, they have been carefully checked and in all cases (except two early experiments on Sr^{89}) have shown decay rates that correspond very closely to those recorded for each nuclide.

The counting rates have also been corrected to zero-thickness by comparison against precipitate-thickness curves that were determined as part of the preparation for this contract. It is hoped that the counting-rate ratios (e.g. the $\frac{Cd115}{Mo99}$ ratio) may be compared with the same ratios measured on the products of an irradiation of normal U_3O_8 by thermal neutrons. In this way, the results from different laboratories may be intercompared without tedious and vulnerable attempts to reduce counting rates to disintegration rates.

E.5.3 Precision of Results

The counting of samples was controlled by the standard statistical procedures used in radiochemistry. As a rule, the precision of the results is estimated to about 5%. In those cases where the counting rate was very low, there will be included in parenthesis immediately after the counting rate, the nine-tenths error converted to percentage of the counting rate. For example, the counting rate of Cd^{115} from sample S-16-L is recorded in Table E.4 as 66(23%). This means that the total number of counts per minute of Cd^{115} (extrapolated to time zero and corrected to zero thickness of precipitate) is 66, and that this number has one chance in ten of being in error by 20%.

Standard factors are taken (from a standard Bi^{210} source) on each counter each working day in this laboratory. Moreover, a careful check has been kept of the background during the last five months, and a shift of as much as 3 cpm would be cause for concern. This constancy of background has been achieved by placing 2-inch bricks of lead under the manual sample changers, thereby reducing to a small fraction those effects that come from other sources of radioactivity that are handled in the basement.

In Tables E.4 and E.5 are listed the extrapolated counting rates for the total sample of each element analyzed. Tests of the filters showed that there was virtually no activity on the second filter paper from each station. However, both first and second papers were treated by the standard dissolution procedures.

The standard practice of laboratories working on these elements is to record the ratio of the counting rate of each element to the Mo^{99}. These are also included in Tables E.4 and E.5.

E.5.4 Surface Shot (T_o is Nov. 191700)

The amount of activity collected at the four stations listed below was quite small:

Station	Gross B Count on Nov.24
S-13-L	151 x 10^3 cpm
S-14-L	53 x 10^3 cpm
S-15-L	64 X 10^3 cpm
S-16-L	165 x 10^3 cpm

As a result, the counting rates of Cd and Cs were so low that they have little significance.

E.5.5 Underground Shot (T_o is Nov. 292000)

The distribution of activity from this shot followed a very unexpected pattern. A heavy surge must have gone from ground-zero in the direction toward Station U-114, because the amount of activity collected there was many times greater than that collected at any of the other three stations included here. Except for this station, gross B activity collected at the other stations was comparable in amount to that collected on the surface shot.

In addition to the four samples from the ACC stations, activity was analyzed from a close-in Air Force paper. The paper was divided into three parts and the different elements analyzed; each one referred to Mo^{99}. It was assumed here that the distribution of activity due to each nuclide would be independent of that part of the paper taken for analysis. It is now thought (from other results) that this assumption is not always strictly true.

One other source of activity collected independently, was also analyzed, but the results of this analysis will be given in the final report because there is some uncertainty whether the sample (a particle resembling slag) contains debris from the surface or the underground shot.

In Table E.5 are listed the results from the underground shot. These are presented in the same general pattern as those from the surface shot.

E.5.6 Discussion and Conclusions

The distinctive fact about these ratios is their variation. Although the precision of the measurements is sometimes low because the total amount of activity was low, there were several samples where the counting levels were high enough to make the maximum error less than 5%. In the underground shot, for example, the statistical errors on the samples from Station U-114-L and the Air Force paper were 1 or 2%. The great variations in the Ag/Mo and Cd/Mo ratios at these stations must be considered accurate to within 3 or 4 %. These results confirm the earlier evidence for fractionation, a term that this laboratory has until recently considered to be a scapegoat for difficulties arising in the course of the analysis.

Once the reality of fractionation has been established, the use of radiochemical results to establish fission-yield curves is seen to be highly vulnerable. There is, however, one interesting ratio that appears to be useful in identifying a shot. This ratio is the Ag^{111}/Cd^{115} ratio, and a survey of a considerable amount of data from former shots shows a remarkable consistency in the values of this ratio. In the case of JANGLE, we have the following Ag/Cd ratios:

	Station
Surface Shot	S-13-L
	S-16-L

The counting data on S-14L and S-15-L is not sufficiently precise to give a valid ratio.

	Station
Underground Shot	U-114-L
	U-115-L
	Air Force Paper J213B

When one considers the great variations in the Ag/Mo and Cd/Mo ratios in Tables E.4 and E.5, it would at first seem remarkable that the Ag/Cd ratios are as consistent as they are. But this is seen to be plausible (though not at all necessary), if one considers the relative volatilities of Pd, Ag and Cd oxides that are formed by the end of the first second in an atomic explosion. In fact, when we consider the periodic variation in

pp. 182 & 183 Deleted

the volatility of oxides of the elements, we are led to make a hypothesis that will certainly be subjected to an exhaustive trial-namely, that fission-product ratios will be most consistent when they involve precursors and final radioactive daughters that have similar volatilities. This is a rather crude hypothesis, and it will likely be considerably refined. It ignores the influence of variations in the half-lives of the precursors as well as several other relatively abstruse points of nuclear physics. Certainly, the constancy of the Ag/Cd ratios is consistent with this hypothesis.

The solution to the problem of fractionation will require an integrated effort by chemists, physicists, and nuclear physicists engaged in this work. It is essentially an attempt to treat rationally the combination of events that can give rise to such variations in radiochemical distribution as those found in the analysis of Jangle debris. The program is being initiated in this laboratory because we realize that it is a problem of central importance in the analysis of atomic bomb debris and the interpretation of the results.